

國立交通大學

材料科學與工程學系

博士論文

側鏈含有奈米結構之高分子電激發光二極體

之合成與分析



**Synthesis and Characterization of Light Emitting
Polymer Presenting Side-Chain-Tethered
Nanostructure**

研究生：周嘉宏 (Chia-Hung Chou)

指導教授：韋光華 (Kung-Hwa Wei)

中華民國 九十五年六月

Table of Content

The list of abbreviations	11
Abstract	12
摘要	14

Chapter 1: Introduction

1-1 Introduction of Light Emitting Polymer and History	15
1-2 Research Motivation	16
1-2-1 The Original of Green Emission in Polyfluorene-based Conjugated Polymers: On-Chain defect Fluorescence	16
1-2-2 keto defect	17
1-2-3 Luminescence Enhancement in Polymer/Nanoparticle Composite Electro-Optic Devices	18
1-3 Materials	18
1-3-1 Polyfluorene (PF)	18
1-3-2 Poly(<i>p</i>-phenylene vinylene) PPV	19
1-3-3 Polyhedral Oligomeric Silsesquioxane (POSS)	21
1-3-4 Nanoparticles	22
1-3-5 Nanoparticle Applications in PLEDs	22

Chapter 2: Polyfluorenes Incorporating Side-Chain-Tethered Polyhedral Oligomeric Silsesquioxane Units

2-1 Introduction Materials	29
2-2 Experimental	31
2-2-1 Materials	32
2-2-2 Characterization	34
2-2-3 Device Fabrication and Testing	34

2-3 Results and Discussions	
A. Polyfluorenes Incorporating Side-Chain-Tethered Polyhedral Oligomeric Silsesquioxane Units Nanocomposites	35
B. Electroluminescence (EL) Characteristics	38
2-4 Conclusions	39

Chapter 3: Polyphenylenevinylene Copolymer Presenting Side-Chain-Tethered Silsesquioxane Units

3-1 Introduction Materials	50
3-2 Experimental	52
3-2-1 Materials	52
3-2-2 Characterization	54
3-2-3 Device Fabrication and Testing	54
3-3 Results and Discussions	
A. Polyphenylenevinylene Copolymer Presenting Side-Chain-Tethered Silsesquioxane Units Nanocomposites	55
B. Electroluminescence (EL) Characteristics	58
3-4 Conclusions	59

Chapter 4: Thiophenol-modified CdS nanoparticles enhance the luminescence of benzoxyl dendron-substituted polyfluorene copolymers

4-1 Introduction	71
4-2 Experimental	73
4-3 Results and Discussions	74
4-3-1 Polyfluorene Side-Chain-Tethered CdS Nanoparticles	74
4-3-2 Electroluminescence (EL) Characteristics	80
4-4 Conclusions	81

Chapter 5: Polyfluorene Copolymer Incorporating Side-Chain-Tethered Gold

Nanoparticles	
5-1 Introduction	92
5-2 Experimental	94
5-2-1 Materials	94
5-2-2 Characterization	95
5-2-3 Device Fabrication and Testing	95
5-3 Results and Discussions	
A. Polyfluorene Side-Chain-Tethered Gold Nanoparticles	96
B. Electroluminescence (EL) Characteristics	97
5-4 Conclusions	99
Chapter 6: Conclusions	108
References and Notes	109



Figure Lists

Chapter 1: Introduction

Figure 1. PLEDs can be used to provide different color. (adapted from http://www.cdlttd.co.uk/technology/37.asp)	25
Figure 2. (a) Typical absorption, photo- and electroluminescence spectra of PPV. ^[34] (b) Cyclic voltammetry of dialkoxy-PPV. ^[35]	25
Figure 3. Polymers with phenyl derivatives in the backbones.....	26
Figure 4. Schematic representation of single-layer OLED	26
Figure 5. The mechanism of Light-emitting process	27
Figure 6. The structure of Polyfluorene (PFs).	27
Figure 7. The structure of Polyhedral Oligomeric Silsesquioxane (POSS).....	28
Figure 8. TEM micrographs and photoluminescence spectra of PPV-quantum dot composites. In each of the three photoluminescence profiles, the blue curve is solution photoluminescence and the red curve is solid-state photoluminescence. (a) 1-Functionalized CdSe nanocrystals blended with PPV (b) pyridine-covered CdSe nanocrystals blended with PPV and (c) composite CdSe nanocrystal-PPV, where PPV was grown from the nanocrystal surface. (adapted from <i>J. AM. CHEM. SOC.</i> 2004 , <i>126</i> , 11322)	28

Chapter 2: Polyfluorenes Incorporating Side-Chain-Tethered Polyhedral

Oligomeric Silsesquioxane Units

Figure 1. ¹ H NMR spectra of (a) 3, (b) Cl-POSS, and (c) 4.	43
Figure 2. FTIR spectra of (a) PFO, (b) PFO-POSS-1%, (c) PFO-POSS-3%, (d) PFO-POSS-5%, and (e) PFO-POSS-10%.	44
Figure 3. X-Ray diffraction curves of PFO-POSS nanocomposite films. (a) PFO, (b) PFO-POSS-1%, (c) PFO-POSS-3%, (d) PFO-POSS-5%, (e) PFO-POSS-10%, and (f) pure Cl-POSS.	44
Figure 4. (a) PL spectra of PFO films before annealing (dotted line) and after annealing	

at 200 °C for 1 h (dashed line) and 2 h (solid line) under a nitrogen atmosphere. (b) FTIR spectra of (i) PFO, (ii) PFO-POSS-5%, and (iii) PFO-POSS-10% before (solid line) and after (dashed line) baking at 200 °C for 6 h.45

Figure 5. UV–Vis absorption and PL spectra of (a) PFO-POSS-1% , (b) PFO-POSS-3%, (c) PFO-POSS-5%, and (d) PFO-POSS-10% films before (dotted line) and after (solid line) annealing at 200 °C for 2 h under a nitrogen atmosphere46

Figure 6. Transmission electron micrographs of (a) PFO-POSS-1%, (b) PFO-POSS-3%, (c) PFO-POSS-5%, and (d) PFO-POSS-10%.47

Figure 7. Electroluminescence spectra of the devices prepared from PFO-POSS and PFO in the configuration ITO/PEDOT/polymer/Ca/Al.48

Figure 8. I–V curves of the devices prepared from PFO-POSS and PFO in the configuration ITO/PEDOT/polymer/Ca/Al.48

Figure 9. UV-vis absorption and Photoluminescence spectrum (excited at 380 nm) in THF of (a) PFO, (b) PFO-POSS-1%, (c) PFO-POSS-3%, (d) PFO-POSS-5%, (e) PFO-POSS-10%.49

Figure 10. TGA curves of polymer at a heating rate of 20 °C/min under nitrogen atmosphere. (a) DSC curves of PFO and PF-POSS-10% at a heating rate of 10 °C /min under nitrogen atmosphere.49

Chapter 3: Polyphenylenevinylene Copolymer Presenting Side-Chain-Tethered Silsesquioxane Units

Figure 1. ¹H NMR spectra of (a) Cl-POSS, (b) POSS-CH₃, and (c) POSS-CH₂Br. ... 62

Figure 2. FTIR spectra of (a) MEHPPV, (b) POSS-PPV1-*co*-MEHPPV, (c) POSS-PPV3-*co*-MEHPPV, (d) POSS-PPV5-*co*-MEHPPV, and (e) POSS-PPV10-*co*-MEHPPV.63

Figure 3A. UV–Vis absorption and PL spectra of (a) MEHPPV, (b) POSS-PPV1-*co*-MEHPPV, (c) POSS-PPV3-*co*-MEHPPV, (d) POSS-PPV5-*co*-MEHPPV, and (e) POSS-PPV10-*co*-MEHPPV recorded in the solid

state.	64
Figure 3B. Normalized (relative to their maximum wavelengths) PL spectra of (a) MEHPPV and (b) POSS-PPV10- <i>co</i> -MEHPPV annealed at room temperature and 150°C in the solid state.	64
Figure 3C. X-ray diffraction spectra of (a) MEHPPV, (b) POSS-PPV1- <i>co</i> -MEHPPV, (c) POSS-PPV3- <i>co</i> -MEHPPV, (d) POSS-PPV5- <i>co</i> -MEHPPV, (e) POSS-PPV10- <i>co</i> -MEHPPV, and (f) Cl-POSS.	65
Figure 3D. Deconvoluted X-ray diffraction spectra of (a) MEHPPV and (b) POSS-PPV10- <i>co</i> -MEHPPV.	65
Figure 4A. (a) Transmission electron micrograph of POSS-PPV10- <i>co</i> -MEHPPV. (b) enlarged view. (c) EDS of POSS-PPV10- <i>co</i> -MEHPPV.	66
Figure 4B. Surface roughness of thin films of (a) MEHPPV. (b) POSS-PPV10- <i>co</i> -MEHPPV.	67
Figure 5. Electroluminescence spectra of the devices prepared from POSS-PPV- <i>co</i> -MEHPPV in the configuration ITO/PEDOT/polymer/Ca/Al.	68
Figure 6. I-L-V curves of the devices prepared from POSS-PPV- <i>co</i> -MEHPPV and MEHPPV in the configuration ITO/PEDOT/polymer/Ca/Al.	68
Figure 7. UV-Vis absorption and PL spectra of (a) MEHPPV, (b) POSS-PPV1- <i>co</i> -MEHPPV, (c) POSS-PPV3- <i>co</i> -MEHPPV, (d) POSS-PPV5- <i>co</i> -MEHPPV, and (e) POSS-PPV10- <i>co</i> -MEHPPV recorded in THF solution.	69
Figure 8. DSC traces of (a) MEHPPV, (b) POSS-PPV1- <i>co</i> -MEHPPV, (c) POSS-PPV3- <i>co</i> -MEHPPV, (d) POSS-PPV5- <i>co</i> -MEHPPV, and (e) POSS-PPV10- <i>co</i> -MEHPPV.	69
Figure 9. TGA traces of (a) MEHPPV, (b) POSS-PPV1- <i>co</i> -MEHPPV, (c) POSS-PPV3- <i>co</i> -MEHPPV, (d) POSS-PPV5- <i>co</i> -MEHPPV, and (e) POSS-PPV10- <i>co</i> -MEHPPV.	70

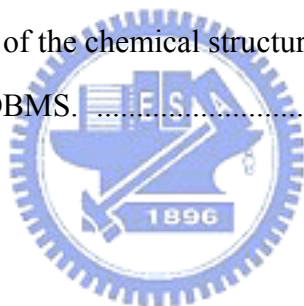
Chapter 4: Thiophenol-modified CdS nanoparticles enhance the luminescence of benzoxyl dendron-substituted polyfluorene copolymers

Figure 1. Normalized UV–Vis absorption spectra recorded in DMF for S-CdS nanoparticles having three different diameters.	84
Figure 2. (a) Photoluminescence spectra of PF [poly-2,7-(9,9-dioctylfluorene)], excited by a xenon lamp at $\lambda_{\max} = 393$ nm, and PF-G0, PF-G1, and PF-G2, all recorded in THF at the same concentration (5×10^{-6} M). (b) Photoluminescence spectra recorded in DMF of (i) PF-G1 in the solid state, using a xenon lamp as the excitation light source, (ii) PF-G1 in the solid state, using a GaN diode laser, and (iii) S-CdS nanoparticles having three different diameters.	85
Figure 3. Photoluminescence spectra of thin films of (a) S-CdS _{3nm} /PF-G1, (b) S-CdS _{4nm} /PF-G1, and (c) S-CdS _{7nm} /PF-G1, normalized with respect to the PL intensity of PF-G1.	86
Figure 4. Photoluminescence spectra of thin films of (a) pure PF-G0, (b) PF-G0 containing 4 wt% S-CdS, (c) pure MEHPPV, (d) MEHPPV containing 4 wt% S-CdS, and (e) PMMA containing 4 wt% S-CdS.	87
Figure 5. A. X-ray diffraction spectra of S-CdS/ PF-G1 nanocomposite. (a) PF-G1 (b) PF-G1 containing 3 wt% S-CdS, (c) PF-G1 containing 4 wt% S-CdS, and (d) PF-G1 containing 8 wt% S-CdS. B. The effect of the amount of S-CdS on the Bragg <i>d</i> spacing of PF-G1. C. FTIR spectra of (a) PF-G1 and (b) PF-G1 containing 4 wt% S-CdS. D. Cyclic voltammogram of the oxidation of polymer.	88
Figure 6. Transmission electron microscopy images of PF-G1 films containing (a) 3 wt% and (b) 4 wt% of S-CdS.	90
Figure 7. Normalized electroluminescence spectra of devices prepared from S-CdS/PF-G1 in the configuration ITO/PEDOT/polymer/Ca/Al.	90
Figure 8. (a) I–V and (b) L–V curves of devices prepared from S-CdS/PF-G1 in the configuration ITO/PEDOT/polymer/Ca/Al.	91

Chapter 5: Polyfluorene Copolymer Incorporating Side-Chain-Tethered Gold Nanoparticles

Figure 1. ¹ H NMR spectra of (a) tris(4-bromophenyl)amine and (b) DBMS.	102
--	------------

Figure 2. XPS spectra [S(2P) region] of PF-DBMS adsorbed onto Au NPs.	103
Figure 3. Normalized UV–Vis absorption spectra and PL emission spectra of PF-DBMS recorded in solution (THF) and from a thin film. The inset displays the thin film after thermal treatment at 100°C for 2 h.	103
Figure 4. (a) Transmission electron microscopy images of Au/PF-DBMS films. The inset displays the lattice image (lattice spacing: ca. 2.3Å) of the Au NPs. (b) Size distribution of Au NPs in the PF-DBMS polymer matrix. (c) TEM images of cross-sections of the device.	104
Figure 5. (a) I–V and (b) L–V curves of devices prepared from Au/PF-DBMS in the configuration ITO/PEDOT/polymer/Ca/LiF/Al.	105
Figure 6. EL spectra of devices prepared from Au/PF-DBMS in the configuration ITO/PEDOT/polymer/LiF/Ca/Al.	106
Figure 7. (a) ¹ H NMR spectra of the chemical structure of all polymers. (b) The chemical structure of the PF-DBMS.	107



Scheme & Table Lists

Chapter 1: Introduction

Scheme 1. (a) The Wessling-Zimmerman precursor route to PPV. (b) End-capping modification of the Gilch polymerization.	24
--	-----------

Chapter 2. Polyfluorenes Incorporating Side-Chain-Tethered Polyhedral

Oligomeric Silsesquioxane Units

Scheme 1. Synthesis of D-POSS-diAF (4) (i) CrO ₃ , acetic anhydride, HCl _(aq) . (ii) aniline, aniline hydrochloride. (iii) K ₂ CO ₃ , KI, DMF/THF (5:4)	40
--	-----------

Scheme 2. Synthesis of PFO-POSS copolymers	41
---	-----------

Table 1. Physical properties of the PFO-POSS copolymers	42
--	-----------

Table 2. Optical properties of the PFO-POSS nanocomposites.	42
---	-----------

Chapter 3: Polyphenylenevinylene Copolymer Presenting Side-Chain-Tethered Silsesquioxane Units

Table 1. Physical Properties of the POSS-PPV- <i>co</i> -MEHPPV Copolymers.	60
---	-----------

Table 2. Optical Properties of the POSS-PPV- <i>co</i> -MEHPPV Nanocomposites.	60
--	-----------

Scheme 1. Synthesis of POSS-PPV- <i>co</i> -MEHPPV copolymers. Reagents and conditions: i, trichloro[4-(chloromethyl)phenyl]silane, HNEt ₃ Cl; ii, K ₂ CO ₃ , DMF/THF; iii, <i>N</i> -bromosuccinimide (NBS)/ AIBN/ CCl ₄ ; iv, <i>tert</i> -BuOK/ THF. ..	61
---	-----------

Chapter 4: Thiophenol-modified CdS nanoparticles enhance the luminescence of benzoxyl dendron-substituted polyfluorene copolymers

Scheme 1. Synthesis of (a) S-CdS and (b) PF-GX and (c) a schematic drawing of the architecture of S-CdS/PF-GX (X = 1, 2).	82
---	-----------

Table 1. Absorption and photoluminescence data for S-CdS/polymer nanocomposites in the solid state.	83
---	-----------

Table 2. Thermal behavior of S-CdS/polymer nanocomposites.83

Chapter 5: Polyfluorene Copolymer Incorporating Side-Chain-Tethered Gold Nanoparticles

Table 1. Absorptions and Quantum Yields for Au NP/Polymer Nanocomposite Solid Films.100

Table 2. Absorptions and Quantum Yields for Polymer Solid Films.100

Table 3. Molecular Weights of the Polymers.101

Scheme 1. Synthesis of (a) PF-DBMS copolymers (b) A schematic drawing of the architecture of Au/ PF-DBMS nanocomposites.101



The list of abbreviations

BuLi	<i>n</i> -butyllithium
CDT	Cambridge Display Technology
CdS	Cadmium Sulfide
DMF	<i>N,N</i> -dimethylformami
DSC	differential scanning calorimetry
FWHM	full width at half maximum, [nm]
GPC	gel-permeating chromatography
HOMO	highest occupied molecular orbital
HTL	hole-transport layer
ITO	indium tin oxide
MEH-PPV	poly[2-methoxy-5-(2-ethylhexyloxy)- <i>p</i> -phenylene vinylene]
S-CdS	Thiophenol-modified cadmium sulfide
PDI	polydispersity index
PEDOT	poly(3,4-ethylenedioxythiophene)
PF	polyfluorene
PFO	poly(9,9-dioctylfluorene)
PF-DBMS	poly{2,7-(9,9'-dioctylfluorene)- <i>co</i> -4-diphenylamino-4'-bipenylmethylsulfide}
PL	photoluminescence
PLED	polymeric light emitting diode
PMMA	poly(methyl methacrylate)
POSS	polyhedral oligomeric silsesquioxane
PPP	poly(<i>p</i> -phenylene)
PPV	poly(<i>p</i> -phenylene vinylene)
PT	polythiophene
Q.E.	quantum efficiency
T_g	glass transition temperature
TGA	thermal gravimetric analysis
THF	tetrahydrofuran
Φ_{PL}	quantum yield of photoluminescence
XPS	X-ray photoelectron spectroscopy

Abstract

The main objective of this dissertation is to study the performance of polymer light emitting diodes involving luminescent polymers incorporating different kinds of inorganic segment in their side chains. In the introduction of this dissertation, we gave an explanation on the historical evolution of polymer nanocomposites light emitting diodes and summarized the literatures in the recent years. In the chapter 2, we have synthesized polyhedral silsesquioxane-tethered polyfluorene copolymers, poly(9,9'-dioctylfluorene-co-9,9'-bis[4-(*N,N*-dipolysilsesquioxane)aminophenyl]fluorene) (PFO-POSS), that have well-defined architectures using Suzuki polycondensation. This particular PFO-POSS molecular architecture increases the quantum yield of polyfluorene significantly by reducing the degree of interchain aggregation; in addition, these copolymers exhibit a purer and stronger blue light by preventing the formation of keto defects. The PPV-POSS molecular architecture also increases the quantum yield significantly by reducing the degree of interchain aggregation were discussed in Chapter 3. This particular molecular architecture of POSS-PPV-co-MEHPPV copolymers possesses not only a larger quantum yield (0.85 vs. 0.19) but also higher degradation and glass transition temperatures relative to those of pure MEHPPV. The maximum brightness of a double-layered-configured light emitting diode (ITO/PEDOT/emissive polymer/Ca/Al) incorporating a copolymer of MEHPPV and 10 mol% PPV-POSS was five times as large as that of a similar light emitting diode incorporating pure MEHPPV (2196 vs. 473 cd/m²).

The presence of a low percentage of thiophenol-modified cadmium sulfide (S-CdS) nanoparticles in the benzoxy-dendritic structure of a copolyfluorene (PF-GX)

substantially improves the efficiency of its light emission were discussed in Chapter 3. The enhancements in photoluminescence and electroluminescence arise mainly from a reduction in the degree of energy transfer from the excited polymer chains to their neighboring polymer chains in the ground state; i.e., there is an increase in the inter-polymer chain distance when CdS nanoparticles are present. We have prepared highly luminescent dendron-substituted copolyfluorenes that incorporate surface-modified cadmium sulfide nanoparticles. A small percentage of these nanoparticles can be incorporated into the dendritic structures upon tailoring the interfaces between the ligands on the nanoparticles and the dendritic structures in the copolyfluorene. Both the photoluminescence and electroluminescence efficiencies of the polymer nanocomposites are dramatically enhanced. Moreover, in order to know the effect to some other nanoparticles, we have tethered gold nanoparticles (Au NPs) to the side chains of poly{2,7-(9,9'-dioctylfluorene)-*co*-4-diphenylamino-4'-biphenylmethylsulfide} (PF-DBMS) through its ArSCH₃ anchor groups. The presence of 1 wt% of the tethered gold NPs led to a reduction in the degree of aggregation of the polymer chains, resulting in a 50% increase in its quantum yield. The electroluminescence of a 1wt% Au/ PF-DBMS device was three times higher in terms of its maximum brightness and its full-width-at-half-maximum emission peak was much narrower than that of a pure PF-DBMS device. These phenomena arise from the photooxidation suppression, hole blocking, and electron transport enhancing effects of the Au NPs were also demonstrated in Chapter 5.

摘要

高分子發光二極體(PLED)是未來發展成大平面的顯示器的重要技術，而大部份的電激發光高分子，由於具有豐富的 π 電子，因此電洞注入特性和傳輸電洞的能力遠比電子注入特性和傳輸電子的能力來的有效率。近期不少研究著重於開發高效率且穩定的發光材料，其中又以藍光材料最受重視。聚芴(Polyfluorene)及其衍生物由於包含一剛性且共平面的雙苯環結構，所以表現出特殊的物理和化學性質；然而，無論是PPV 或者是PF系列元件在製成薄膜時，由於材料累積濃度過高造成分子堆疊或產生excimer，嚴重影響光色以及降低發光效率；此外，PF系列由於C9位置容易產生氧化現象(keto defect)，也會改變元件原有穩定的發光光色。為了改善這些缺點，選擇導入多立面體聚矽氧烷(POSS)於高分子材料之側鏈期望以防止氧化及減少分子堆疊，使得高分子的光色及熱穩定性進一步改良，可廣泛地應用在顯示器的發光材料上。此方法所合成之高分子奈米複合材料可提升發光高分子之發光效率、元件效率並提升其耐熱度及穩定性。在本文的第二及第三章節，我們將分別討論POSS在Polyfluorene(PF) 與 Polyphenyl vinylene (PPV)中所扮演的角色。另外一部分，有鑒於高分子內部螢光發光效率最高僅達25%的物理限制，高分子與無機材料的結合便受到了矚目；雖近期有磷光高分子發光二極體之開發，但合成時必須使用重金屬，來源恐不穩定。因此，本研究嘗試以膠體化學法合成半導體材料量子點（其直徑小於10 奈米）製備一系列S-CdS/PF-GX (X=1, 2)之奈米複合發光材料，並藉由實驗證實，導入少量改質的量子點(S-CdS)，不但可有效地提昇螢光及電激發光效率至原來之兩倍至三倍，同時也增強原本材料在製程元件後的穩定度及電性。在第五章中我們選擇用金奈米粒子並對其特性作進一步的探討。含有1wt%的金奈米粒子之聚芴高分子共聚物提高了原本的量子效率與光學穩定性；同時在元件部份，與純聚芴高分子共聚物比較，高分子藉由鍵結金奈米粒子之元件也具有較優異的表現。

Chapter 1: Introduction

1-1 Introduction of Light Emitting Polymer and History

Since the discovery of PLEDs in 1989^[1], significant effort has been directed into the development of red, green and blue materials that exhibit high efficiency and stability under normal operating conditions, and to enable integration into flat panel display (FPD) applications (Figure 1). From 1989 until now, LEDs is probably the most important application maintaining the researchers' interest towards conjugated (conducting) polymers, although in recent years we witness a growing interest towards other relevant applications such as sensors and photovoltaics. Hundreds of academic research groups around the world have contributed to the development of electroluminescent polymers. An even more pronounced research activity is being held in industry. Several newly born R&D companies such as Cambridge Display Technologies (CDT, spin-off from Cambridge University), Covion Organic Semiconductors and UNIAX (spin-off from UCSB), are targeted at development of high efficiency, long life-time EL polymers. A huge commercial potential, connected with the possibility of solution fabrication of EL devices, and, particularly, flat and/or flexible displays, attracted in the business such industrial giants as Dow Chemical, DuPont, IBM, Kodak and Philips.^[2] PLEDs utilize the same physics principles as LEDs but use polymers as the active light-emitting layer. It has many advantages when compared to normal inorganic LEDs. Simple and cost-efficient manufacturing and the ability to generate a uniform area of light demonstrate that PLEDs exhibit excellent promise for current and future electronic and optical applications. The first PLEDs used poly(phenylene vinylene) PPV as the emitting layer. PPV is an undoped conjugated polymer, which has a molecular structure given

in Figure 2. Today many other polymers such as polythiopenes, polypyridine, poly(pyridyl vinylenes) and polyphenylene have been used to emit light (Figure 3). Light emitting diodes consist of active or emitting layers placed between a cathode (typically aluminum or calcium) and an anode (ITO, indium tin oxide). A diagram of a typical PLED is shown in Figure 4. When the two electrodes are connected electrons are injected from the cathode into the p^* -band semiconducting polymer and holes are injected from an electrode into the p -band. The oppositely charged carriers in the two bands meet within the polymer films and recombine (return to their ground state) radiatively to give off light.^[3] (Figure 5)

1-2 Research Motivation



1-2-1. The Original of Green Emission in Polyfluorene-based Conjugated Polymers: On-Chain defect Fluorescence.

Conjugated polymers have been studied in great detail as electroluminescent materials for use in organic light emitting diodes. Significant progress has been made in understanding the fundamental working processes involved in generating efficient, reliable light across the entire visible spectrum. Polyfluorene-based materials have been investigated extensively because of the many attractive properties they possess. Additional experimental results are needed to discern the nature of the unwanted green emission that often appears during device operation and quantum efficiencies need to be significantly improved. The currently most challenging topic for conjugated polymers applications is blue emission color stability. All available poly(*para*-phenylene) (PP)-type materials, which are the most promising family of

blue light emitters, are prone to degradation, resulting in an unwanted change in color due to the emergence of low energy green emission peak. However, vital to overcome the problem and to provide suitable future synthetic strategies. The low-energy emission band has been mostly attributed to reordering of the polymer chains and subsequent aggregate^[4] or excimer formation.^[5] It will be shown in the following that both excimer and aggregate formation cannot explain the presented experimental observations and can therefore be ruled out as the main origins of the energy emission band of polyfluorene-type polymers as suggested previously.^[6] Instead, the experimental observations show fluorescence from an on-chain oxidative defect to be the source of this emission band.

1-2-2. keto defect

Low-energy emission bands have been identified in all PPP-type polymers upon thermal,^[7] photo-, and/ or electrical degradation. Recently, the occurrence of this emission band has been correlated to presence of ketonic defects incorporated into the polymer backbone in the form of 9-fluorenones. Furthermore, fluorene-fluorenone copolymers has established a quantitative correlation between the 9-fluorenone content and the low-energy emission band intensity. However, no unambiguous verdict about the nature of the emission (emission from the aggregation or excimer) could be found. This identification is, however, crucial for determining future synthetic approaches: Influencing the solid state packing of the polymer chains by bulky side chains,^[8] spiro-linked compounds,^[9] or disorder induced by the copolymerization of fluorine with e.g., anthracene^[10] could effectively hinder aggregate or excimer formation. Fluorescence emission from oxidative (on-chain) defects, on the contrary, can only be excluded by improving the oxidative stability of

the polymers.

1-2-3. Luminescence Enhancement in Polymer/Nanoparticle Composite

Electro-Optic Devices

Polymer light emitting diodes have a good chance to become the main display system in the near future since diodes have many advantages concerning preparation and operation over other display systems. However, material with single species often can not meet all the stringent criteria of industrial applications. The major drawbacks of the PLEDs have been operating life times and insufficient device radiances.

Recently, it has been shown that incorporating oxide nanoparticles into a PPV derivative enhances the PLED current density and radiance by an order of magnitude.

In this thesis, we have to improve or tailor material properties with composite and develop finely tailored nanocomposite materials for emissive or non emissive display technology. An efficient way to obtain promising new materials is to modify existing potential materials with doping of semiconductor nanoparticles are described.

1-3 Materials

1-3-1. Polyfluorene (PF)

Fluorene is a polycyclic aromatic compound, which received its name due to strong violet fluorescence which arises from highly conjugated planar π -electron system. The 2,7-Positions in fluorene are the most reactive sites towards electrophilic attack, which allows construction of a fully conjugated rigid-rod polymer chain by substitution reactions, whereas the methylene bridge provides an opportunity

to modify the processability of the polymer by substituents, without perturbing the electronic structure of the backbone. The varieties, excellent optical and electronic properties, and high thermal and chemical stability of polyfluorenes (PFs) make them an attractive class of materials for polymer light-emitting diodes (PLEDs). Different aspects of syntheses, properties and LED applications of fluorene-based conjugated polymers and co-polymers have been highlighted in several recent reviews.^[11] In fact, polyfluorenes are the only class of conjugated polymers that can emit a whole range of visible colors with relatively high quantum efficiency.

It is well known that PFs are the most promising class of blue-emitting materials. The original problem associated with undesirable “green emission band” was shown to be a result of exciton trapping on the electron deficient fluorenone defect sites. The color purity can be reestablished via 1) careful purification of the monomer (complete elimination of mono-substituted units), 2) inserting a protecting layer between the PF and reactive cathode material, 3) introducing hole-trapping sites (most commonly, triarylamine units), which would compete with fluorenone defects, minimizing the excitone formation on the latter, 4) introducing bulky substituents into PF backbone, which would minimize the exciton trapping on fluorenone defects. Furthermore, introducing of different conjugated moieties into PF backbone allows for efficient color tuning in these materials.

1-3-2. Poly(*p*-phenylene vinylene) PPV

Conjugated polymers are organic semiconductors in which the π -molecular orbitals are delocalized along the polymer backbone. Polymer-based OLEDs are attractive due to their excellent film forming properties and their ease of application

over large surfaces through simple, economically viable coating techniques such as spin coating or ink-jet printing. Small molecule emissive materials are typically coated as thin films via vacuum-deposition which is difficult over large areas and is not as cost effective. As previously stated, PPV was the first polymer that was shown to display electroluminescence. Since direct synthesis of PPV produces an insoluble material, an alternative route was developed to allow the spin-coating of a soluble precursor polymer from solution (Scheme 1). Poly(*p*-phenylene vinylene) (PPV) is a highly stable conjugated polymer. Its yellow color is due to an absorption band centered at ~400–420 nm (depending on the method of synthesis) with an on-set corresponding to a band gap of ~2.5 eV.^[12] The HOMO and LUMO levels in PPV can be accessed in cyclic voltammetry experiments, which, under proper conditions, reveal chemically reversible oxidation and reductions waves (Figure 2a). The deduced electrochemical gap corresponds reasonably well to the optical band gap. There are number of synthetic strategies elaborated for preparation of PPV homo- and co-polymers:^[13]

1. Thermoconversion (Wessling-Zimmerman route)
2. Chemical vapor deposition (CVD)
3. Ring-opening metathesis polymerization (ROMP)
4. The Gilch polycondensation
5. Chlorine precursor route (ROMP) (Gilch modification)
6. Non-ionic route (Gilch modification)
7. Knoevenagel polycondensation
8. Heck coupling polymerization
9. Wittig(-Horner) Condensation
10. Miscellaneous.

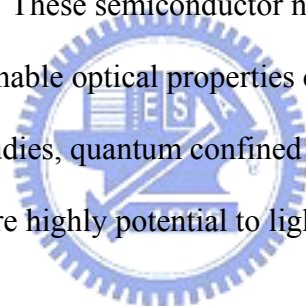
Being a relatively good electron donor, PPV and its derivatives can be chemically doped by strong oxidating agents and strong acids, affording highly conductive p-doped materials (with conductivity up to $\sim 10^4 \text{ S/cm}^5$). The yellow-green fluorescence of PPV is featured by a vibronically structured emission band with peaks maxima at 520 and 551 nm (Figure 2b).

1-3-3. Polyhedral Oligomeric Silsesquioxanes (POSS)

Organic-inorganic nanocomposites with well-defined architectures have attracted a great deal of attention since they not only have synergistic properties, but can also be tailored to specific technical applications^[14]. One class of inorganic component-polyhedral oligomeric silsesquioxanes (POSS) has nanometer-sized structure with high surface area and controlled porosity has been demonstrated to an efficient method in the design of hybrid materials^[15-27]. POSS has two unique features : (1) the chemical composition is a hybrid, intermediate ($\text{RSiO}_{1.5}$) between that of silica (SiO_2) and silicones (R_2SiO). (2) POSS molecules are physically large, POSS consists of a rigid, cubic silica core with a 0.53 nanometer side length and can have organic functional groups connected to the vertices of the cubic core for further reaction (Figure 7). Due to its versatile functional groups and high solubility in several solvents, POSS molecules can form covalent bonds with themselves or organic monomers. POSS molecules are typically stable up to 400°C , which are higher than the thermal degradation temperatures of most polymers. Their incorporation into some polymers has lead to enhancements in thermal stability and mechanical properties. For instance, POSS molecules have been successfully incorporated into acrylics^[15], styryls^[16], epoxy^[17] and polyethylene^[24].

1-3-4. Nanoparticles

One of the most interesting subjects in materials science is a quantum confinement effect in low-dimensional systems as quantum wells, quantum wires, and quantum dots. Nanoparticles play an important role for nanotechnology and livelihood applications, for example catalysts, light-emitting diode, etc. Recently, many kinds of metal, metal oxide or semiconductor nanoparticles were reported for applications, such as Au or CdSe nanoparticles for bio-labeling and solar devices, TiO₂ nanoparticles for photo-catalysis materials, Co, CoFe₂O₄ and Fe₂O₃ nanoparticles for magnetic applications. For semiconductor nanoparticles with sizes close to their Bohr exciton radius (typically between 1-10 nm), the size-dependent band gap results in tunable optical properties. These semiconductor nanoparticles are termed as quantum dots because their tunable optical properties can be predicted by quantum mechanics. Among these studies, quantum confined semiconductor nanoparticles, such as CdS and CdSe/ZnS, are highly potential to light emitting diode devices.

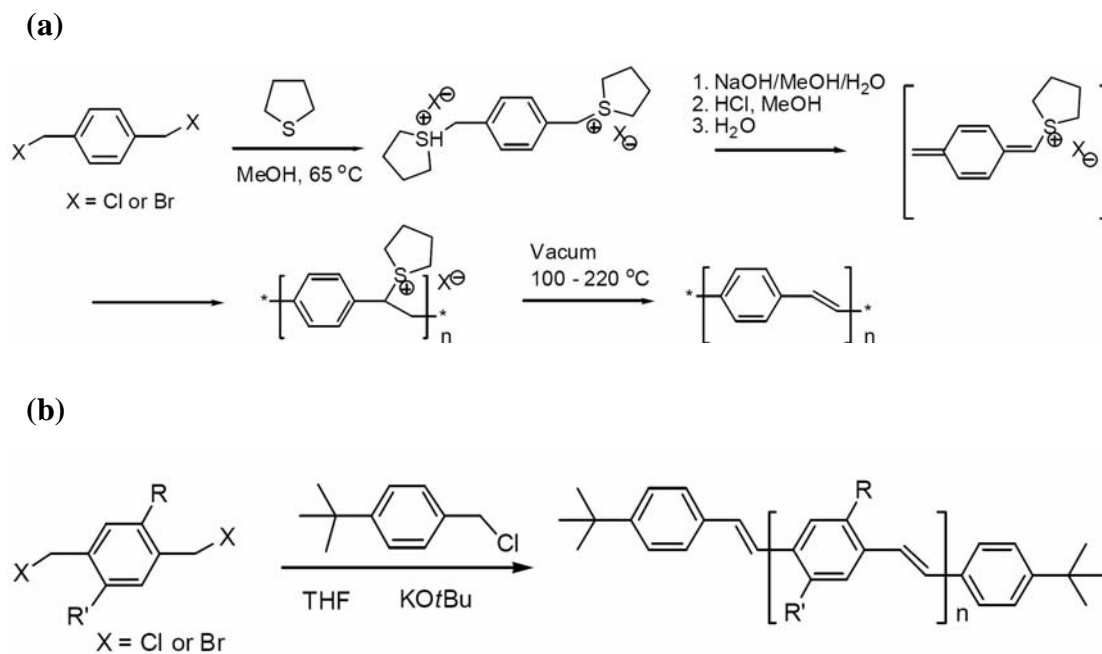


1-3-5. Nanoparticle Applications in PLEDs

The potential use of polymer light-emitting diodes is ultimately limited by their low quantum efficiency as well as by their poor stability due to oxygen. A recent study found that blending Au NPs with polyfluorene resulted in enhanced luminescent stability.^[28] Blue polymer light-emitting diodes with enhanced luminescent stability were obtained by incorporating 5-10 nm gold nanoparticles as the quenchers of the triplet states of blue emitting polymer. The nanocomposite light-emitting diodes exhibited an enhanced quantum efficiency due to the roughening of the surface onto which the Al cathode is deposited and to balanced charge injection. On the other hand, in polymer-nanoparticle composites, uniform dispersion of the

nanoparticles carries advantages over cases where nanoparticle aggregation dominates. Such dispersion has been particularly difficult to obtain in the case of composites prepared from nanoparticles and conjugated polymers. One recent study found that cadmium selenide nanocrystals, or quantum dots, can be integrated into thin films of poly(paraphenylene vinylene) (PPV) without aggregation.^[29] (Figure 8) The ability to tailor and disperse quantum dots in PPV thin films in this fashion dramatically impacts the photophysical properties of these materials relative to conventional blends. While PPV coverage is emphasized here, the novel quantum dot growth methods, and the general polymerization methodology, carry the potential for broad applicability that will enable new physical studies and device fabrication using polymer-quantum dot composite materials.





Scheme 1. (a) The Wessling-Zimmerman precursor route to PPV. (b) End-capping modification of the Gilch polymerization.

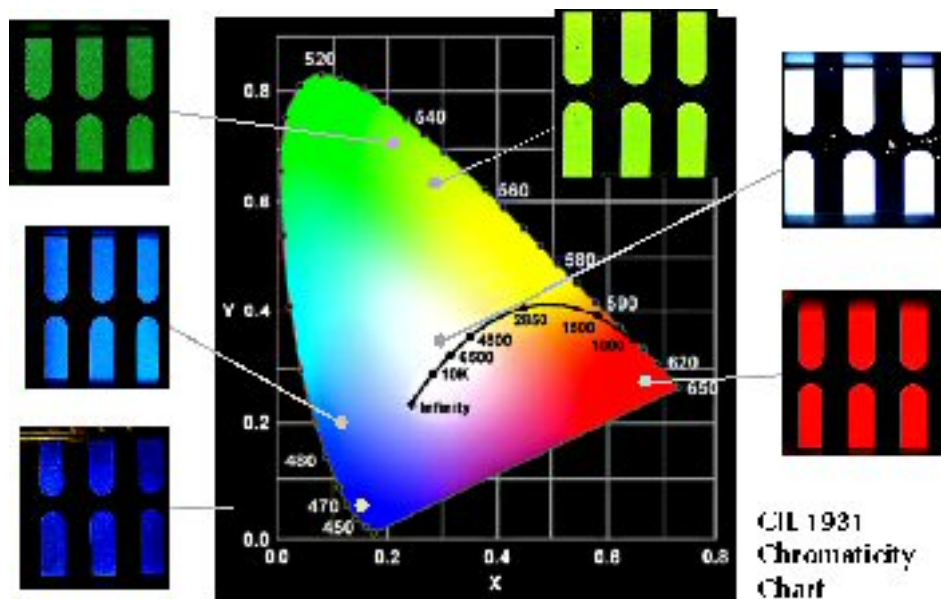


Figure 1. PLEDs can be used to provide different color. (adapted from <http://www.cdtltd.co.uk/technology/37.asp>)

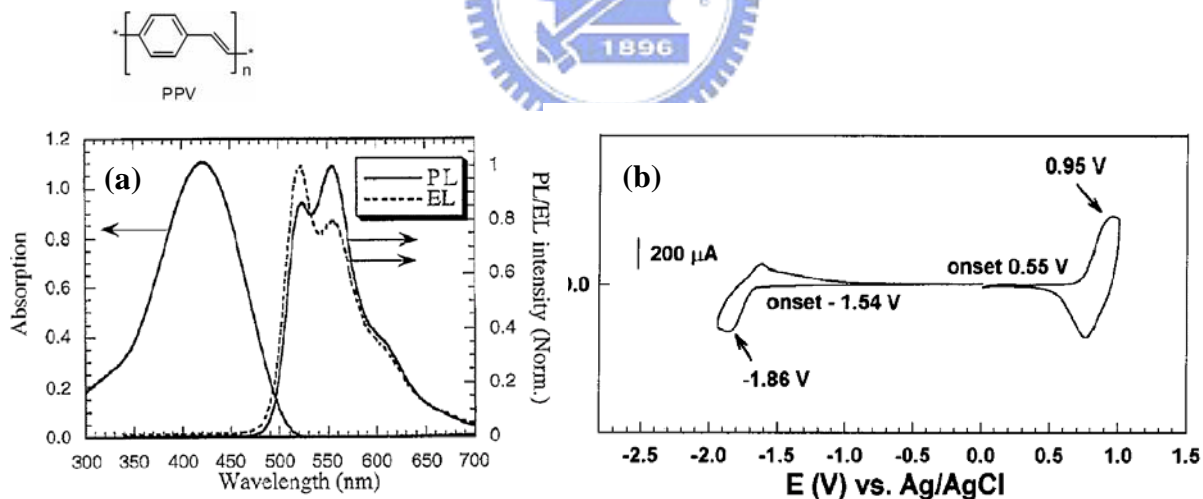


Figure 2. (a) Typical absorption, photo- and electro- luminescence spectra of PPV.^[34]

(b) Cyclic voltammetry of dialkoxy-PPV.^[35]

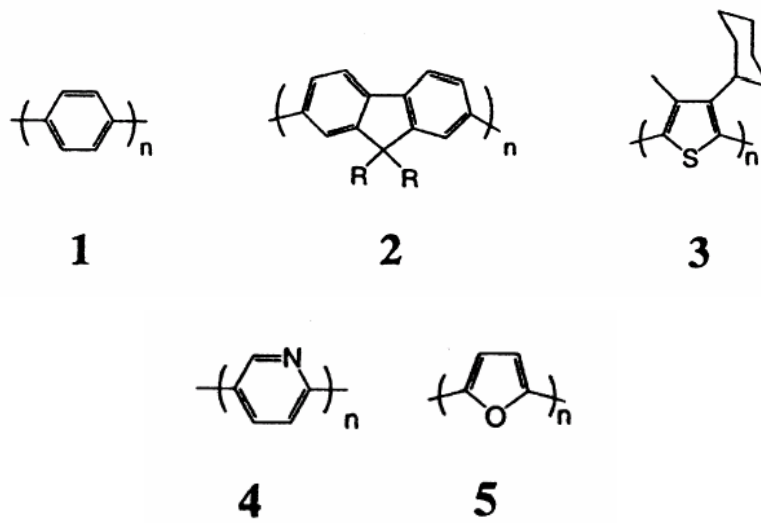


Figure 3. Polymers with phenyl derivatives in the backbones.

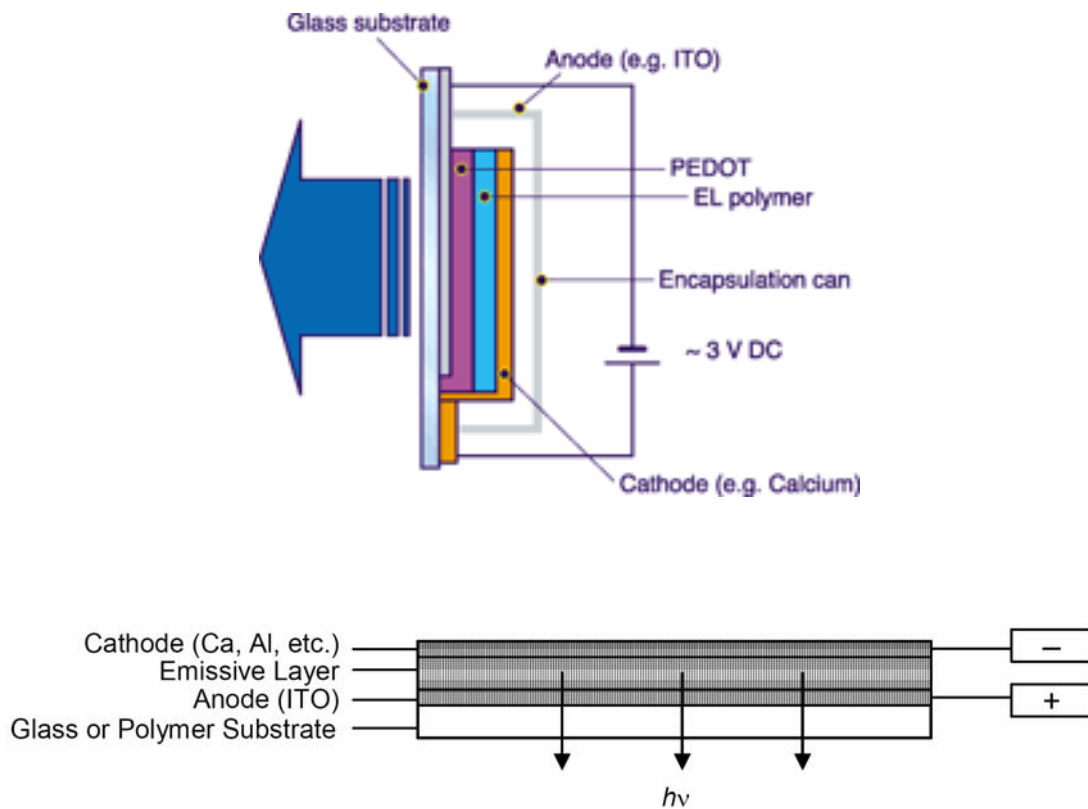


Figure 4. Schematic representation of single-layer OLED

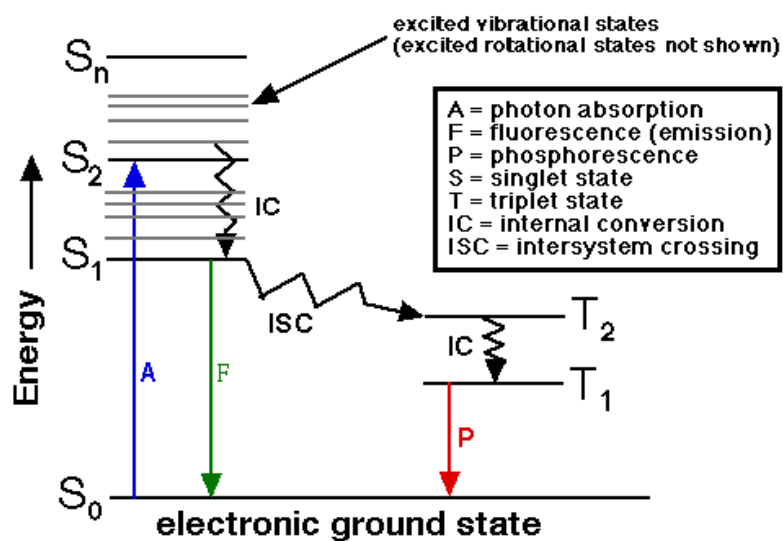


Figure 5. The mechanism of Light-emitting process.

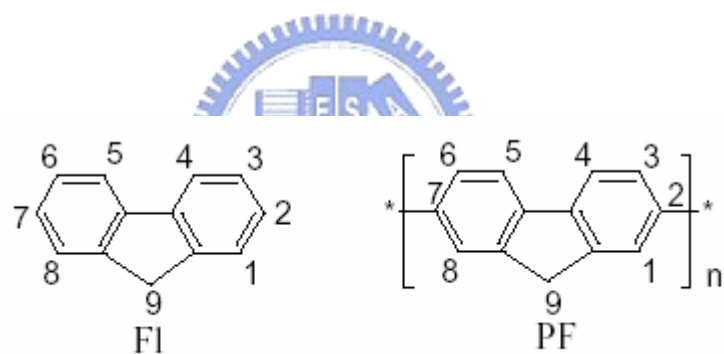


Figure 6. The structure of Polyfluorene (PFs).

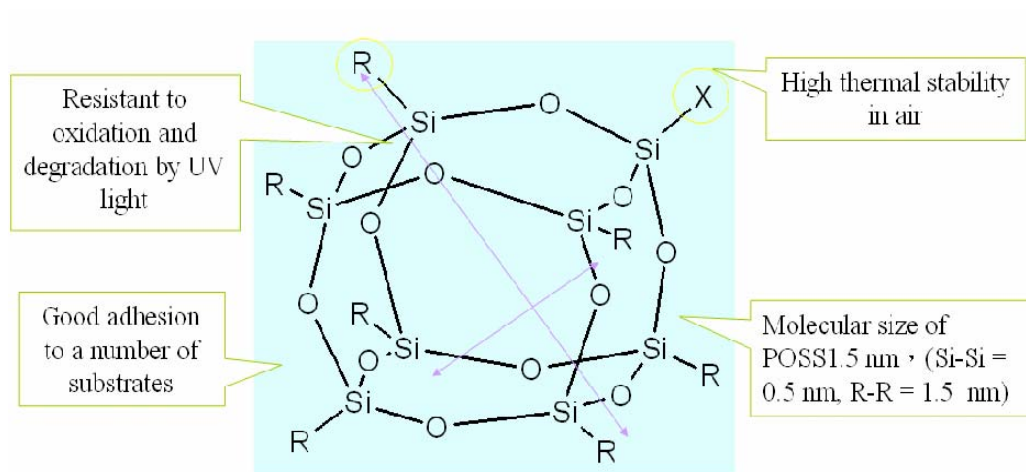


Figure 7. The structure of Polyhedral Oligomeric Silsesquioxane (POSS).

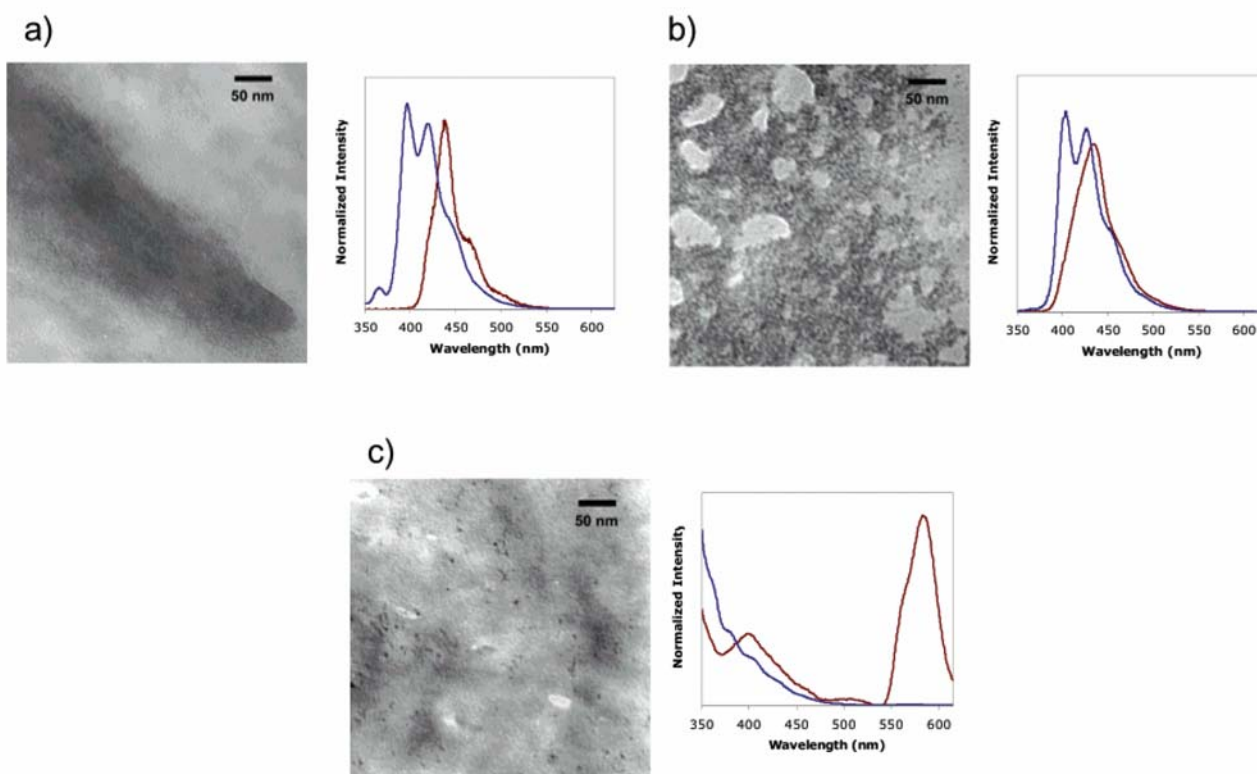


Figure 8. TEM micrographs and photoluminescence spectra of PPV-quantum dot composites. In each of the three photoluminescence profiles, the blue curve is solution photoluminescence and the red curve is solid-state photoluminescence. (a) 1-Functionalized CdSe nanocrystals blended with PPV (b) pyridine-covered CdSe nanocrystals blended with PPV and (c) composite CdSe nanocrystal-PPV, where PPV was grown from the nanocrystal surface. (adapted from *J. AM. CHEM. SOC.* **2004**, *126*, 11322)

Chapter 2: Polyfluorenes Incorporating Side-Chain-Tethered Polyhedral Oligomeric Silsesquioxane Units

2-1 Introduction Materials

Semiconducting polymers have been studied extensively for their potential applications in electroluminescent displays,^[32] solar cells,^[33] and thin film organic transistors.^[34] One of the most promising conjugated polymers is polyfluorene, which has been applied widely for its characteristic of emitting blue light.^[35-38]

Polyfluorenes may be functionalized readily by modifying the C-9 position of the fluorene monomer; such modification can, for instance, provide good solubility in common organic solvents that allows further processing. In the solid state, polyfluorene and its derivatives exhibit adequate photoluminescence (PL) and electroluminescence (EL) efficiencies.^[8, 39-40] The application of polyfluorenes in light emitting diodes, however, has been hampered by the appearance of green electroluminescence (ca. 530 nm) in addition to the desired peak at 425 nm; this green electroluminescence has been attributed to either intermolecular interactions, which lead to the formation of aggregates,^[41-47] or to the presence of emissive keto defect sites that arise as a result of thermo- or electro-oxidative degradation of the polyfluorene backbone.^[48] A detailed discussion of this phenomenon has been presented elsewhere.^[48b] As a result, the expected blue emission from polyfluorene becomes an undesired blue-green color in LED applications.

Several approaches have been adopted to reduce the formation of aggregation or keto defect in polyfluorenes, including the introduction of bulky side chains, using cross-linked structures, improving the oxidative stability of pendant groups or chain ends,^[45] and limiting chain mobility by blending it with a high- T_g polymer.^[47] One

of the most recent approaches involves incorporation of polyhedral oligomeric silsesquioxane (POSS) into the conjugated polymer. The first such study was undertaken by attaching POSS covalently to the chain ends of poly(2-methoxy-5-[2-ethylhexyloxy]-1,4-phenylenevinylene) (MEHPPV) and poly(9,9'-dioctylfluorene) (PFO), which resulted in enhanced thermal stability of the devices prepared from these modified polymers.^[45] The density of the polymer chain ends, however, decreases as the molecular weight of the polymer increases, which limits the amount of POSS that can be attached (ca. 1.2%). Another study involved a synthesis of a bridged polyfluorene copolymer by using fluorene tetrabromide monomers featuring a siloxane bridge. The thermal stability of a device made from this siloxane-bridged polyfluorene appears to be better than that prepared from pure PFO.^[48] A third related study involved attaching polyfluorene to the functionalized vertices on the cubic polyhedral silsesquioxane core units to form starlike structures; these polymers possessed improved thermal and optoelectronic characteristics. The amount of POSS content in the polyfluorene was ca. 3.8%.^[48] The enhanced electroluminescence characteristics in these polyfluorenes have been attributed to POSS imparting a reduction in either the degree of aggregation and excimer formation or the number of keto defects. The molecular architecture that polyfluorene possessed in the latter two studies cannot be defined easily. Previously, we synthesized a polyimide-side-chain-tethered POSS as an approach to lowering its dielectric constant.^[49a] In this present study, we took a copolymer approach by synthesizing polyfluorene-tethered POSS in a well-defined architecture. To the best of our knowledge, the introduction of an inorganic side group, such as POSS, into the C-9 position of polyfluorene has not been explored previously. We believe that by developing a POSS/polyfluorene copolymer having well-defined architecture we will be able to tailor its luminescence properties more

precisely by modifying the molecular structure. In this paper, we report the synthesis and characterization of fluorene-based random copolymers featuring tethered polyhedral oligomeric silsesquioxanes (POSS) units.

Scheme 1 displays the synthetic procedure we used to prepare the POSS-dibromide monomer (D-POSS diAF), in which cyclopentyl-POSS was covalently bonded to the C-9 carbon atom of the fluorine unit through a 4-aminophenyl spacer. We used POSS-dibromide as a co-monomer, which, together with 2,7-dibromo-9,9'-dioctylfluorenone (5), were reacted with 2,7-bis(4,4,5,5-tetramethyl-1,3,2-dioxaborolan-2-yl)fluorene (6) through Suzuki coupling followed by end capping. Scheme 2 presents the complete synthetic procedure for the preparation of POSS-tethered polyfluorene. The extended 9,9'-bis(4-aminophenyl)fluorenyl core, which is readily accessible, offers the following additional advantages: (1) Direct attachment of the benzyl groups of POSS to the C-9 carbon atom of the fluorene unit is avoided; such benzyl linkages are potentially susceptible to photooxidation, which may cause degradation and failure of the polymer LEDs.^[49b, 8] (2) The introduction of the 4-aminophenyl spacer reduces the steric hindrance imposed by POSS.^[50] The insertion of a rigid phenylene spacer between the POSS side chain and the polymer backbone may lead to a shielding effect on the polyfluorene main chain, while leaving the reaction sites of the macromonomer accessible for the palladium-catalyzed polymerization reaction. (3) Through this copolymerization approach, the amount of POSS incorporated into the polyfluorene may be tuned by controlling the amount of POSS-dibromide monomer used in the polymerization.

2-2 Experimental

2-2-1. Materials

2,7-Dibromo-9,9'-dioctylfluorenone (5),^[50] 2,7-bis(4,4,5,5-tetramethyl-1,3,2-dioxaborolan-2-yl)fluorene (6),^[51] and the chlorobenzylcyclopentyl-POSS^[52] were synthesized according to literature procedures. THF was distilled under nitrogen from sodium benzophenone ketyl; other solvents were dried using standard procedures. All other reagents were used as received from commercial sources unless otherwise stated.

Chlorobenzylcyclopentyl-POSS. ¹H NMR (300 MHz, CDCl₃): δ 7.64 (d, *J* = 8.1 Hz, 2H), 7.37 (d, *J* = 8.1 Hz, 2H), 4.57 (s, 2H), 2.26–1.21 (m, 56H), 1.16–0.81 (m, 7H) ppm. ²⁹Si NMR (600 MHz, THF): δ -67.8, -68.2, -79.6 ppm.

Synthesis of 9,9'-Bis(4-aminophenyl)-2,7-dibromofluorene (3). A mixture of 2,7-dibromo-9-fluorenone (2) (3.0 g, 8.88 mmol), aniline (4.0 g, 4.30 mmol), and aniline hydrochloride (1.15 g, 8.88 mmol) was heated at 150 °C under nitrogen for 6 h. The reaction mixture was then slowly added into water (150 mL) and extracted with ethyl acetate (3 × 50 mL). The combined extracts were dried (MgSO₄), the solvent was evaporated, and the residue was purified by column chromatography (hexane/ethyl acetate, 4:1) to afford 3 (3.23 g, 72%). ¹H NMR (CDCl₃): δ 7.52 (d, *J* = 8.1 Hz, 2H), 7.44 (4H), 6.90 (d, *J* = 8.1 Hz, 4H), 6.53 (d, *J* = 8.1 Hz, 4H), 3.58 (s, 4H) ppm. Anal. Calcd for C₂₅H₁₈Br₂N₂ (%): C, 59.31; H, 3.58; N, 5.53. Found: C, 59.38; H, 3.62; N, 5.47.

Synthesis of 9,9'-bis[4-(*N,N*-dipolysilsesquioxane)aminophenyl]fluorene

(D-POSS-diAF) (4). 9,9-Bis(4-aminophenyl)-2,7-dibromofluorene (200 mg, 0.395 mmol) was stirred with K_2CO_3 (764 mg, 5.53 mmol) and KI (262 mg, 1.58 mmol) in DMF (5 mL) and THF (4 mL) at room temperature for 1 h. A small amount of Cl-POSS (888 mg, 0.832 mmol) was added and then the whole mixture was heated at 70 °C for 3 h. The reaction mixture was then slowly poured into water (150 mL) and extracted with chloroform (3×30 mL). The combined extracts were dried ($MgSO_4$), the solvents were evaporated, and the residue was purified by column chromatography (hexane/ chloroform, 1:10) to afford 4 (0.69 g, 68%). 1H NMR ($CDCl_3$): δ 7.62-7.63 (m, 14H), 7.01-6.84 (m, 8H), 4.81 (s, 2H), 4.27 (s, 4H), 2.06–1.18 (m, 112H), 1.14–0.79 (m, 14H) ppm. Anal. Calcd for $C_{109}H_{154}Br_2O_{24}N_2Si_{16}$ (%): C, 52.67; H, 6.24; N, 1.13. Found: C, 52.11; H, 6.21; N, 1.07.

General Procedure for the Synthesis of Alternating Copolymers PFO-POSS.

Aqueous potassium carbonate (2 M) and aliquate 336 were added to a solution of the POSS-appended fluorene dibromide monomer 4, dibromide 5, and diboronate 6 in toluene. The mixture was degassed and purged with nitrogen three times. The catalyst, tetrakis(triphenylphosphine)palladium (3.0 mol%), was added in one portion under a nitrogen atmosphere. The solution was then heated at 90 °C and vigorously stirred under nitrogen for 5 days. End-group capping was performed by heating the solution under reflux for 6 h sequentially with phenylboronic acid and bromobenzene. After cooling, the polymer was recovered by precipitating it into a mixture of methanol and acetone (4:1). The crude polymer was collected, purified twice by reprecipitation from THF into methanol, and subsequently dried under vacuum at 50 °C for 24 h. The 1H and ^{13}C NMR spectra of PFO and PFO-POSS appear to be identical because of the low content of POSS in the latter polymer.

2-2-2. Characterization.

^1H , ^{13}C , and ^{29}Si nuclear magnetic resonance (NMR) spectra of the compounds were obtained using a Bruker DRX 300 MHz spectrometer. Mass spectra of the samples were obtained on a JEOL JMS-SX 102A spectrometer. Fourier transform infrared (FTIR) spectra of the synthesized materials were acquired using a Nicolet 360 FT-IR spectrometer. Gel permeation chromatographic analyses were performed on a Waters 410 Differential Refractometer and a Waters 600 controller (Waters Styragel Column). All GPC analyses of polymers in THF solutions were performed at a flow rate of 1 mL/min at 40 °C; the samples were calibrated using polystyrene standards.

Thermogravimetric analysis (TGA) and differential scanning calorimetry (DSC) measurements were performed under a nitrogen atmosphere at heating rates of 20 and 10 °C/min, respectively, using Du Pont TGA-2950 and TA-2000 instruments, respectively. UV–Vis absorption and photoluminescence (PL) spectra were recorded on a HP 8453 spectrophotometer and a Hitachi F-4500 luminescence spectrometer, respectively. Before investigating the thermal stability of the synthesized polymers, their polymer films were annealed in air at 200 °C for 2 h.

2-2-3. Device Fabrication and Testing.

The electroluminescent (EL) devices were fabricated on an ITO-coated glass substrate that was precleaned and then treated with oxygen plasma before use. A layer of poly(ethylene dioxythiophene):poly(styrene sulfonate) (PEDOT:PSS, Baytron P from Bayer Co.; ca. 40-nm thick) was formed by spin-coating from its aqueous solution (1.3 wt%). The EL layer was spin-coated at 1500 rpm from the corresponding toluene solution (15 mg mL^{-1}) on top of the vacuum-dried PEDOT:PSS layer. The

nominal thickness of the EL layer was 65 nm. Using a base pressure below 1×10^{-6} Torr, a layer of Ca (30 nm) was vacuum deposited as the cathode and a thick layer of Al was deposited subsequently as the protecting layer. The current–voltage characteristics were measured using a Hewlett–Packard 4155B semiconductor parameter analyzer. The power of the EL emission was measured using a Newport 2835-C multi-function optical meter. The brightness was calculated using the forward output power and the EL spectra of the devices; a Lambertian distribution of the EL emission was assumed.

2-3 Results and Discussions

A. Polyphenylenevinylene Copolymer Presenting Side-Chain-Tethered

Silsesquioxane Units Nanocomposites

Figure 1 displays the ^1H NMR spectra of 9,9'-bis(4-aminophenyl)-2,7-dibromo-fluorene (3), Cl-POSS, and D-POSS-diAF (4). The peak for the NH protons shifted downfield from 3.59 ppm for 3 to 4.48 ppm for 4, while the CH_2 peak of Cl-POSS shifted upfield from 4.47 to 4.21 ppm in D-POSS-diAF. The ratio of the peak areas of the benzylic CH_2 and NH protons is ca. 2:1. Taken together, all of these data suggest that Cl-POSS had reacted with 4-aminophenyl fluorene to form D-POSS-diAF. Table 1 lists the thermal properties and molecular weight distributions of the PFO-POSS copolymers. Both the thermal degradation and glass transition temperature increased as the amount of POSS in PFO increased, presumably because the tethered POSS enhanced the thermal stability and retarded the polymer chain mobility. The molecular weights of the PFO-POSS copolymers decreased upon increasing the POSS content; this phenomenon can be attributed to the steric hindrance caused by POSS during the polymerization process. Figure 2 displays FTIR spectra of PFO copolymers containing different amounts of POSS. The

FTIR spectrum of POSS displays two major characteristic peaks in the range 1000–1180 cm^{-1} (Si–O–Si stretching). The Si–C band at 1074 cm^{-1} , however, overlaps with the Si–O–Si band and, thus, could not be observed clearly.

Figure 3 displays the X-ray diffraction curves of Cl-POSS, PFO, and PFO-POSS. We observed no X-ray diffraction peaks for pure PFO. There are three distinct diffraction peaks at $2\theta = 8.3, 19.1,$ and 26.1° observed for Cl-POSS (Fig. 3f), which correspond to d -spacings of 10.5, 4.6 and 3.3 Å, respectively. The d -spacing of 10.5 Å reflects the size of the Cl-POSS molecules; the other two spacings reflect the rhombohedral crystal structure of POSS molecules.^[15] The presence of a small crystal peak of POSS in PFO indicates a mild degree of aggregation of POSS molecules. The DSC curves of pure PFO^[53] indicate a value of T_g of 62 °C, a crystallization exothermic peak (T_c) at 98 °C, and a melting endothermic peak (T_m) at 155 °C (see the Supporting Information). Only a small T_m at 166 °C appears in the curve for PFO-POSS-10%; the disappearance of the T_g and T_c peaks in this case (PFO containing 10% POSS) can be explained by the fact that the mobility of the PFO main chains, including chain folding, is severely retarded by the steric hindrance imposed by the bulky side-chain-tethered POSS units, as has been reported in the literature.^[54] The UV–Vis and photoluminescence spectra of PFO and PFO-POSS recorded in THF are presented in the Supporting Information. Table 2 lists the wavelengths of the absorption and PL maxima and the quantum yields of PFO-POSS. The absorption and emission peak maxima of PFO occur at 384 and 418 nm, respectively; these values are close to those reported in the literature.^[55] We observed no aggregation band in these spectra because THF is a good solvent for PFO. The absorption and emission peaks for PFO and PFO-POSS are almost identical. For each polymer, the absorption peak maximum in solution (THF) is located between 384 and 362 nm, with

a slight blue shift caused by the presence of POSS; the PL maxima occur at similar wavelengths for all of the polymers. The quantum yields of the PFO-POSS copolymers increased substantially as the amount of tethered POSS increased. In particular, the quantum yield of PFO containing 10% POSS was 54% higher than that of pure PFO (0.86 vs. 0.55). This finding can be attributed to the steric hindrance caused by the POSS units preventing aggregation of the PFO main chains, which, in turn, reduces the degree of dimer formation after excitation. This phenomenon is a result of the particular side-chain-tethered POSS architecture that we have employed: it has not been reported in previous studies of POSS/PFO copolymers. The other significant effect that the incorporation of the silsesquioxane into PFO side chain causes is the persistence of luminescence behaviour after thermal treatment of PFO-POSS. The stability of both color and luminescence at elevated temperatures are critical for polymer LEDs because sometimes the operating temperature of these devices exceeds 86 °C. Next, we investigated in detail the effect that thermal treatment has on POSS-incorporated PFO. Figure 4a displays the photoluminescence spectra of PFO as a solid film after heat treatment at 200 °C; in all cases, the absorption peaks at 386 nm remain. Other than the main peak at 425 nm, we observe an additional small peak, at ca. 530 nm, in the spectrum of PFO film exposed at 200 °C for 1 h. The green emission peak at 530 nm increased in intensity, while the intensity of the main 425 nm peak reduced quite dramatically, after annealing the PFO film for 2 h. Figure 4b indicates that, after thermal treatment, the intensity of the keto peak (C=O, 1713 cm⁻¹) in the FTIR spectra decreases as the amount of POSS in PFO increases: almost no keto peak appears in the spectrum of the sample containing 10% POSS. Undesired fluorescence emission resulting from the oxidation defects in polymer chains can be reduced by improving the thermal oxidative properties of the polymers.^[48b, 15] In this case, the bulky siloxane units

attached to 4-aminophenyl spacer appear to provide a good shield for the neighboring dialkyl groups from oxidation because the thermal degradation temperature of siloxane units is higher than that of dialkyl chains, which is evident in the TGA results of POSS/PFO copolymer in table 1.

Figure 5 presents the normalized absorption and PL emission spectra of the annealed PFO-POSS films with respect to that of their fresh films. The fact that the absorption λ_{max} of PFO-POSS in Figures 5c and 5d appears at the same wavelength before and after heating suggests that the thermal treatment did not disrupt the conjugation in these PFO-POSS samples. The PL spectrum of PFO containing 1% POSS exhibits a much smaller shoulder at 530 nm than that for the pure PFO after the same thermal treatment. This peak was reduced further when 3% POSS (Fig. 5b) was present and became an insignificant shoulder at ca. 500 nm when $\geq 5\%$ POSS was incorporated into PFO (Figs. 5c and 5d). These results suggest that the tethered POSS units not only reduced the aggregation of PFO molecular chains but also prevented keto defects from forming upon thermal treatment. Figure 6 presents transmission electron microscopy (TEM) images of different PFO-POSS samples; these images clearly reveal that no large aggregates have formed, but small domains of POSS are present, and the POSS domains are dispersed well in the polymer matrix.

B. Electroluminescence (EL) Characteristics.

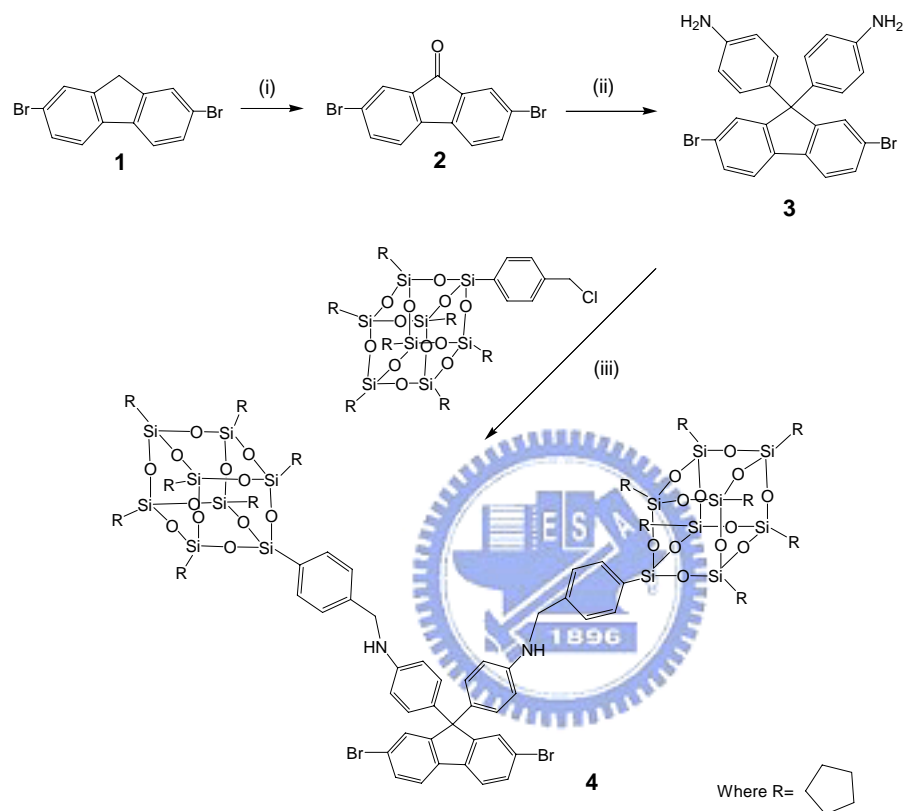
Figure 7 displays the electroluminescence (EL) spectra of PFO-POSS devices. The EL device prepared from PFO emits a weak blue signal at 425 nm and a more-intense green signal in the range 470–600 nm, which is presumably due to the aggregation and keto defects discussed previously. When 5% POSS was included in PFO, the intensity of the peak at 425 nm increased, but the intensity of the green

emission remained approximately the same. In the case where 10% POSS was incorporated in PFO, the green emission in the range 470–600 nm was reduced sharply, while the peak at 425 nm became the major emission peak and had an intensity much larger than that exhibited by the device prepared from pure PFO. The reduction in the green emission is apparently due to the presence of the siloxane units. The introduction of bulky siloxane units into polyfluorene side chain presumably serves a dual function; it not only hinders oxidation of fluorenes but also increases the interchain distance, thereby retarding the interchain interactions and leading to a reduction of excitons migration to defect sites as discussed in a previous study.^[56] Figure 8 displays the variations of the current density and brightness of the EL devices. The turn-on voltage increased to 5.8 V for PFO containing 10% POSS from 5.4 V for the pure-PFO EL device. A significant increase (68%) in the maximum brightness of the PFO-POSS-10%-based device occurred relative to that of the pure-PFO EL device (392 vs. 234 cd/m^2) at a drive voltage of 10 V and a current density of 576 mA/cm^2 . These improvements might be due to a combination of a lesser degree of aggregation and fewer keto defects being formed upon the incorporation of POSS into PFO.

2-4 Conclusions

We have synthesized a novel polyfluorene side-chain-tethered polyhedral silsesquioxane that has a well-defined architecture. This particular molecular architecture of PFO-POSS increases the quantum yield of polyfluorene significantly by reducing the degree of interchain aggregation; it also results in a purer and stronger blue light being emitted from the EL device by preventing the formation of keto defects.

Scheme 1 Synthesis of D-POSS-diAF (4) (i) CrO_3 , acetic anhydride, $\text{HCl}_{(\text{aq})}$. (ii) aniline, aniline hydrochloride. (iii) K_2CO_3 , KI, DMF/THF (5:4).



Scheme 2 Synthesis of PFO-POSS copolymers

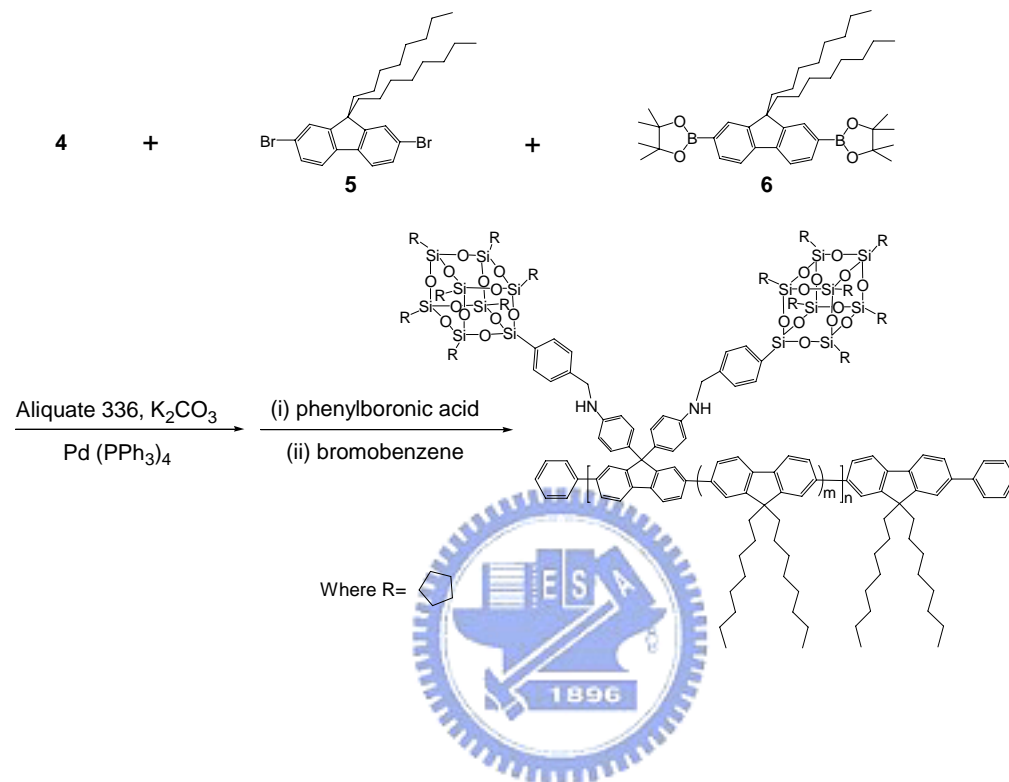


Table 1. Physical properties of the PFO-POSS copolymers.

	T_d^a (°C)	M_n	M_w	PDI	Yield(%)
PFO	372	27,000	51,000	1.86	96
PFO-POSS-1%	382	21,000	42,000	1.96	78
PFO-POSS-3%	381	20,000	37,000	1.85	68
PFO-POSS-5%	397	16,000	31,000	1.93	79
PFO-POSS-10%	416	12,000	24,000	1.97	65

^a Temperature at which 5% weight loss occurred, based on the initial weight.

Table 2. Optical properties of the PFO-POSS nanocomposites.

	λ_{\max} (UV, nm)		λ_{\max} (PL, nm) ^a		quantum yield
	solution ^b	film	solution ^b	film	film ^c
PFO	384	390	418 (441)	425 (448)	0.55
PFO-POSS-1%	374	383	417 (440)	423 (447)	0.57
PFO-POSS-3%	374	381	417 (437)	423 (447)	0.64
PFO-POSS-5%	372	381	417 (437)	423 (447)	0.67
PFO-POSS-10%	362	380	416 (436)	422 (446)	0.86

^a The data in parentheses are the wavelengths of shoulders and subpeaks.

^b The absorption and emission measured in THF.

^c PL quantum yield estimated relative to a sample of poly-2,7-(9,9'-dioctylfluorene) ($\Phi_{\text{FL}}=0.55$).

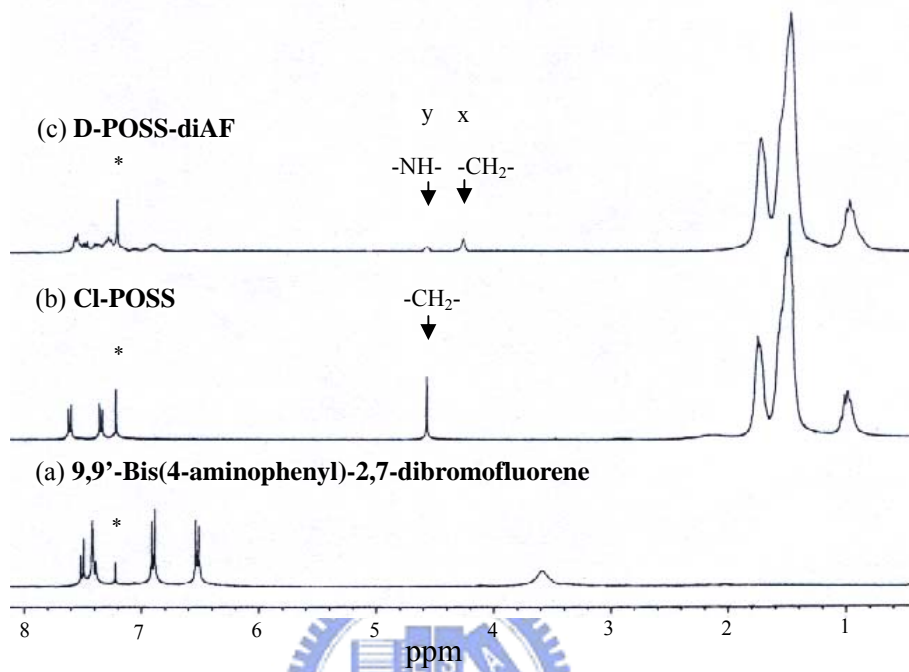


Figure 1. ^1H NMR spectra of (a) 3, (b) Cl-POSS, and (c) 4.

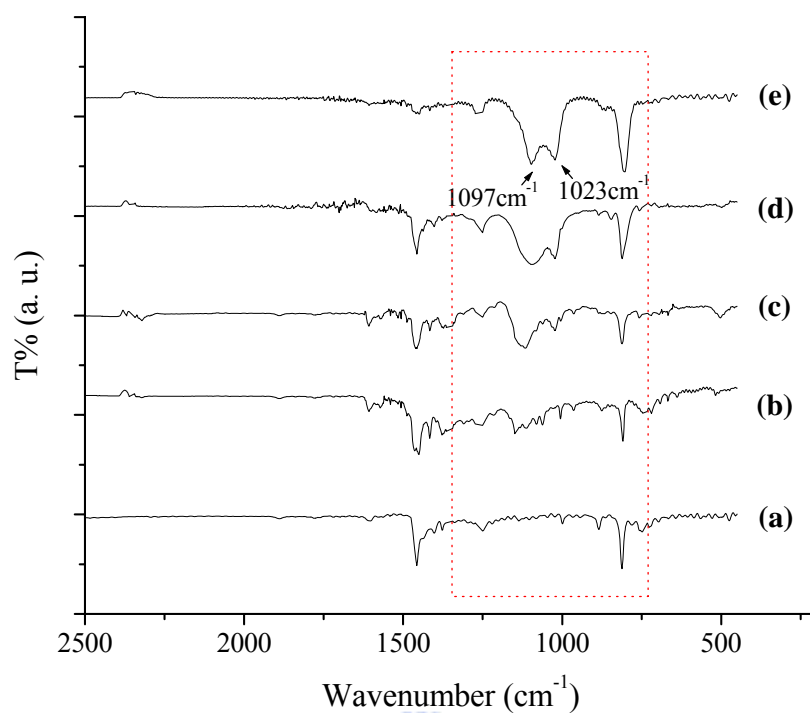


Figure 2. FTIR spectra of (a) PFO, (b) PFO-POSS-1%, (c) PFO-POSS-3%, (d) PFO-POSS-5%, and (e) PFO-POSS-10%

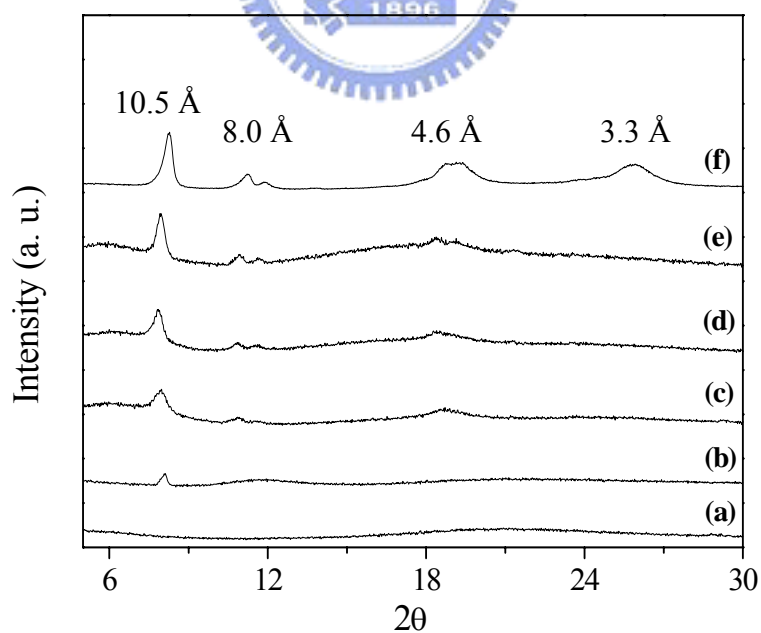


Figure 3. X-Ray diffraction curves of PFO-POSS nanocomposite

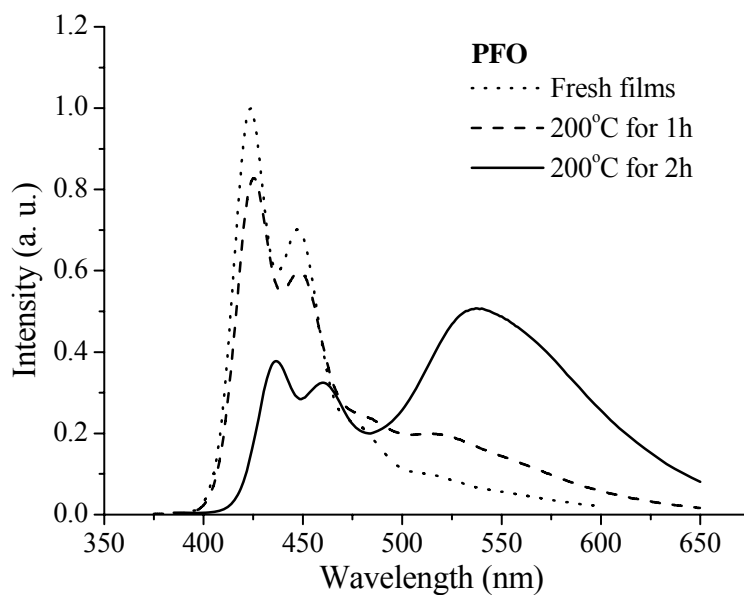


Figure 4 (a) PL spectra of PFO films before annealing (dotted line) and after annealing at 200 °C for 1 h (dashed line) and 2 h (solid line) under a nitrogen atmosphere.

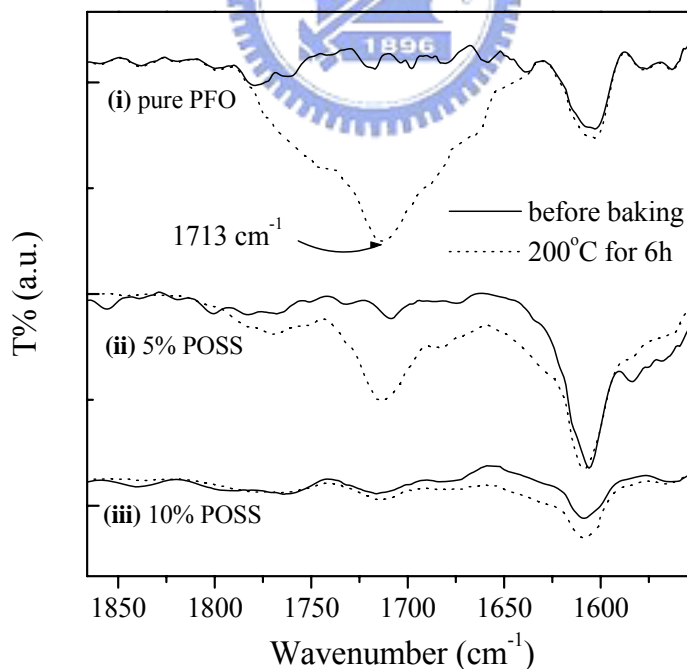


Figure 4 (b) FTIR spectra of (i) PFO, (ii) PFO-POSS-5%, and (iii) PFO-POSS-10% before (solid line) and after (dashed line) baking at 200 °C for 6 h.

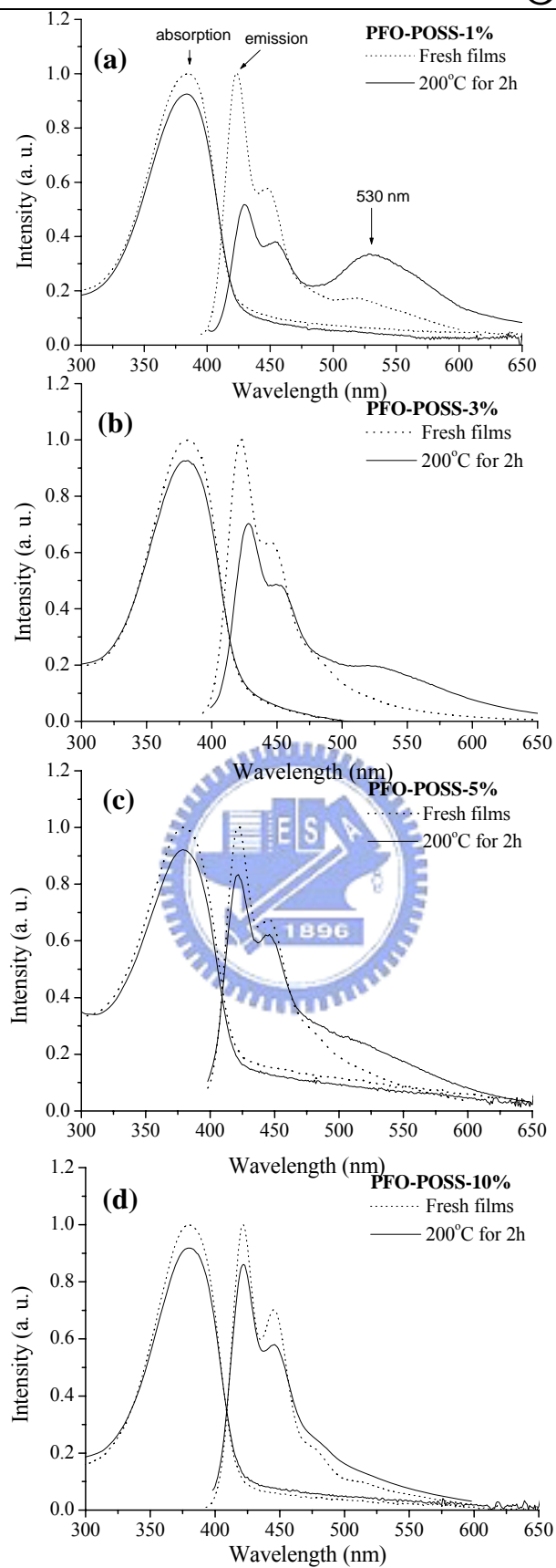


Figure 5. UV-Vis absorption and PL spectra of (a) PFO-POSS-1% , (b) PFO-POSS-3%, (c) PFO-POSS-5%, and (d) PFO-POSS-10% films before (dotted line) and after (solid line) annealing at 200 °C for 2 h under a nitrogen atmosphere.

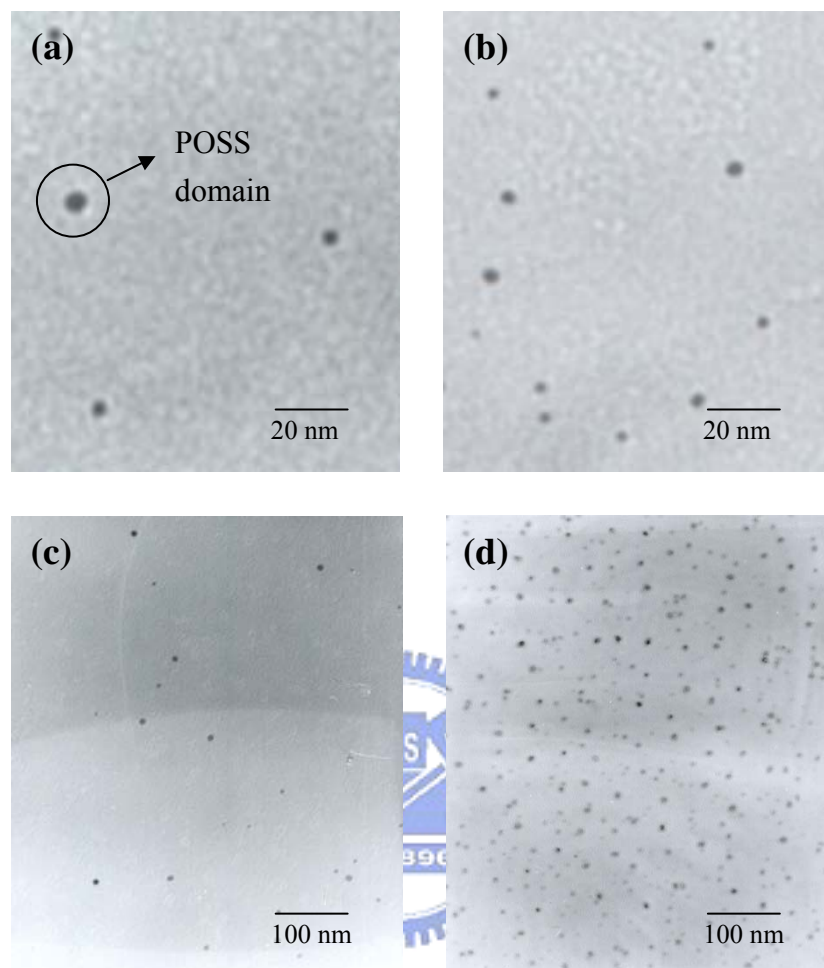


Figure 6. Transmission electron micrographs of (a) PFO-POSS-1%, (b) PFO-POSS-3%, (c) PFO-POSS-5%, and (d) PFO-POSS-10%.

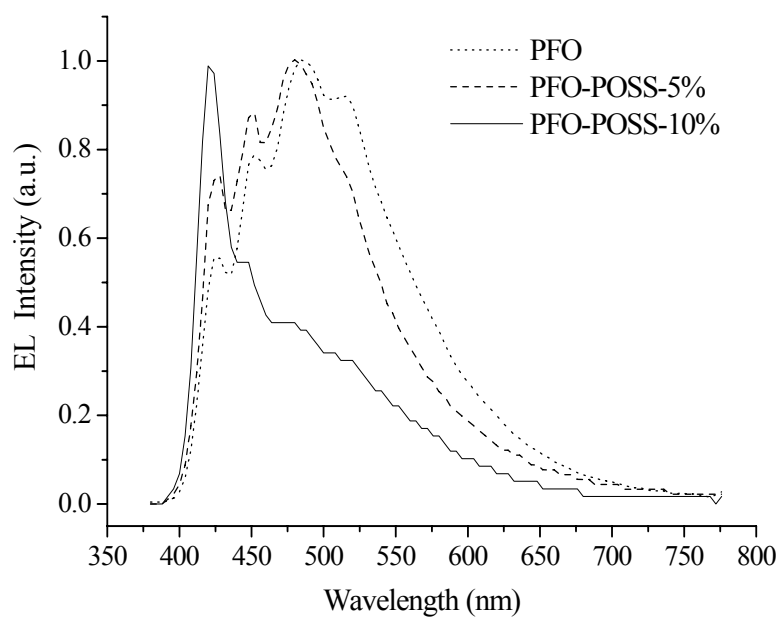


Figure 7. Electroluminescence spectra of the devices prepared from PFO-POSS and PFO in the configuration ITO/PEDOT/polymer/Ca/Al.

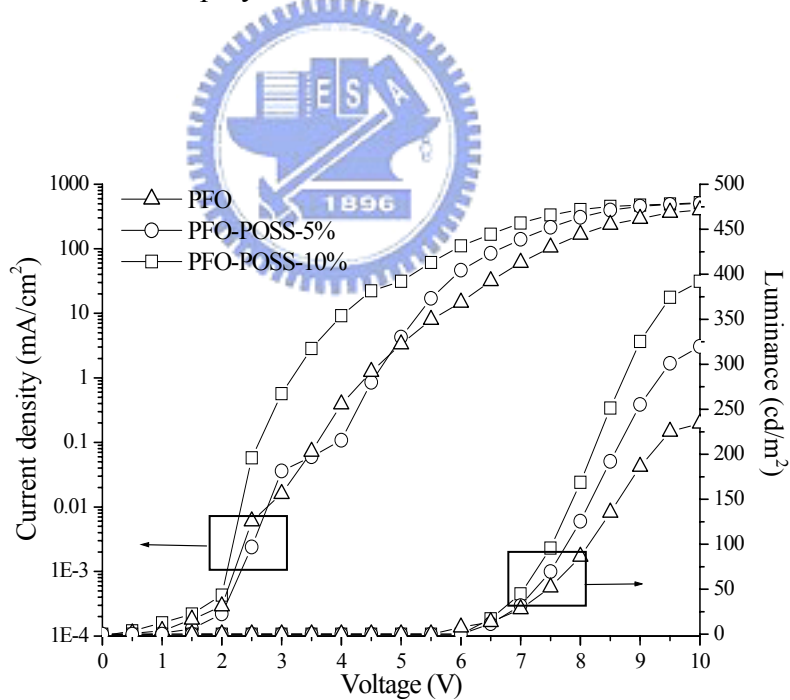


Figure 8. I–V curves of the devices prepared from PFO-POSS and PFO in the configuration ITO/PEDOT/polymer/Ca/Al.

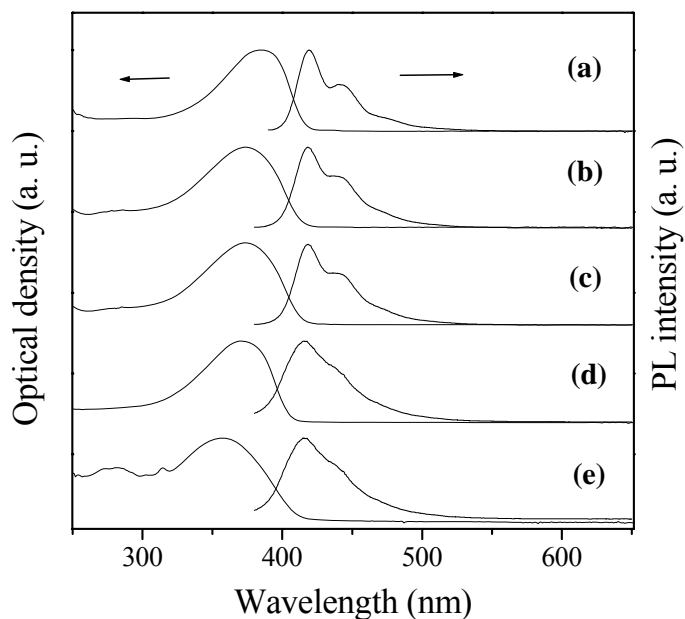


Figure 9. UV-vis absorption and Photoluminescence spectrum (excited at 380 nm) in THF of (a) PFO, (b) PFO-POSS-1%, (c) PFO-POSS-3%, (d) PFO-POSS-5%, (e) PFO-POSS-10%

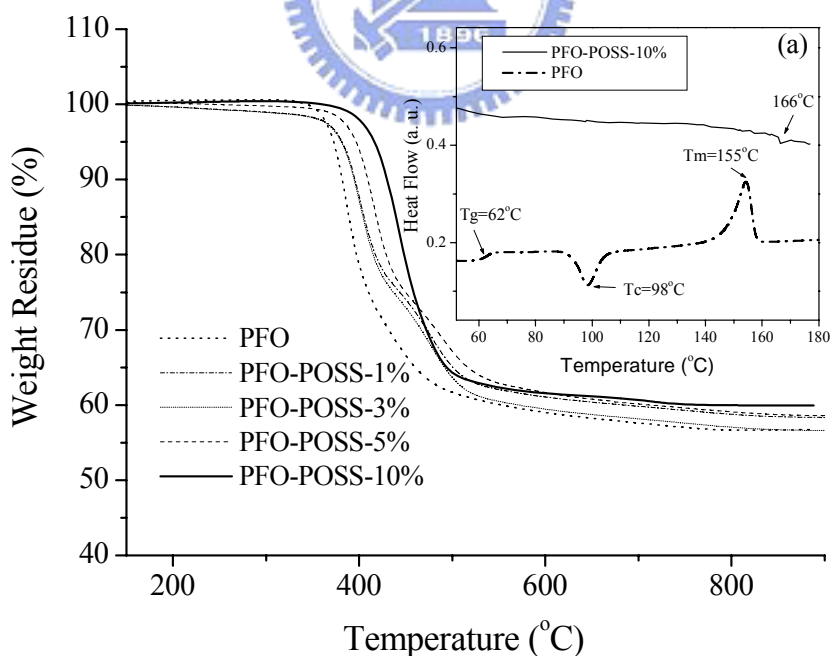


Figure 10. TGA curves of polymer at a heating rate of 20 °C/min under nitrogen atmosphere. (a) DSC curves of PFO and PFO-POSS-10% at a heating rate of 10 °C/min under nitrogen atmosphere.

Chapter 3: Enhanced Luminance and Thermal Properties of Polyphenylenevinylene Copolymer Presenting Side-Chain-Tethered Silsesquioxane Units

3-1 Introduction Materials

Emissive media based on electroluminescent (EL) polymers are currently under development for a number of display applications,^[27, 57, 58] including large-area flat-panel displays that can be driven at low voltage. Polymer light-emitting diodes (PLEDs) are very promising candidates for the development of low-cost, multicolored, large-area flat-panel displays because their molecular structures are readily modified and because they can be handled using a range of wet processing techniques.^[59-60] A number of issues remain to be resolved, however, before commercialization of these devices can occur. The formation of excimers resulting from the aggregation of their molecular chains in the solid state, and rather short operating lifetimes, owing to their low thermal stabilities. Several attempts have been made to reduce the formation of aggregates of polymer chains in the solid state. One such approach is the introduction of bulky organic units into the side chains of the polymer. This tactic has been used, for example, in the case of poly(*p*-phenylenevinylene) (PPV)-based alternating copolymers containing conjugated phenylenevinylene segments and nonconjugated spacers;^[61-63] these bulky side groups disrupt the packing of the polymer chains, which results in the formation of amorphous PPVs displaying reduced aggregation. Another approach to improving the efficiency of the devices is to blend hole-transporting and electron-transporting materials to balance the injected charges.^[64-66a] When such a device is operated for a long time, however, this method can cause some defect to occur in some cases.^[66b-d] When such a device is operated for a long time,

however, this method can cause some phase separation to occur, which is detrimental to the device's performance. Other approaches include improving the antioxidative properties of the pendant groups or chain ends^[67] and limiting chain mobility by blending^[52] with a high- T_g polymer. One approach to not only preventing polymer chains from aggregating but also to improving the antioxidative properties of their pendant groups is to use inorganic pendant groups as the side chains of the conjugated polymers.

The chemistry of polyhedral oligomeric silsesquioxane (POSS) covalently bonded to organic polymers has been developed recently. One set of members of the polyhedral oligomeric silsesquioxane family are octamers having the general formula $(\text{RSiO}_{1.5})_8$; they consist of a rigid, cubic silica core having a nanopore diameter of ca. 0.3–0.4 nm.^[23] The incorporation of $(\text{RSiO}_{1.5})_8$ into some polymers leads to an enhancement of their thermal stability and mechanical properties.^[68-69]

The first study in which POSS and conjugate polymers were combined involved tethering POSS to the chain ends of poly(2-methoxy-5-[2-ethylhexyloxy]-1,4-phenylenevinylene) (MEHPPV)^[70] and the luminescent polymer poly(9,9'-dioctylfluorene) (PFO). The enhanced electroluminescence of these nanostructured polymers was attributed to POSS imparting a reduction in the degree of either aggregation or excimer formation.^[67]

The approach of tethering POSS at the ends of a polymer's chain, however, limits the number of POSS units that can be attached. In a previous study, we synthesized a series of side-chain-tethered POSS derivatives of polyimide as a method of lowering its dielectric constant.^[71] More recently, side-chain-tethered PF-POSS copolymers have been synthesized; they display a stronger and purer blue electroluminescence.

^[71a] In this paper, we report a new series of asymmetric PPV derivatives presenting POSS units in their side chains. We synthesized these polymers using the Gilch

polymerization method. We incorporated the POSS units into the PPV to improve its thermal stability and EL characteristics. The bulky silsequioxane group was introduced at the meta position of the phenyl substituents to inhibit intermolecular interactions between the resulting polymer chains. Such meta substitution also helps to provide an amorphous state and better processibility. To the best of our knowledge, the introduction of an inorganic side group, such as POSS, into PPV-based alternating copolymers has not yet been described. We believe that developing POSS/poly(*p*-phenylene vinylene) copolymers having well-defined architectures will allow its luminescence properties to be tailored more precisely through modifications of its molecular structure.

3-2 Experimental Section

3-2-1. Materials

Chlorobenzylcyclopentyl-POSS^[70a] was synthesized according to literature procedures. THF was distilled under nitrogen from sodium benzophenone ketyl; other solvents were dried using standard procedures. All other reagents were used as received from commercial sources, unless otherwise stated.

Chlorobenzylcyclopentyl-POSS. ¹H NMR (300 MHz, CDCl₃): 7.64 (d, *J* = 8.1 Hz, 2H), 7.37 (d, *J* = 8.1 Hz, 2H), 4.57 (s, 2H), 2.26–1.21 (m, 56H), 1.16–0.81 (m, 7H) ppm. ²⁹Si NMR (600 MHz, THF): –67.8, –68.2, –79.6 ppm.

Synthesis of POSS-CH₃ (1).

2,5-Dimethylphenol (238 mg, 1.95 mmol) was stirred with K₂CO₃ (4.58 g, 33.18 mmol) and KI (1.57 g, 9.48 mmol) in DMF (30 mL) and THF (15 mL) at room temperature for 1 h. A small amount of Cl-POSS (2.0 g, 1.95 mmol) was added and

then the whole mixture was heated at 70 °C for 3 h. The reaction mixture was then slowly poured into water (300 mL) and extracted with chloroform (3 × 50 mL). The combined extracts were dried (MgSO₄), the solvents were evaporated, and the residue was purified by column chromatography (hexane/ chloroform, 1:10) to afford **1** (1.86 g, 81%). ¹H NMR (300 MHz, CDCl₃): δ 7.70 (d, *J* = 8.1 Hz, 2H), 7.51–7.31 (b, 3H), 7.03 (d, *J* = 6.9 Hz, 1H), 6.67 (s, 1H), 5.09 (s, 2H), 2.37 (s, 3H), 2.32 (s, 3H), 2.27–1.21 (m, 56H), 1.17–0.81 (m, 7H) ppm.

Synthesis of POSS-CH₂Br (**2**).

A mixture of POSS-CH₃ (**1**; 600 mg, 0.510 mmol), NBS (198.6 mg, 1.02 mmol), and AIBN (8.0 mg) was heated under reflux in carbon tetrachloride under nitrogen for 3 h. The reaction mixture was filtered to remove succinimide, the solvent was evaporated, and the residue was purified by column chromatography (hexane/chloroform, 1:10). ¹H NMR (300 MHz, CDCl₃) δ: 7.73 (d, *J* = 8.1 Hz, 2H), 7.59 (d, *J* = 6.9 Hz, 1H), 7.38 (d, *J* = 8.1 Hz, 2H), 7.09 (d, *J* = 6.9 Hz, 1H), 7.01 (s, 1H), 5.18 (s, 2H), 4.73 (s, 2H), 4.57 (s, 2H), 2.26–1.21 (m, 56H), 1.16–0.81 (m, 7H) ppm. Anal. Calcd for C₅₀H₇₆Br₂O₁₃Si₈ (%): C, 47.30; H, 6.03. Found: C, 47.18; H, 6.09.

General Procedure for the Synthesis of Copolymers POSS-PPV-*co*-MEHPPV.

A solution of potassium *tert*-butoxide (1 M in THF) was added to a solution of the monomer in dry THF, and then the mixture was stirred for 4 h. End-group capping was performed by heating the solution under reflux for 1 h in the presence of tetrabutylbenzyl bromide. Addition of the THF solution to methanol precipitated the polymer, which was collected, washed with methanol, and stirred in a mixture of methanol and water (1:1) for 1 h. The polymer was collected, washed with methanol,

filtered, and dried at 50 °C for 24 h. After cooling, the polymer was recovered by precipitating it into a mixture of methanol and acetone (4:1). The crude polymer was collected, purified twice by reprecipitation from THF into methanol, and subsequently dried under vacuum at 50 °C for 24 h. The ^1H and ^{13}C NMR spectra of MEHPPV and PPV-POSS appear to be identical because of the low content of POSS in the latter polymer.

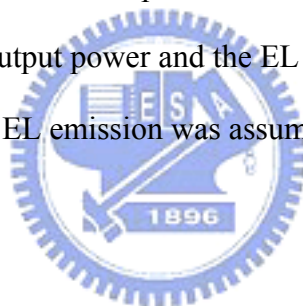
3-2-2. Characterization.

^1H , ^{13}C , and ^{29}Si nuclear magnetic resonance (NMR) spectra of the compounds were obtained using a Bruker DRX 300 MHz spectrometer. Mass spectra of the samples were obtained on a JEOL JMS-SX 102A spectrometer. Fourier transform infrared (FTIR) spectra of the synthesized materials were acquired using a Nicolet 360 FT-IR spectrometer. Gel permeation chromatographic analyses were performed on a Waters 410 Differential Refractometer and a Waters 600 controller (Waters Styragel Column). All GPC analyses of polymers in THF solutions were performed at a flow rate of 1 mL/min at 40 °C; the samples were calibrated using polystyrene standards. Thermogravimetric analysis (TGA) and differential scanning calorimetry (DSC) measurements were performed under a nitrogen atmosphere at heating rates of 20 and 10 °C/min, respectively, using Du Pont TGA-2950 and TA-2000 instruments, respectively. UV–Vis absorption and photoluminescence (PL) spectra were recorded on a HP 8453 spectrophotometer and a Hitachi F-4500 luminescence spectrometer, respectively. Before investigating the thermal stability of the synthesized polymers, their polymer films were annealed in air at 200 °C for 2 h.

3-2-3. Device Fabrication and Testing.

The electroluminescent (EL) devices were fabricated on an ITO-coated glass

substrate that was precleaned and then treated with oxygen plasma before use. A layer of poly(ethylene dioxythiophene):poly(styrene sulfonate) (PEDOT:PSS, Baytron P from Bayer Co.; ca. 40-nm thick) was formed by spin-coating it from an aqueous solution (1.3 wt%). The EL layer was spin-coated, at 1500 rpm from the corresponding toluene solution (15 mg mL^{-1}), on top of the vacuum-dried PEDOT:PSS layer. The nominal thickness of the EL layer was 65 nm. Using a base pressure below 1×10^{-6} Torr, a layer of Ca (35 nm) was vacuum deposited as the cathode and a thick layer of Al was deposited subsequently as the protecting layer. The current–voltage characteristics were measured using a Hewlett–Packard 4155B semiconductor parameter analyzer. The power of the EL emission was measured using a Newport 2835-C multi-function optical meter. The brightness was calculated using the forward output power and the EL spectra of the devices; a Lambertian distribution of the EL emission was assumed.



3-3 Results and Discussion

A. Polyphenylenevinylene Copolymer Presenting Side-Chain-Tethered Silsesquioxane Units Nanocomposites

Figure 1 displays the ^1H NMR spectra of Cl-POSS, POSS- CH_3 (1), and POSS- CH_2Br (2). The CH_2 peak of Cl-POSS (4.47 ppm) shifted downfield to 5.14 ppm in POSS- CH_3 . The ratio of the peak areas of the benzylic CH_2 and CH_2Br protons is ca. 1:2. Taken together, these data suggest that Cl-POSS had reacted with 2,5-dimethylphenol to form POSS- CH_3 . Table 1 lists the thermal properties and molecular weight distributions of the POSS-PPV-*co*-MEHPPV copolymers. Both the thermal degradation and glass transition temperatures increased substantially as the amount of POSS in MEHPPV increased, particularly for the case where 10 mol% POSS was tethered to MEHPPV: we observed an 83 °C increase in the value of T_d

and a disappearance of any glass transition.^[72] This situation arose because the tethered bulky POSS enhanced the thermal stability and retarded the mobility of the polymer main chain. The molecular weights of the POSS-PPV-*co*-MEHPPV copolymers decreased upon increasing the POSS content; this phenomenon can be attributed to the steric hindrance caused by the POSS units during the polymerization process. Figure 2 displays FTIR spectra of MEHPPV copolymers containing different amounts of POSS. The FTIR spectrum of POSS displays two major characteristic peaks: the Si-C band at 1038 cm⁻¹ and the Si-O-Si band at 1123 cm⁻¹.

Table 2 lists the wavelengths of the absorption, the location of the PL maxima, and the quantum yields of POSS-PPV-*co*-MEHPPV. The absorption and emission peak maxima of MEHPPV occurred at 499 and 553 nm, respectively; these values are close to those reported in the literature.^[70] We observed no aggregation band in these spectra because THF is a good solvent for MEHPPV. The absorption and emission peaks for MEHPPV and POSS-PPV-*co*-MEHPPV are almost identical. For each polymer, the absorption peak maximum in solution (THF) is located between 499 and 494 nm, with a slight blue shift caused by the presence of POSS; the PL maxima occur at similar wavelengths for all of the polymers. Figure 3A presents the normalized absorption and PL emission spectra of the MEHPPV-POSS copolymer films. The quantum yields of the POSS-PPV-*co*-MEHPPV copolymers increased substantially as the amount of tethered POSS increased.^[80] In particular, the quantum yield of MEHPPV containing 10% POSS was four times higher than that of pure MEHPPV (0.87 vs. 0.19). We attribute this finding to the steric hindrance caused by the POSS units in preventing aggregation of the PPV main chains, which, in turn, reduces the degree of dimer formation after excitation. This improved quantum yield, which has not been reported in any previous studies of POSS/PPV

copolymers, is a direct result of employing this particular side-chain-tethered POSS architecture.

For fresh MEH-PPV film, the yellowish peak at ~590 nm originates from single chain exciton emissions,^[76] whereas the reddish peak at 630 nm is related to emissions from interchain species, such as aggregates or excimers.^[76a] The difference in the PL spectra of the fresh MEH-PPV and POSSPPV-*co*-MEHPPV film is small because both polymer chains have not reached equilibrium states by their preparation process (i.e. spin-coating). By annealing the polymer films at higher temperatures as in the work by Schwartz^[77] and Yang Yang^[78] et al., one could see some more profound changes in their PL spectra. For instance, Figure 3B shows that after annealing MEHPPV film at 150°C for 2 h under air, its PL spectrum displays a red-shifted broad main peak at 630 nm, indicating formation of aggregates. While the main emission peak for annealed POSS-PPV10-*co*-MEHPPV film remain near 590 nm, with a weak peak at 630 nm. Therefore, at the equilibrium states, there is a distinct difference in their PL spectra, due to the bulky and rigid POSS groups tethered to the side of MEHPPV chains. The same phenomena are also observed in EL spectra (Figure 5).

We have carried out by X-ray diffraction for confirming that interchain distance of PPV was increased by side-chain-tethered POSS. Figure 3C displays the X-ray diffraction curves of Cl-POSS, MEHPPV, and PPV-POSS. There are three distinct diffraction peaks at $2\theta = 8.3, 19.1, \text{ and } 26.1^\circ$ for Cl-POSS (Fig. 3f), which correspond to *d*-spacings of 10.5, 4.6 and 3.3 Å, respectively. The *d*-spacing of 10.5 Å reflects the size of the Cl-POSS molecules; the other two spacings are owing to the rhombohedral crystal structure of POSS molecules.^[79] For pure MEHPPV and

PPV-POSS copolymers, it is evident that they are amorphous and have no side chain alignment. The nearly amorphous structure of pure MEHPPV (Figure 3C-a) originates from the two highly asymmetric substituents, the methoxy and 2-methoxy 5-(2'-ethoxyhexyloxy) for MEH-PPV.^[79] When POSS molecules were tethered to PPV, the average interchain distance increased appreciably from X-ray diffraction results. For instance, in the presence of 10% POSS (PPV-POSS-10%), the inter-chain distance increases to 4.6 Å (19.5°) from 4.0 Å (22.0°) for MEHPPV after deconvolution of the X-ray diffraction curve.

Figure 4A presents a transmission electron microscopy (TEM) image of our POSS-PPV10-*co*-MEHPPV sample.^[81] This image reveals that no large aggregates were formed, but small domains of POSS are present; these POSS domains are dispersed evenly in the polymer matrix—a situation that we confirmed by analyzing this sample's energy dispersive spectrum (EDS; Figure 4A-(c)). The topology of POSS-PPV-*co*-MEHPPV copolymers films were studied with atomic force microscopy (AFM). Figure 4B shows the height image and the phase image of MEH-PPV and POSS-PPV10-*co*-MEHPPV polymer films prepared with chlorobenzene as the solvent. The surface roughness of PPV-POSS film is larger than that of pure MEHPPV (0.496 nm vs. 0.206 nm) due to the presence of POSS. The phase images also show that POSS groups are dispersed homogeneously in the whole system.

B. Electroluminescence (EL) Characteristics

Figure 5 displays the electroluminescence (EL) spectra of POSS-PPV-*co*-MEHPPV devices. The EL device prepared from MEHPPV emits a strong peak at 590 nm and a vibronic signal in the range 610–620 nm, which is due presumably to the aggregation of MEHPPV and its excimer formation, as discussed

earlier. The introduction of bulky siloxane units into the PPV side chains presumably increases the interchain distance, thereby retarding interchain interactions and leading to a reduction in the degree of exciton migration to defect sites.^[62]

Figure 6 displays the variations in the current density and brightness of the EL devices.

The turn-on voltage decreased to 2.5 V for PPV containing 10% POSS from 3.5 V for the pure-MEHPPV EL device. As indicated in Figure 6, a more than four-fold

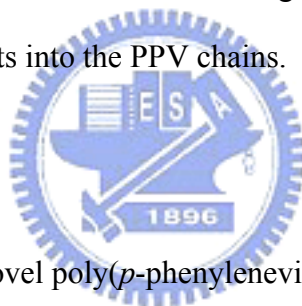
increase occurred in the maximum brightness of the

POSS-PPV10-*co*-MEHPPV-based device relative to that of the pure-MEHPPV EL

device (2196 vs. 473 cd/m²) at a drive voltage of 9.5 V. The efficiency of

POSS-PPV10-*co*-MEHPPV is 1.83 cd/A at a current density of 1221 A/m².

These improvements might be due to a decreased degree of aggregation upon the incorporation of the POSS units into the PPV chains.



3-4 Conclusions

We have synthesized a novel poly(*p*-phenylenevinylene) side-chain-tethered polyhedral silsesquioxane (POSS-PPV-*co*-MEHPPV) that possesses a well-defined architecture. This particular molecular architecture of PPV-POSS increases the quantum yield of MEHPPV significantly by reducing the degree of interchain aggregation; it also results in a much brighter red light from the EL device by decreasing the degree of aggregation between the polymer chains.

Table 1. Physical Properties of the POSS-PPV-*co*-MEHPPV Copolymers.

	T_g (°C)	T_d^a (°C)	M_n	M_w	PDI	Yield (%)
MEHPPV	71	370	61,000	111,000	1.82	78
POSS-PPV1-<i>co</i>-MEHPPV	90	381	55,000	107,000	1.95	66
POSS-PPV3-<i>co</i>-MEHPPV	96	395	52,000	98,000	1.88	64
POSS-PPV5-<i>co</i>-MEHPPV	*	417	48,000	91,000	1.90	69
POSS-PPV10-<i>co</i>-MEHPPV	*	453	39,000	73,000	1.87	60

^a Temperature at which 5% weight loss occurred, based on the initial weight.

* The glass transition disappeared because of the steric hindrance imposed on the main molecular chains by the POSS units.

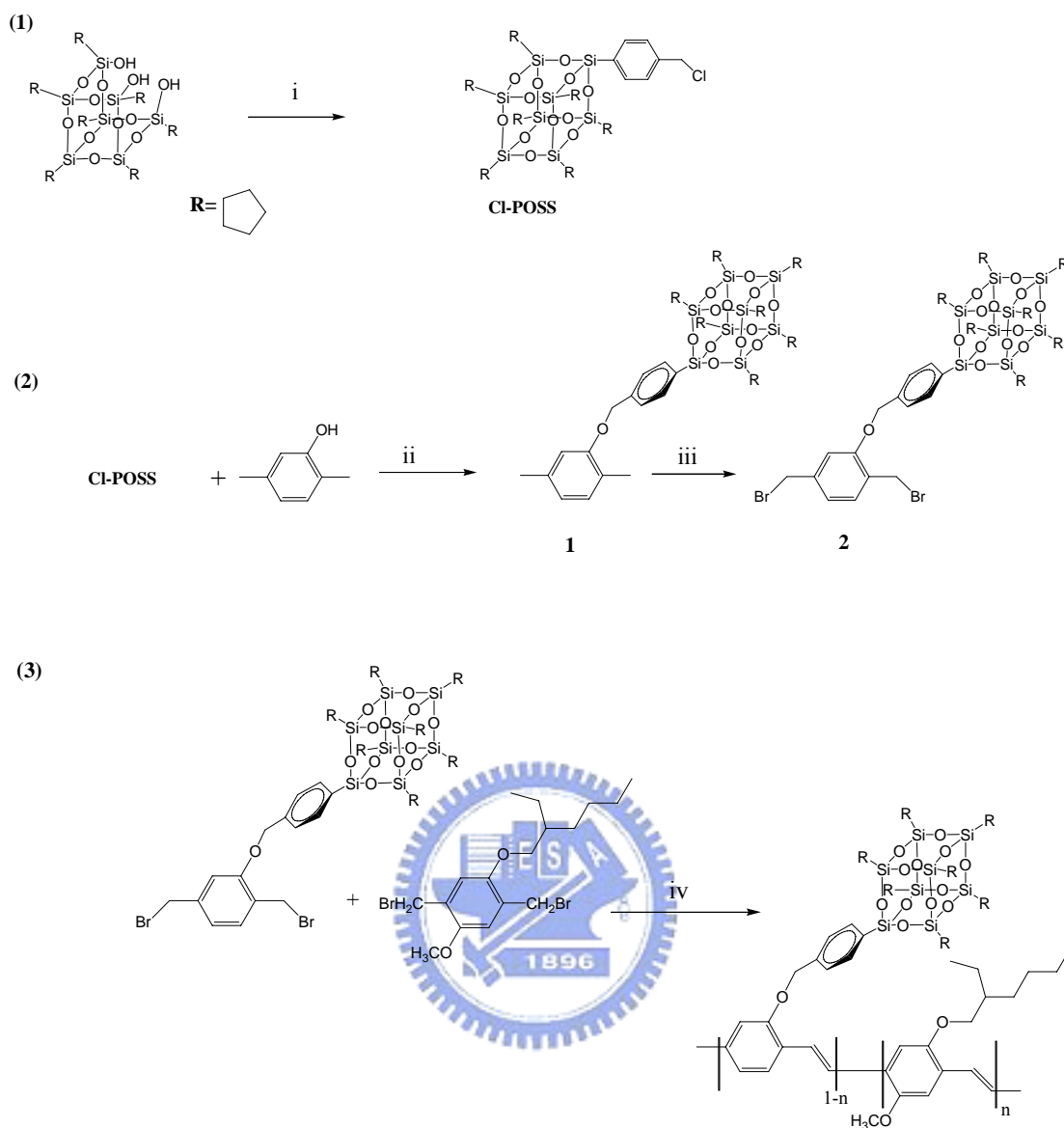
Table 2. Optical Properties of the POSS-PPV-*co*-MEHPPV Nanocomposites.

	λ_{\max} (UV, nm)		λ_{\max} (PL, nm) ^a		QY
	solution ^b	film	solution ^b	film	
MEHPPV	499	517	553 (592)	591 (634)	0.19
POSS-PPV1-<i>co</i>-MEHPPV	499	512	552 (591)	588 (633)	0.43
POSS-PPV3-<i>co</i>-MEHPPV	498	512	552 (591)	586 (632)	0.62
POSS-PPV5-<i>co</i>-MEHPPV	497	511	552 (591)	585 (631)	0.84
POSS-PPV10-<i>co</i>-MEHPPV	494	505	551 (590)	584 (631)	0.87

^a The data in parentheses are the wavelengths of the shoulders and subpeaks.

^b The absorption and emission were measured in THF.

^c PL quantum yield estimated relative to a sample of Rhodamine 6G ($\Phi_f = 0.95$)^[73-75].



Scheme 1^a. Synthesis of POSS-PPV-*co*-MEHPPV copolymers.

^a Reagents and conditions: i, trichloro[4-(chloromethyl)phenyl]silane, HNEt₃Cl; ii, K₂CO₃, DMF/THF; iii, *N*-bromosuccinimide (NBS)/ AIBN/ CCl₄; iv, *tert*-BuOK/ THF.

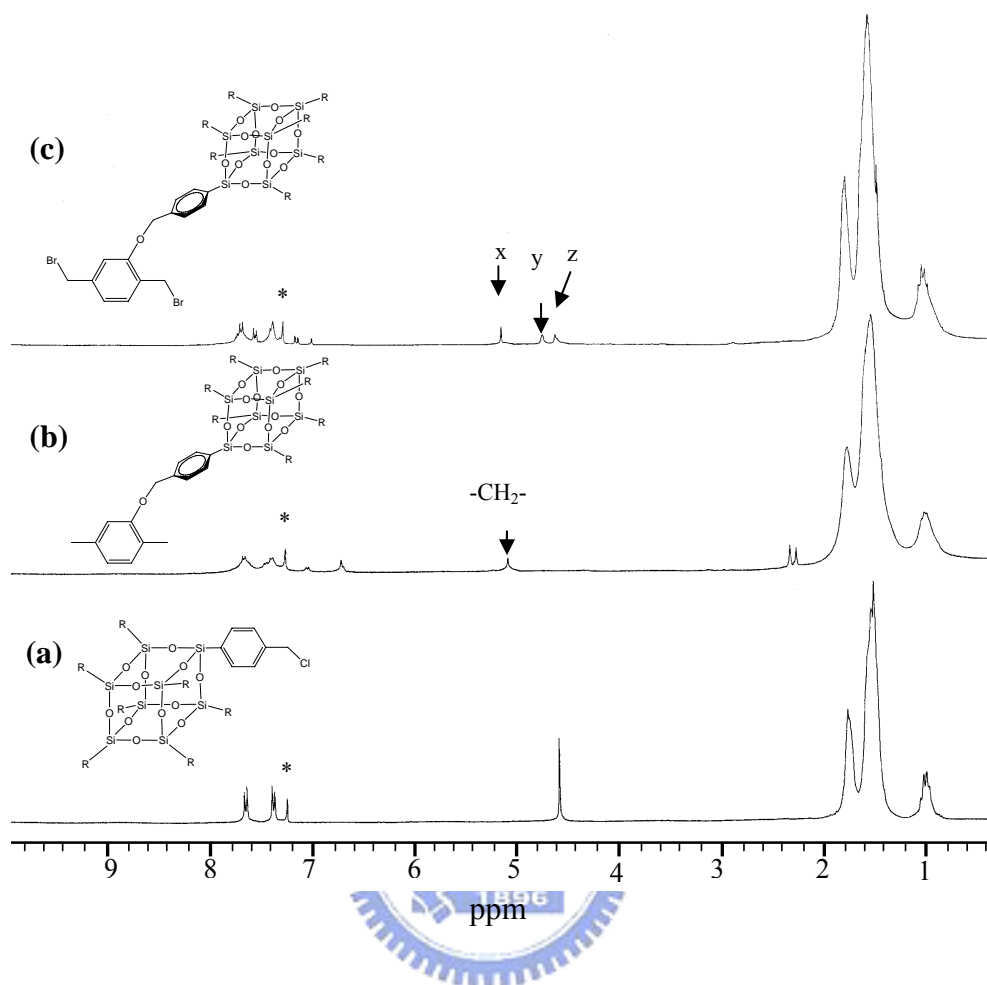


Figure 1 ^1H NMR spectra of (a) Cl-POSS, (b) POSS-CH₃, and (c) POSS-CH₂Br.

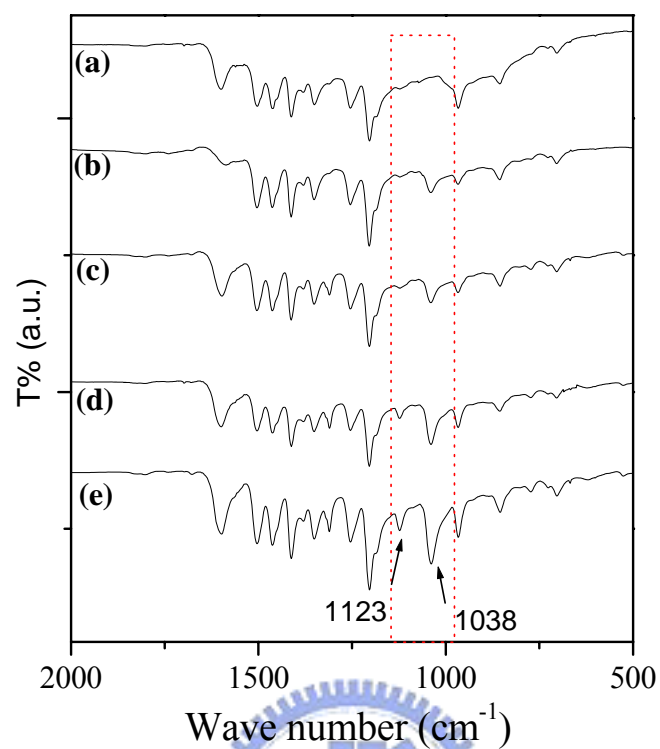


Figure 2 FTIR spectra of (a) MEHPPV, (b) POSS-PPV1-*co*-MEHPPV, (c) POSS-PPV3-*co*-MEHPPV, (d) POSS-PPV5-*co*-MEHPPV, and (e) POSS-PPV10-*co*-MEHPPV.

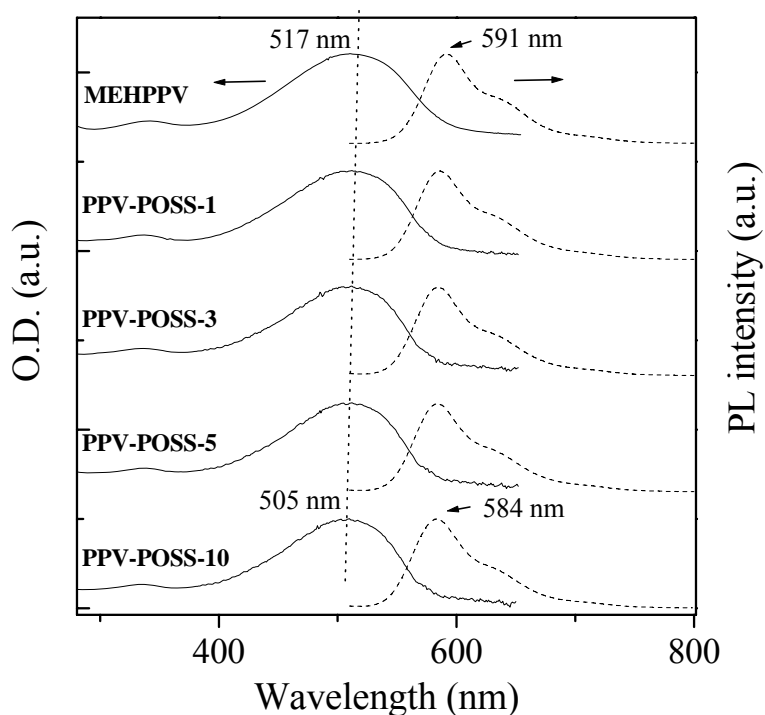


Figure 3A. UV-Vis absorption and PL spectra of (a) MEHPPV, (b) POSS-PPV1-*co*-MEHPPV, (c) POSS-PPV3-*co*-MEHPPV, (d) POSS-PPV5-*co*-MEHPPV, and (e) POSS-PPV10-*co*-MEHPPV recorded in the solid state.

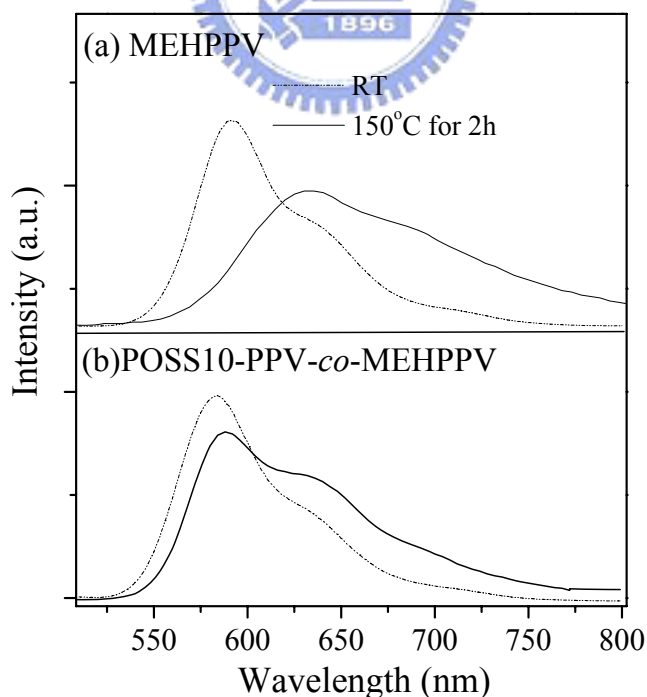


Figure 3B. Normalized (relative to their maximum wavelengths) PL spectra of (a) MEHPPV and (b) POSS-PPV10-*co*-MEHPPV annealed at room temperature and 150°C in the solid state.

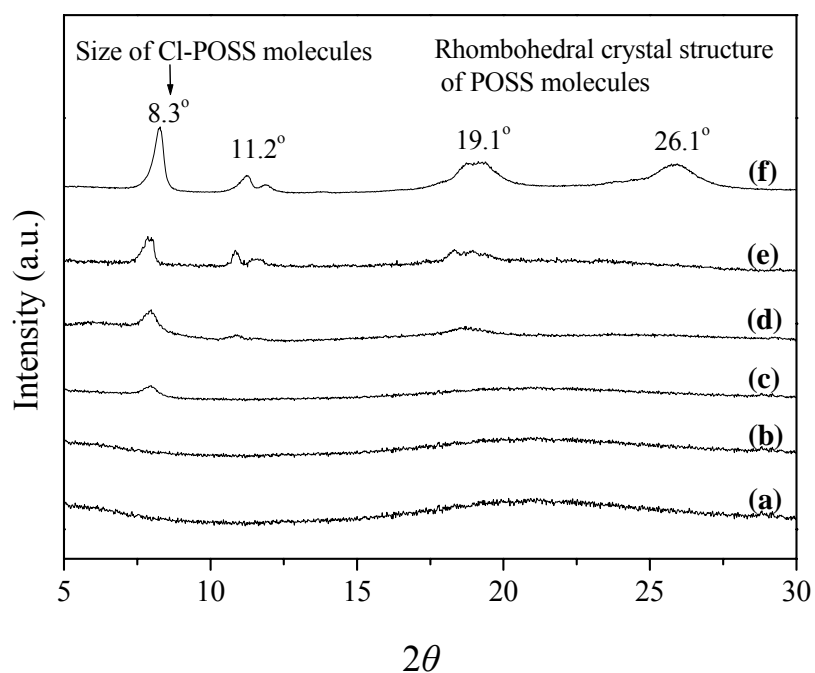


Figure 3C. X-ray diffraction spectra of (a) MEHPPV, (b) POSS-PPV1-*co*-MEHPPV, (c) POSS-PPV3-*co*-MEHPPV, (d) POSS-PPV5-*co*-MEHPPV, (e) POSS-PPV10-*co*-MEHPPV, and (f) Cl-POSS.

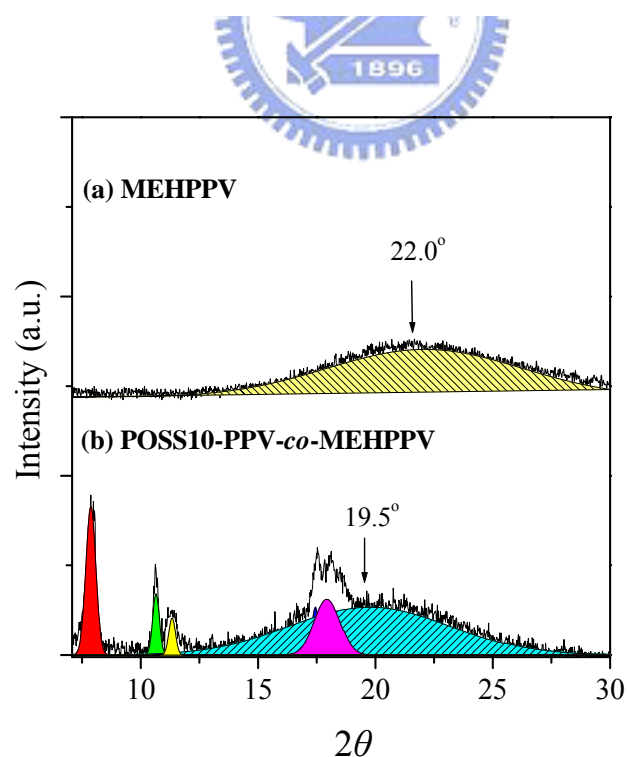


Figure 3D. Deconvoluted X-ray diffraction spectra of (a) MEHPPV and (b) POSS-PPV10-*co*-MEHPPV.

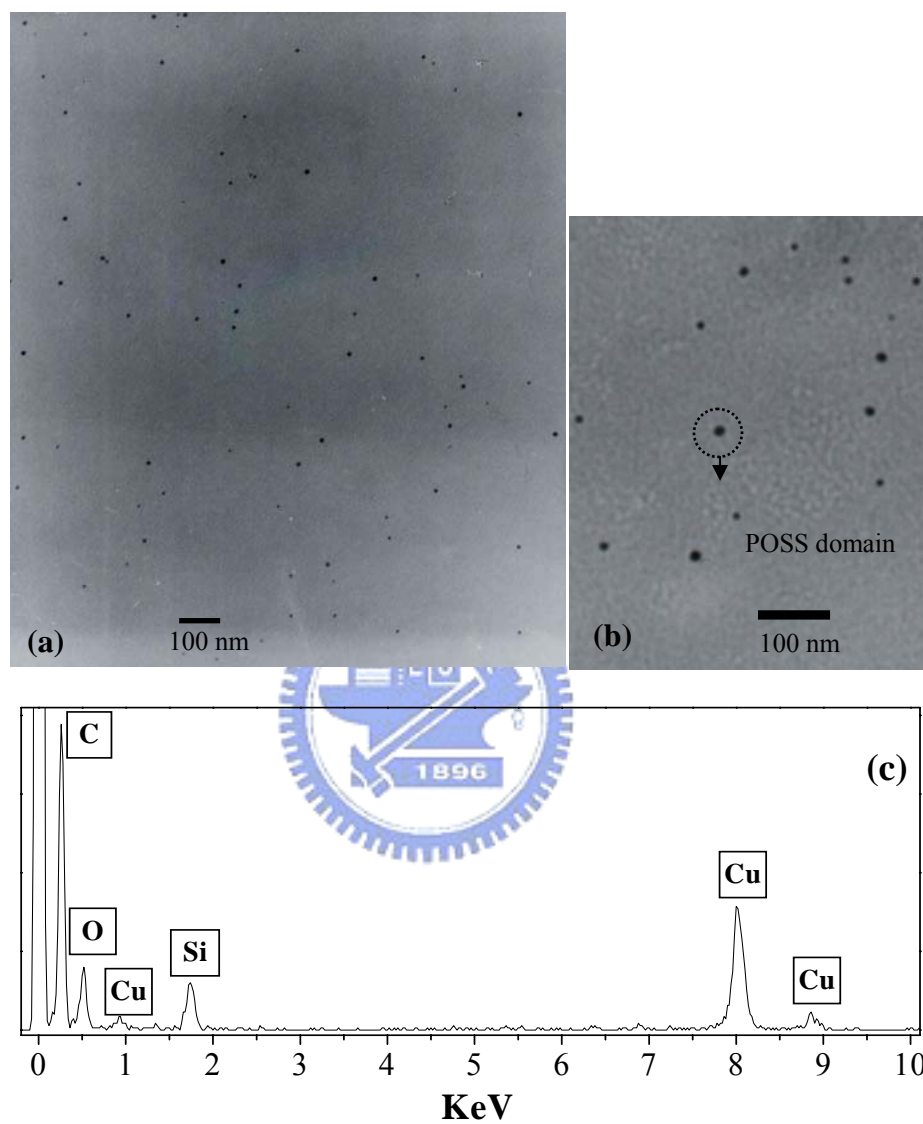


Figure 4A. (a) Transmission electron micrograph of POSS-PPV10-*co*-MEHPPV. (b) enlarged view. (c) EDS of POSS-PPV10-*co*-MEHPPV.

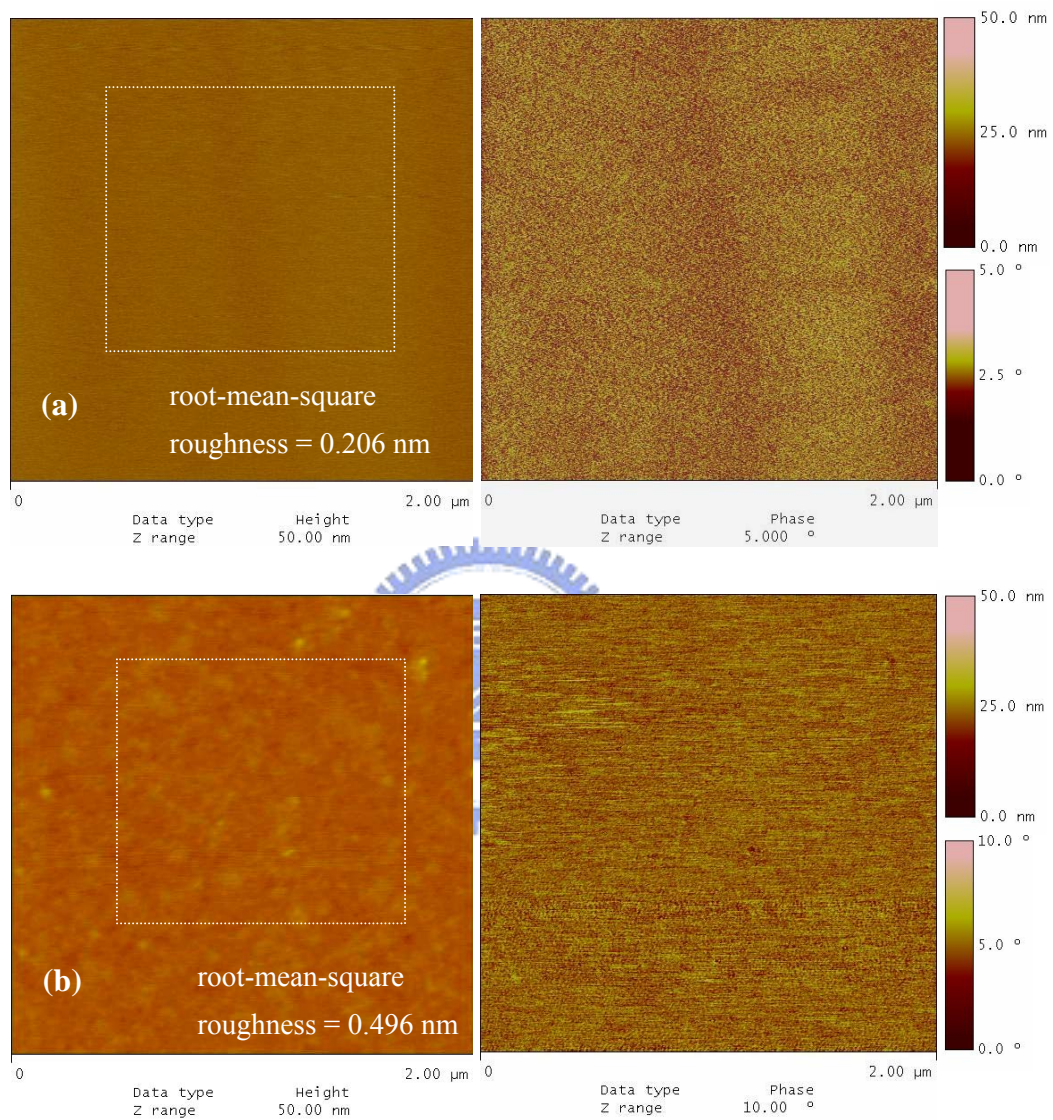


Figure 4B. Surface roughness of thin films of (a) MEHPPV. (b) POSS-PPV10-*co*-MEHPPV.

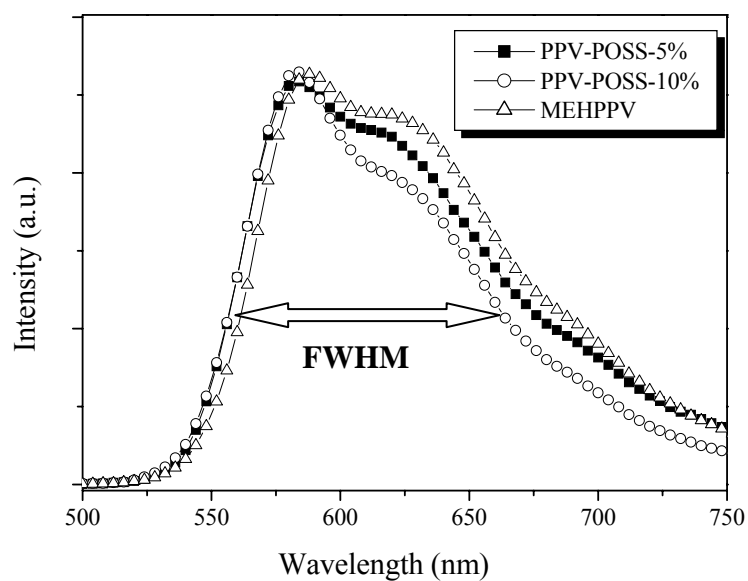


Figure 5. Electroluminescence spectra of the devices prepared from POSS-PPV-co-MEHPPV in the configuration ITO/PEDOT/polymer/Ca/Al.

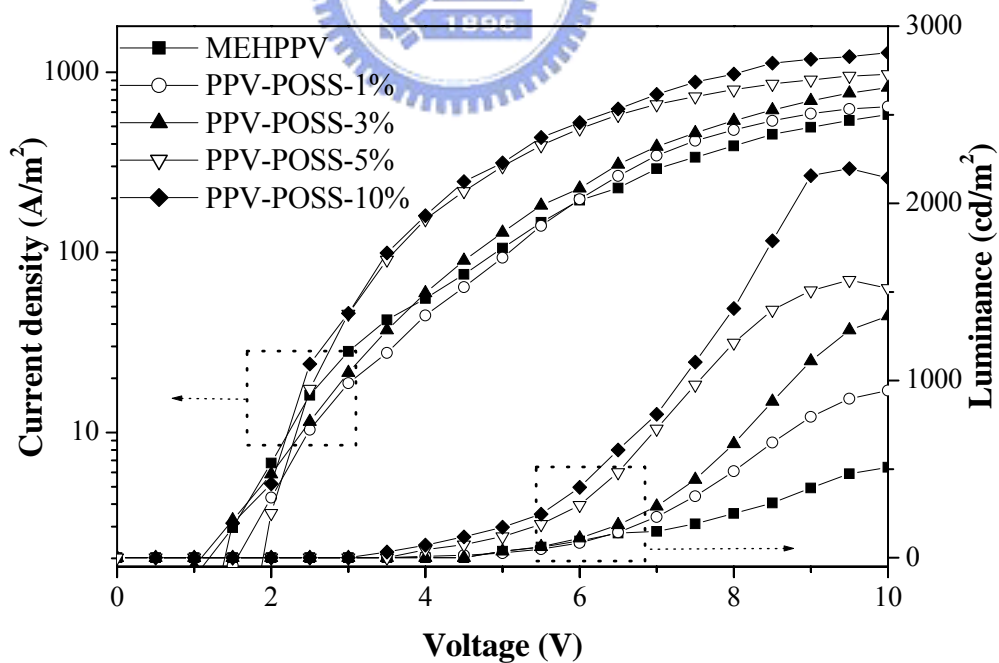


Figure 6. I-L-V curves of the devices prepared from POSS-PPV-co-MEHPPV and MEHPPV in the configuration ITO/PEDOT/polymer/Ca/Al.

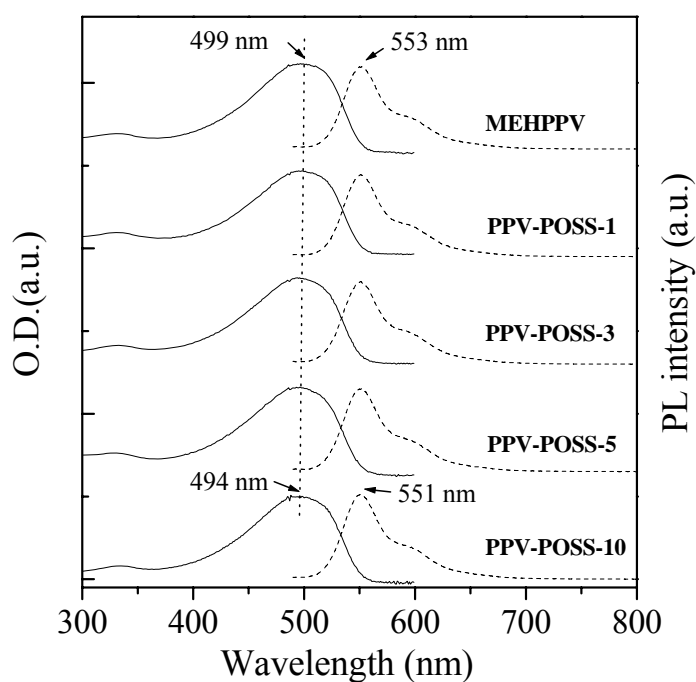


Figure 7. UV-Vis absorption and PL spectra of (a) MEHPPV, (b) POSS-PPV1-*co*- MEHPPV, (c) POSS-PPV3-*co*-MEHPPV, (d) POSS-PPV5-*co*-MEHPPV, and (e) POSS-PPV10-*co*-MEHPPV recorded in THF solution.

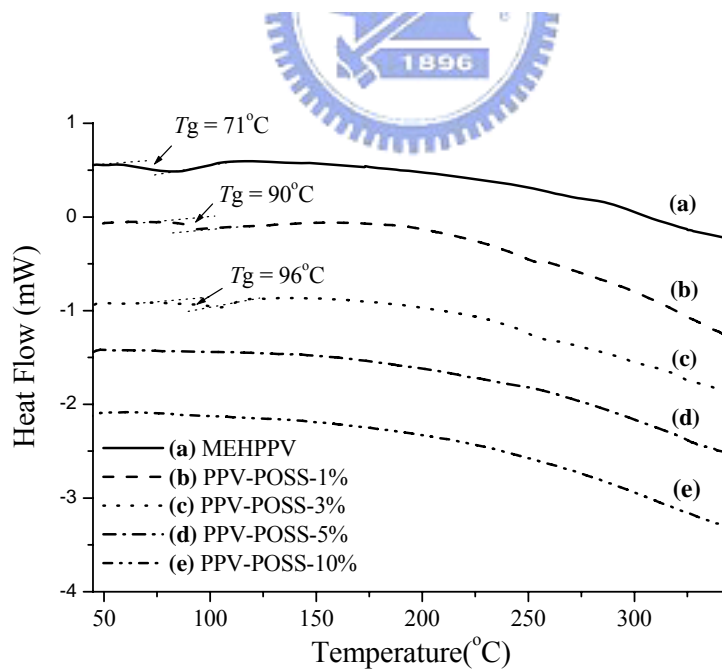


Figure 8. DSC traces of (a) MEHPPV, (b) POSS-PPV1-*co*-MEHPPV, (c) POSS-PPV3-*co*-MEHPPV, (d) POSS-PPV5-*co*-MEHPPV, and (e) POSS-PPV10-*co*-MEHPPV.

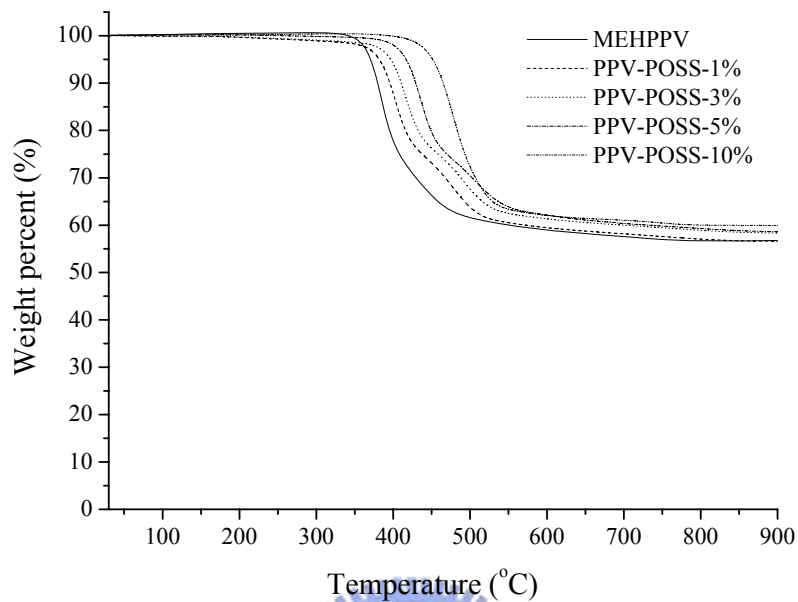


Figure 9. TGA traces of (a) MEHPPV, (b) POSS-PPV1-*co*-MEHPPV, (c) POSS-PPV3-*co*-MEHPPV, (d) POSS-PPV5-*co*-MEHPPV, and (e) POSS-PPV10-*co*-MEHPPV.

Chapter 4: Thiophenol-modified CdS nanoparticles enhance the luminescence of benzoxyl dendron-substituted polyfluorene copolymers

4-1 Introduction

Conjugated aromatic polymers have attracted a considerable amount of interest over the past few decades because their semiconducting and electroactive properties allow them to be used in a diverse range of applications, such as in batteries, electronic devices, and light-emitting diodes. In particular, the development of blue light-emitting polymers remains critical to the fabrication of full-color organic displays. Polyfluorene^[82–84] layers have emerged as potential sources of blue light for light-emitting diodes because of their relatively high photoluminescence efficiencies.^[85] Indeed, their photo- and thermostabilities are better than those of poly(phenylene vinylene) derivatives.^[86–90] Although these polymers exhibit relatively high photoluminescence quantum efficiencies and good thermal stabilities, their device applications are hampered by their tendency to form aggregates in the solid state. Moreover, most organic chromophores, such as those in polymers, quench to different degrees at various concentrations in the solid state, and this phenomenon leads to broad emission bands and losses in efficiency and purity of color. Attempts at improving the luminescence efficiency of polymers have followed two approaches: steric hindrance approach and the electronic approach. The steric hindrance approach involves altering the interchain distance between polymers by attaching bulky side groups—e.g., dendritic structures—to the main chain of the polymer; such modifications prevent aggregate formation or concentration quenching. The luminescence efficiencies in these copolymers have been improved in several cases, but this phenomenon occurs in conjunction with a

decrease in the molecular weight of the polymers, owing to synthetic yield constraints. The electronic approach involves combining materials having higher quantum yields into luminescent polymers.^[91] For example, one method combines conjugated organic polymers with wide-band-gap semiconductor nanoparticles.^[91] Several reports have described^[92–96] the energy levels and electron transport properties of these polymer–nanoparticle nanocomposites; complex phenomena can appear as a result of the sensitivity of the surface ligands and the sizes of the band gaps in the nanoparticles. For instance, the photoluminescence of poly[2-methoxy-5-(ethylhexyloxy)-1,4-phenylene vinylene] (MEH-PPV) can be quenched when nanoparticles are present at a higher concentration, or energy can be transferred from the polymer to the nanoparticles.^[97–99] To the best of our knowledge, however, no one has reported that polymer luminance can be improved by the presence of CdS nanoparticles—possibly because the interactions between these nanoparticles and the polymer segments had not been designed properly or because high concentrations of nanoparticles in a polymer can lead to quenching effects caused by offset band edges between the polymer and the nanoparticles.

In this paper, we propose a new approach to improving polymer luminescence by attaching dendritic structures to polyfluorene (dendritic copolyfluorene) and then incorporating a low percentage of surface-modified semiconductor nanoparticles into the polymer.^[100–101] Dendritic copolyfluorene^[102] contains multiple functional groups that increase both the solubility of the polymer and the number of its interaction sites. By tailoring the interface between the ligands on the nanoparticles and the dendritic structures, a small percentage of the surface-modified cadmium sulfide nanoparticles can be incorporated into the polymer. We have investigated the effect that the addition of these nanoparticle has on the polymer’s photoluminescence (PL) and electroluminescence (EL) efficiencies.

4-2 Experimental

4-2-1. Materials

Surface-modified CdS nanoparticles were synthesized by reacting cadmium acetate dihydrate [$\text{Cd}(\text{OAc})_2 \cdot 2\text{H}_2\text{O}$], sodium sulfide (Na_2S), and thiophenol (HSC_6H_5) in methanol at room temperature, using a variation of the kinetic trapping method.

^[106–107] The diameters of the synthesized CdS can be adjusted by changing the ratio of the three ingredients. These CdS nanoparticles are termed “S-CdS” nanoparticles, indicating that the surface ligands on the CdS nanoparticles are thiophenol units.

After filtration, the S-CdS nanoparticles were collected and then dispersed in DMF.

From the absorption edge (λ_e) in their UV–Vis spectra, the S-CdS nanoparticles were determined to have diameters of ca. 3, 4, and 7 nm. ^[108–109]

The synthesis of the dendritic polyfluorene was performed using a typical Suzuki coupling reaction protocol. The copolymerization of dendritic monomers and 2,7-bis(4,4,5,5-tetramethyl-1,3,2-dioxaborolan-2-yl)-9,9-dioctylfluorene was performed using $\text{Pd}(\text{PPh}_3)_4$ as a catalyst and Aliquat 336 as a phase-transfer reagent in a mixture of toluene and aqueous potassium carbonate (2.0 M). A detailed description of the synthesis of these dendritic copolyfluorenes is available to elsewhere. ^[102, 8] The copolymers were named PF-GX, where X represents the number of generations of the dendron ($X = 0, 1, \text{ or } 2$). S-CdS/DMF was added to a previously prepared dendritic copolyfluorene PF-GX ($X = 0, 1, 2$) in DMF solution and stirred overnight. PF-G1, the polyfluorene possessing one dendron generation, had a weight-average molecular weight (M_w) of 65 kDa and a polydispersity of 1.9; PF-G2, the polyfluorene having two dendron generations, had a M_w of 40 kDa and a polydispersity of 2.2. The mixture of S-CdS/PF-GX in DMF was dried under vacuum at 313 K for 2 h and then maintained at 383 K for another 24 h to obtain the

S-CdS/PF-GX nanocomposite film. Scheme 1 outlines the synthesis of the nanocomposites formed from the thiophenol-modified CdS nanoparticles and the dendritic copolyfluorenes.

4-3 Results and Discussion

4-3-1. Polyfluorene Side-Chain-Tethered CdS Nanoparticles

Figure 1 displays the UV–Vis absorption spectra of three differently sized thiophenol-modified CdS (S-CdS) nanoparticles in DMF. The sharp absorption peak at $\lambda = 269$ nm is due to the benzene ring in the thiophenol and the broad absorption peaks at $\lambda = 360, 410,$ and 460 nm arise from CdS nanoparticles having diameters of 3, 4, and 7 nm, respectively. The maximum photoluminescence peaks of the S-CdS_{3nm}, S-CdS_{4nm}, and S-CdS_{7nm} nanoparticles in DMF (Figure 2b) occurred at 546, 590, and 655 nm, respectively, when these solutions were excited separately with light at $\lambda_{\text{exe}} = 360, 410,$ and 460 nm, respectively. The small peaks at $\lambda = 480, 519,$ and 604 nm, for S-CdS_{3nm}, S-CdS_{4nm}, and S-CdS_{7nm}, respectively, originate from defects on the surfaces of the CdS nanoparticles.

Figure 2 presents the photoluminescence spectra of PF, PF-G0, PF-G1, and PF-G2 recorded in THF. The maximum PL peak of PF-G1, excited at $\lambda_{\text{exe}} = 394$ nm, is located at $\lambda = 425$ nm; the two additional peaks at $\lambda = 454$ and 486 nm are due to vibronic progression of C=C bond stretching. PF, PF-G0, and PF-G1 have nearly equal photoluminescence intensities, which indicates that their fluorophores are well-separated in solution. In comparison, the signal for PF-G2 has about twice the PL intensity, which reflects the larger transition moment arising from the effect of higher conjugation in this dendritic structure.

To more fully understand the photophysics of PF-G1, we investigated films of pure PF-G1 and PF-G1 incorporated with the various-sized S-CdS nanoparticles.

We excited the samples using a broadband ($\Delta\lambda = 10$ nm) xenon lamp having a central wavelength of 394 nm and a narrow-band GaN diode laser. Figure 2(b) displays the results of this study. We observed clear vibronic features at 425, 445, 472, 508, 544, and 598 nm for all of the PF-G1 films. In particular, the first three of these vibronic peaks overlap with the $1s_e-1s_h$ exciton absorption peaks of S-CdS_{4nm} and S-CdS_{7nm} quantum dots. Hence, it appears that the only possible energy transfer in this case is from PF-G1 to the CdS nanoparticles, but this situation requires further confirmation.^[110] In addition, the broad absorption features of the S-CdS quantum dots that appear below 400 nm may also improve the photon absorption efficiency of the composite films.

Figure 3 displays the PL spectra of PF-G1 thin films containing the different-sized S-CdS nanoparticles. We controlled the thicknesses of these films to within 53–56 nm, as measured using an α -step instrument. When excited using a xenon lamp at 394 nm, the main PL peaks for these nanocomposites are located at the same wavelength as that of pure PF-G1, but the intensities of these peaks are affected dramatically by the amount and size of the incorporated S-CdS. For instance, in Figure 3a we observe that when 4 wt% of S-CdS_{3nm} nanoparticles are added to PF-G1, the intensity of the PL peak at 425 nm increased by more than 2.5 times relative to that of pure PF-G1. This effect becomes more pronounced as the size of CdS nanoparticles increases, as illustrated in Figures 3b and 3c. The intensities of the peaks at 425 nm of the PF-G1 thin films incorporating 4- and 7-nm-diameter CdS nanoparticles increased by 3.1 and 3.4 times, respectively, relative to that of pure PF-G1. We did not observe any peaks between 500 and 700 nm for S-CdS nanoparticles present in PF-G1, presumably due to the low S-CdS concentration that we used. The intensity of the PL peak at 425 nm in 4 wt% S-CdS_{7nm}/PF-G2 was more than 3 times that of pure PF-G2, with no appearance of the CdS PL peak (see

the supporting information). To fully understand this behavior, we performed two control experiments. The first considered the light emission of the S-CdS nanoparticles; the second was concerned with whether other luminescent polymers lacking dendritic structures behave in a similar manner. Figure 4 illustrates that no detectable PL peaks appeared when the same amount (4 wt %) of S-CdS was present in optically inactive poly(methyl methacrylate) (PMMA). Moreover, the addition of the same amount of S-CdS nanoparticles into PF-G0 and MEH-PPV did not substantially change the intensities or locations of the PL peaks of these polymers. This finding indicates that the CdS nanoparticles themselves emit relatively weak light in the nanocomposites, if at all. What is more interesting, however, is the role that CdS plays in the PL enhancement of the dendritic polymers. There are two possible mechanisms through which CdS nanoparticles enhance the PL of copolyfluorene, i.e., through steric hindrance or through electronic phenomena. The first of these mechanisms proposes that an increase in the inter-polymer chain distance in the nanocomposites leads to a decrease in dimer formation. In the pure PF-G1 polymer, dimers form as a result of the close proximity of polymer chains when they are excited. The inter-polymer chain distances in the S-CdS/PF-GX (X = 1, 2) nanocomposites increases upon incorporating the S-CdS nanoparticles into the dendritic polymers. Figure 5A shows X-ray diffraction spectra of S-CdS/PF-G1 obtained by deducting the glass substrate background (i.e. the difference between polymer on substrate and substrate).^[111] The packing of PF-G1 chains in the solid state was found to be amorphous by X-ray diffraction experiments, with two broad correlation peaks. The peak that remains at $2\theta = 20.1^\circ$ (d - spacing = 4.4 Å), despite the variation in the amount of CdS nanoparticles, is due to the average C-C intermolecular distance (i.e. the distance between the pendent group of the polymer chains) of PF-G1, while the other peak at lower diffraction angle that changes with

the amount CdS nanoparticles is a measurement of the average inter polymer chain distance as reported in a previous study of dendritic polyfluorene.^[112] Figure 5B shows that the average inter-chains distance of PF-G1 in the nanocomposite increases with the amount of CdS nanoparticles. For instance, in the presence of 4wt% CdS_{4nm} nanoparticles, the inter-chain distance in PF-G1 increases to 28.5 Å from 12.6 Å for pure PF-G1. As the CdS in PF-G1 increase to 8%, the peak shifted to a diffraction angle smaller than the limit of the X-ray instrument and seemed to suggest that the polymer chains are further apart, indicating that disordering of polymer chains could have happened (i.e. polymer chain solid packing break). One of the reasons that inter-chain distance increase in the presence of CdS nanoparticles is possibly due to the selective distribution of the nanoparticles into the dendritic regions of the structure, which results from the relatively strong interaction between the benzyl groups of the dendrons and the phenyl groups of the thiophenol ligands of CdS (Scheme 1). Figure 5C presents the Fourier transform infrared (FTIR) spectra of PF-G1 and the PF-G1 nanocomposite containing 4 wt% CdS_{4nm}. In comparing these two spectra, we detect several significant differences that originate from the addition of the S-CdS nanoparticles. The features near 500 cm⁻¹ may be due to low-frequency ring bending and deformation modes. The peaks near 990 cm⁻¹ are due to the breathing mode of the benzene ring, and the peaks near 1600 cm⁻¹ originate from C=C stretching. The inclusion of S-CdS nanoparticles significantly quenches the deformation and breathing modes for the benzene rings; this observation indicates that there is a possibility that π - π stacking occurs to a large extent between the phenyl groups of thiophenol and the dendritic units in PF-G1. The interactions between aromatic rings via π -stacking (i.e. the van der Waals contact between aromatic ring)^[114] are at the origin of many phenomena of organic material science^[113] and biological chemistry,^[115] and can be determined by the oxidation potential of the

material during electron detachment. Another piece of supporting evidence of CdS nanoparticles bound to the dendrons can therefore be found in the oxidation potential change, when the π -stacking of thiophenol surfactant on CdS with the phenyl groups in the dendron structure occurs. The inset in Figure 5D shows that the oxidation potential (E_{ox}) of S-CdS/PF-G1 decrease with the increasing amount of CdS.^[116] For example, in the presence 8 wt % CdS_{4nm} nanoparticles, the E_{ox} reduced to 1.24V from 1.30V for pure PF-G1. Although this change is small, it is enough to reflect the fact that there exists a possibility that π - π stacking formed to some extent^[115, 117] since the volume percentage of CdS in PF-G1 is one fourth of the weight percentage (density of CdS vs. PF-G1 is close to 4:1). By combining the FTIR, oxidation potential, and X-ray diffraction results, it can reasonably be concluded that the incorporation of S-CdS nanoparticles into the dendritic polyfluorene chains have happened, and that leads to increased distance between polymer chains. This phenomenon implies that the free volume in the nanocomposites is larger than that of the pure polymer because the inter-polymer chain distance is a one-dimensional representation of the free volume. The glass transition temperatures (T_g) of the S-CdS/copolyfluorene nanocomposites at various compositions are summarized. (see the supporting information). Our hypothesis is supported by the fact that the value of T_g for 8 wt% S-CdS/PF-G1 is depressed to 74.3 °C from 90.5 °C for pure PF-G1. We also found that the values of T_g decreased upon increasing the diameter of the S-CdS nanoparticles. The depression is also apparent in the case of the PF-G2 nanocomposites (from 59.1 for pure PF-G2 to 54.3 °C); the low value of T_g of PF-G2, relative to that of PF-G1, is due to the presence of a greater number of chain ends in the second-generation dendron. Figure 6 displays transmission electron microscopy (TEM) images of 4 wt% S-CdS/PF-G1; it is clear that the S-CdS nanoparticles did not form large aggregates in the PF-G1 matrix. The other possible mechanism for the

increased luminance results from electronic interactions occurring between CdS and PF-G1, but this type of interaction is difficult to verify because of the low concentration of nanoparticles in PF-G1. Thus, in this study, we found no evidence for energy transfer occurring from PF-G1 to the CdS nanoparticles.

To obtain a quantitative assessment of the luminance enhancement, we used Beer's law to determine the normalized luminescence efficiency of these nanocomposites. Table 1 lists the values of the normalized photoluminescence with respect to the molecular concentration. Substantial improvements in the photoluminescence of the composite systems occurred when a small weight percentage of S-CdS nanoparticles was present in either PF-G1 or PF-G2. For instance, we found a two fold improvement in the photoluminescence per fluorene chromophore for 4 wt% S-CdS/PF-G1 relative to that of pure PF-G1 (i.e., the quantum yield increased from 0.22 to 0.46). For the second-generation dendritic polymer nanocomposite, S-CdS/PF-G2, the photoluminescence per fluorene chromophore increased by more than 1.8-fold relative to that of pure PF-G2 (i.e., the quantum yield increased from 0.55 to 0.99). This phenomenon can be explained quantitatively using the equation:^[103]

$$\eta_{\text{PL}} = \phi_{\text{FL}}/\phi_{\text{A}} = k_{\text{r}}/(k_{\text{r}} + k_{\text{nr}}) \quad (1)$$

where η_{PL} is the fluorescence yield, ϕ_{FL} is the number of photons emitted, and ϕ_{A} is the number of photons absorbed. The terms k_{r} and k_{nr} represent the rates of decay of the radiative and combined non-radiative processes, respectively. The S-CdS nanoparticles in PF-G1 cause a decrease in k_{nr} , which in turn results in an increase in η_{PL} . The observation that the incorporation of CdS nanoparticles into the dendritic polymer structures reduces the degree of energy transfer from the isolated polymer

chains to an inter-chain dimer is also evident in the electroluminescence of the S-CdS/PF-G1 device.

4-3-2. Electroluminescence (EL) Characteristics

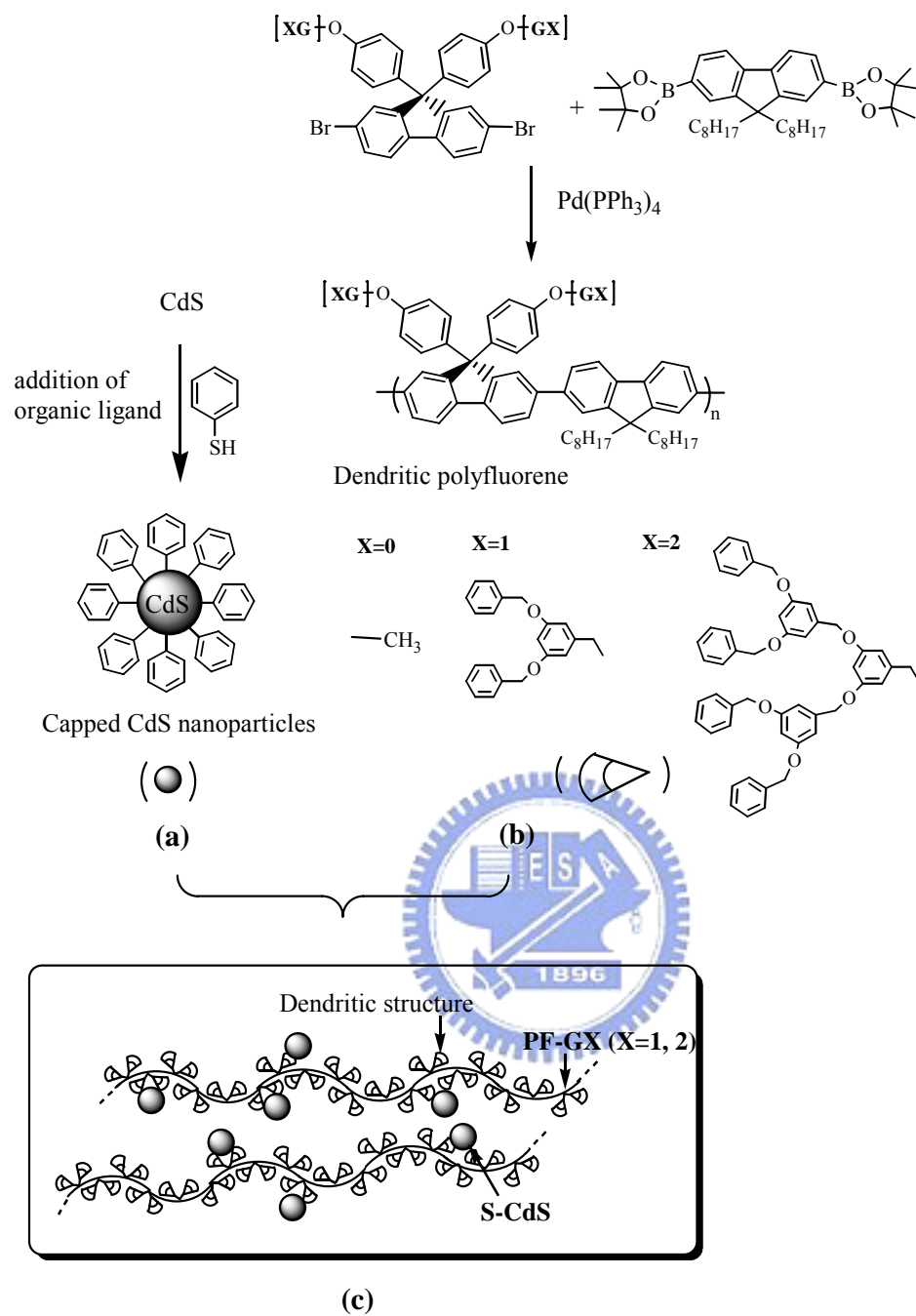
We fabricated double-layer LED devices having the configuration ITO/PEDOT:PSS/polymer/Ca/Al, where PEDOT:PSS [poly(3,4-ethylenedioxythiophene) doped with poly(styrenesulfonic acid) (Batron-P 4083)] was used as the hole injection/transporting layer at a thickness of 150 nm. A thin layer of Ca (35 nm) was employed as the cathode, which was coated with a 180-nm-thick layer of Al. The thickness of the emissive layer was ca. 80 nm. Figure 7 displays the normalized electroluminescence of the devices. The similarities between the EL and PL spectra of both the pure PF-G1 and S-CdS/PF-G1 devices indicate that the same excitation processes occur in each case. The EL device prepared from pure PF-G1 emits blue light at 426 nm and a weak green light in the range 465–550 nm. In the case where 8% S-CdS was incorporated into PF-G1, the green emission in the range 465–550 nm reduced sharply, while the peak at 426 nm became a sharper and major emission peak. In addition, the full width at the half-maximum (FWHM) of the peak of 8% S-CdS/PF-G1 reduced to 49 nm from a value of 112 nm for pure PF-G1, indicating that it emits a purer blue light. Compared with its PL spectrum, the change in relative intensities in vibronic structure indicates that aggregate emission is dominant in its EL process.^[104–105] This behavior has also been observed in polyfluorene derivatives, namely for PF-POSS.^[105] Figure 8 displays the variations of the current density and brightness of the EL devices. The turn-on voltage increased to 4.5 V for PF-G1 containing 8% S-CdS from 4 V for the pure-PF-G1 EL device. A more-than-fourfold increase in the maximum brightness of the 8% CdS/PF-G1-based device occurred relative to that of

the pure-PF-G1 EL device (1196 vs. 298 cd/m^2) at a drive voltage of 10 V and a current density of 644 mA/cm^2 . These improvements are probably due to the lower degree of aggregation that occurred upon incorporating S-CdS into PF-G1.

4-4 Conclusions

Placing a small amount of surface-tailored CdS nanoparticles into the dendritic structure of copolyfluorene substantially improves the efficiency of the polymer's light emission as well as the purity of the emitted light. The enhancements in photoluminescence and electroluminescence are due mainly to a reduction in the concentration of inter-polymer excimers through which energy transfer occurs from the excited polymer chains to their neighboring ground state polymer chains; i.e., the CdS nanoparticles caused an increase in the inter-polymer chain distance.





Scheme 1 Synthesis of (a) S-CdS and (b) PF-GX and (c) a schematic drawing of the architecture of S-CdS/PF-GX (X = 1, 2).

Table 1: Absorption and photoluminescence data for S-CdS/polymer nanocomposites in the solid state.

Sample	$\epsilon^{[a]}$ ($M^{-1} \text{ cm}^{-1}$)	O.D. ^[b] $\lambda = 394 \text{ nm}$	L ^[c] (nm)	M ^[d] (mol cm^{-3})	$\eta^{[e]}$
PF-G1	4.48×10^4	0.326	95	0.771	0.22
3 wt% S-CdS/PF-G1	4.61×10^4	0.301	106	0.620	0.39
4 wt% S-CdS/PF-G1	4.91×10^4	0.293	88	0.680	0.46
8 wt% S-CdS/PF-G1	4.92×10^4	0.290	90	0.655	0.44
PF-G2	7.70×10^4	0.192	76	0.328	0.55
3 wt% S-CdS/PF-G2	7.62×10^4	0.203	84	0.317	0.78
4 wt% S-CdS/PF-G2	7.51×10^4	0.226	81	0.372	0.99

^[a] Values of the decadic molar extinction coefficient were determined from UV–Vis spectra recorded in THF ($\epsilon = \text{O.D.}/c l$), where c is the concentration of the compound in solution, and l is the path length of the sample.

^[b] The optical density (absorbance) in the solid state.

^[c] The thickness of the thin film.

^[d] The concentration of the fluorescent chromophore in each composite film.

^[e] Quantum yield estimated using poly[2,7-(9,9-dioctylfluorene)] ($\eta = 0.55$) as the reference. See ref. [8].

Table 2: Thermal behavior of S-CdS/polymer nanocomposites.

Sample	T_g ($^{\circ}\text{C}$) ^[a]
PF-G1	90.5
3% S-CdS_{4nm}/PF-G1	88.0
4% S-CdS_{4nm}/PF-G1	81.4
8% S-CdS_{4nm}/PF-G1	74.3
4% S-CdS_{3nm}/PF-G1	85.4
4% S-CdS_{7nm}/PF-G1	76.5
PF-G2	59.1
3% S-CdS_{4nm}/PF-G2	57.2
4% S-CdS_{4nm}/PF-G2	54.3

^[a] The value of T_g was determined by differential scanning calorimetry (DSC) under a nitrogen atmosphere using a heating rate of $10 \text{ }^{\circ}\text{C min}^{-1}$.

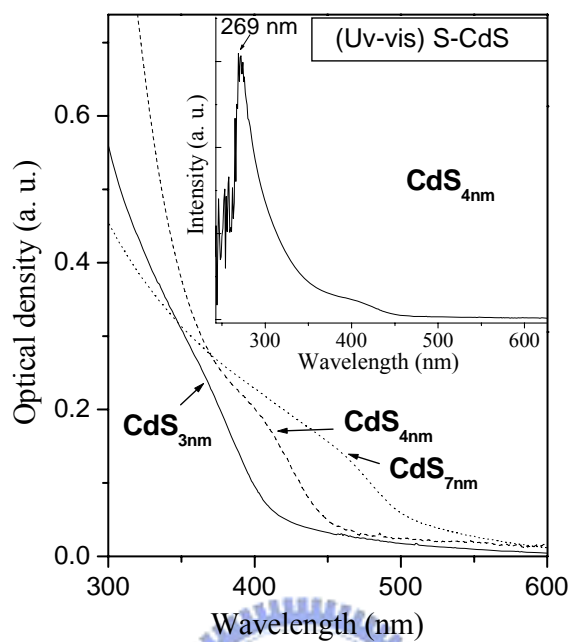


Figure 1. Normalized UV–Vis absorption spectra recorded in DMF for S-CdS nanoparticles having three different diameters.

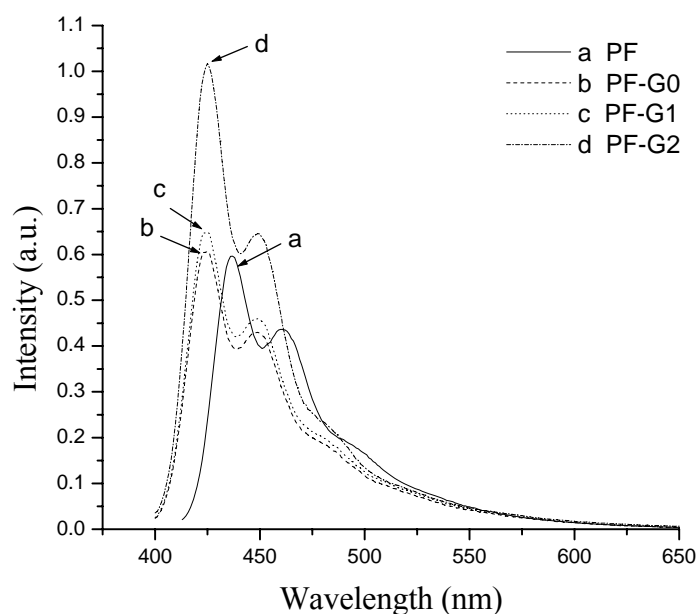


Figure 2 (a) Photoluminescence spectra of PF [poly-2,7-(9,9-dioctylfluorene)], excited by a xenon lamp at $\lambda_{\text{max}} = 393$ nm, and PF-G0, PF-G1, and PF-G2, all recorded in THF at the same concentration (5×10^{-6} M).

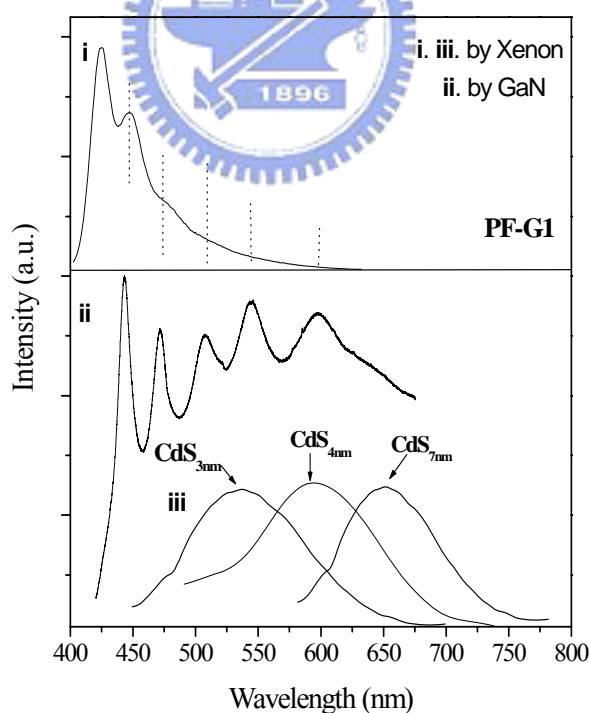


Figure 2 (b) Photoluminescence spectra recorded in DMF of (i) PF-G1 in the solid state, using a xenon lamp as the excitation light source, (ii) PF-G1 in the solid state, using a GaN diode laser, and (iii) S-CdS nanoparticles having three different diameters.

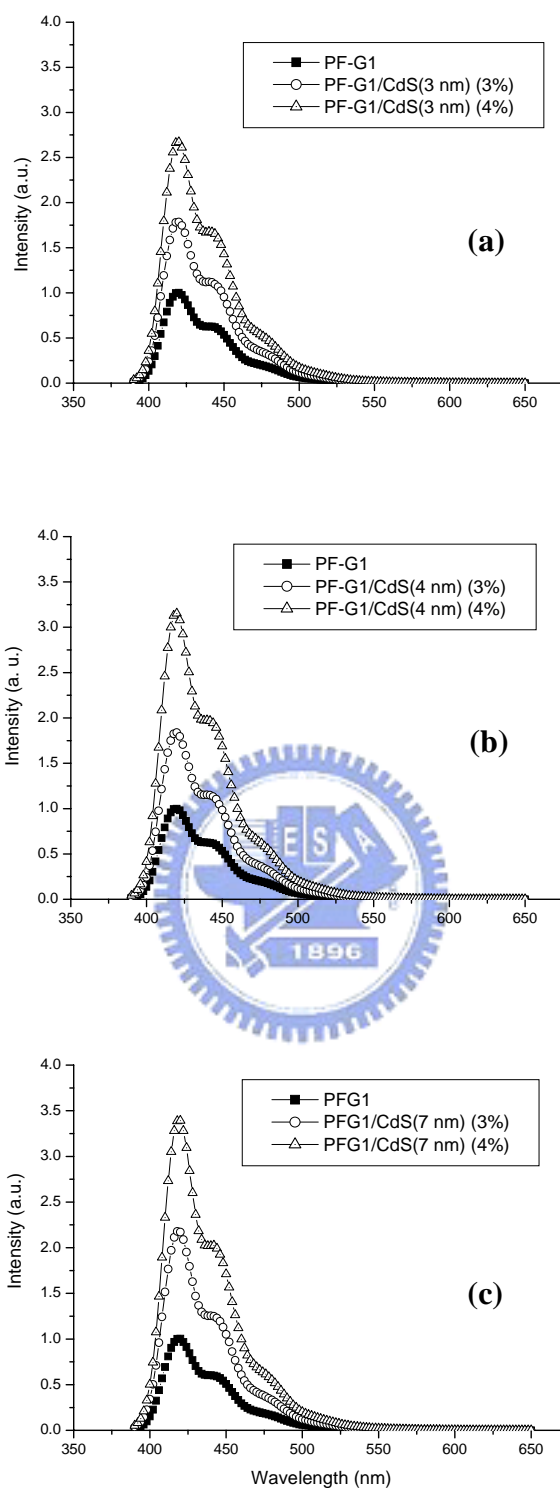


Figure 3. Photoluminescence spectra of thin films of (a) S-CdS_{3nm}/PF-G1, (b) S-CdS_{4nm}/PF-G1, and (c) S-CdS_{7nm}/PF-G1, normalized with respect to the PL intensity of PF-G1.

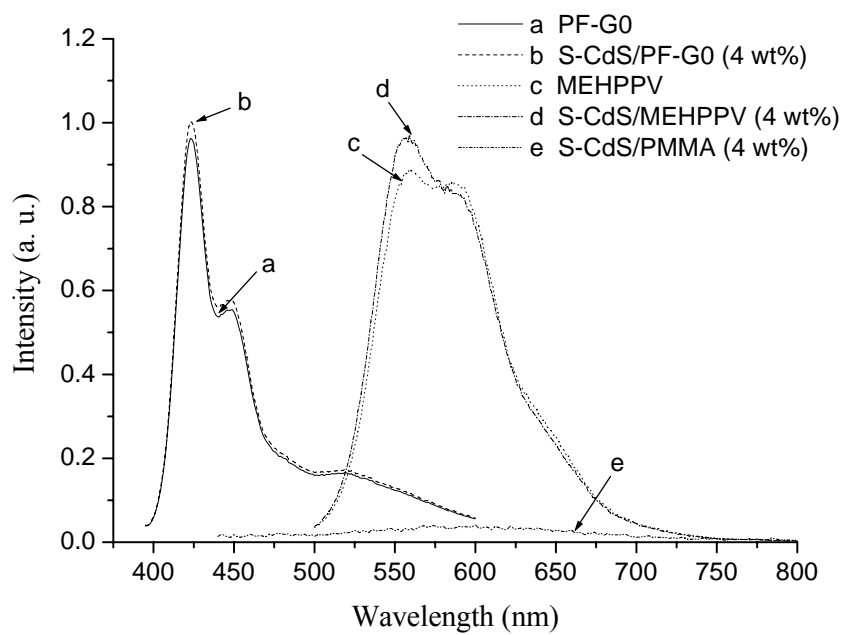


Figure 4. Photoluminescence spectra of thin films of (a) pure PF-G0, (b) PF-G0 containing 4 wt% S-CdS, (c) pure MEHPPV, (d) MEHPPV containing 4 wt% S-CdS, and (e) PMMA containing 4 wt% S-CdS.

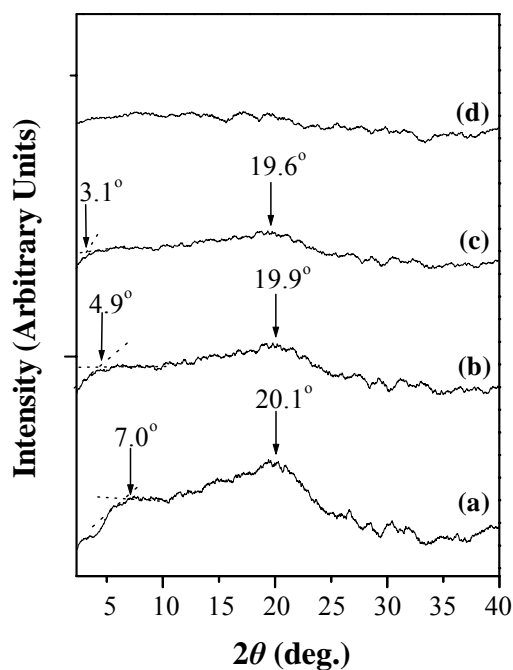


Figure 5A. X-ray diffraction spectra of S-CdS/PF-G1 nanocomposite. (a) PF-G1 (b) PF-G1 containing 3 wt% S-CdS, (c) PF-G1 containing 4 wt% S-CdS, and (d) PF-G1 containing 8 wt% S-CdS.

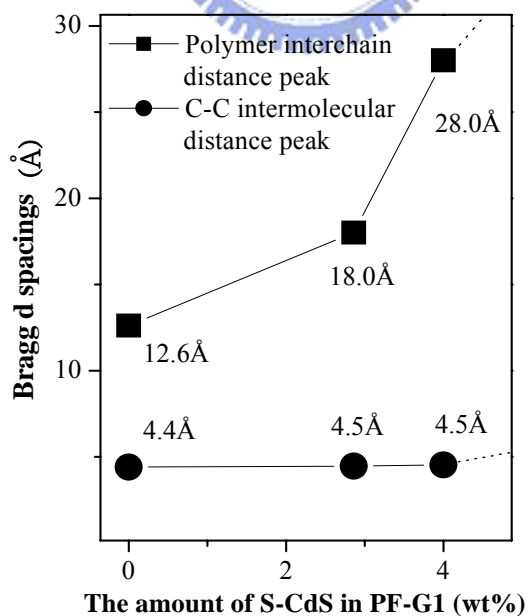


Figure 5B. The effect of the amount of S-CdS on the Bragg d spacing of PF-G1.

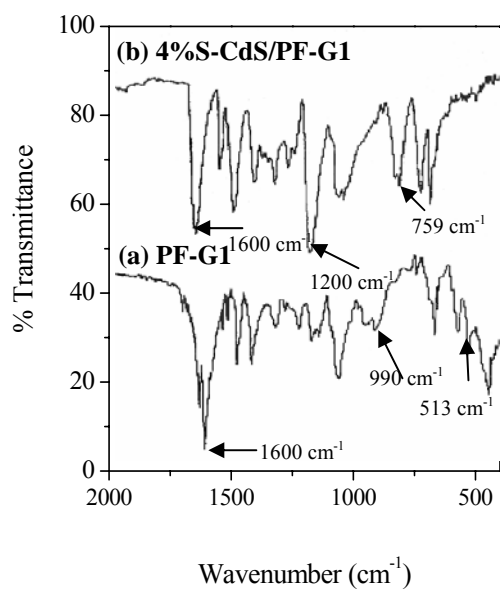


Figure 5C. FTIR spectra of (a) PF-G1 and (b) PF-G1 containing 4 wt% S-CdS.

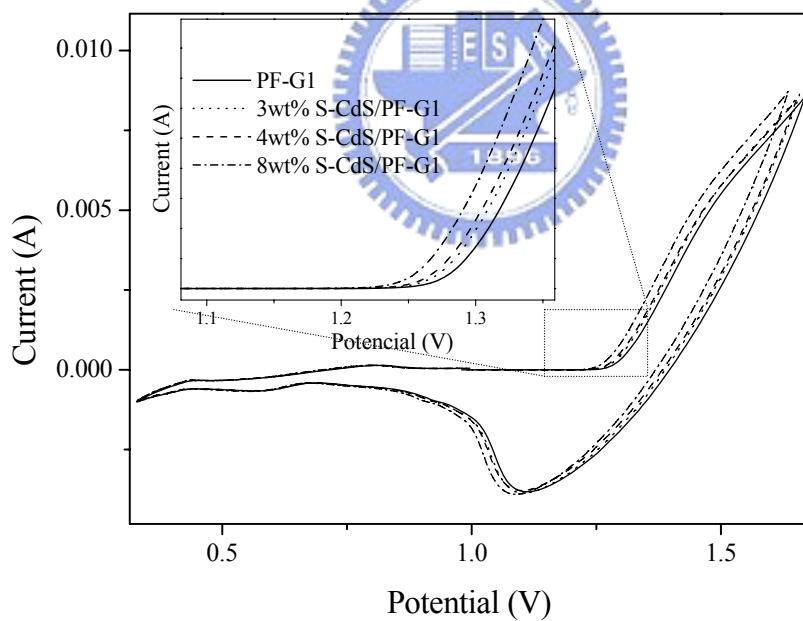


Figure 5D. Cyclic voltammogram of the oxidation of polymer.

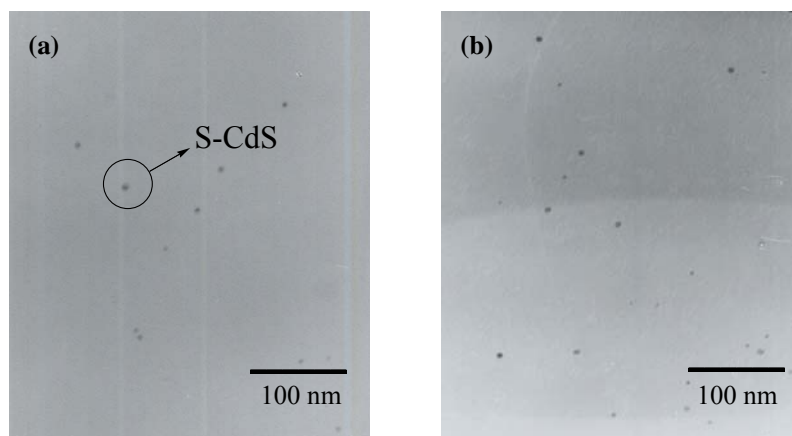


Figure 6. Transmission electron microscopy images of PF-G1 films containing (a) 3 wt% and (b) 4 wt% of S-CdS.

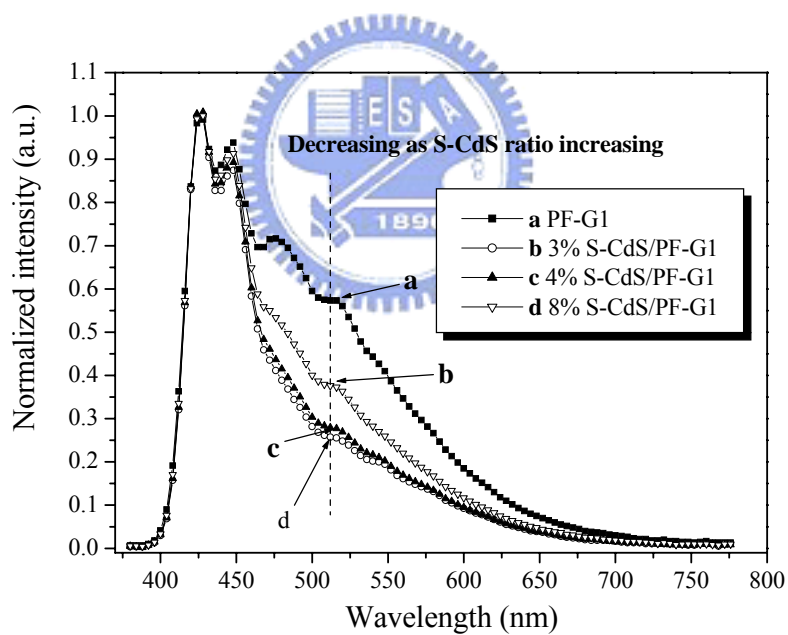


Figure 7. Normalized electroluminescence spectra of devices prepared from S-CdS/PF-G1 in the configuration ITO/PEDOT/polymer/Ca/Al.

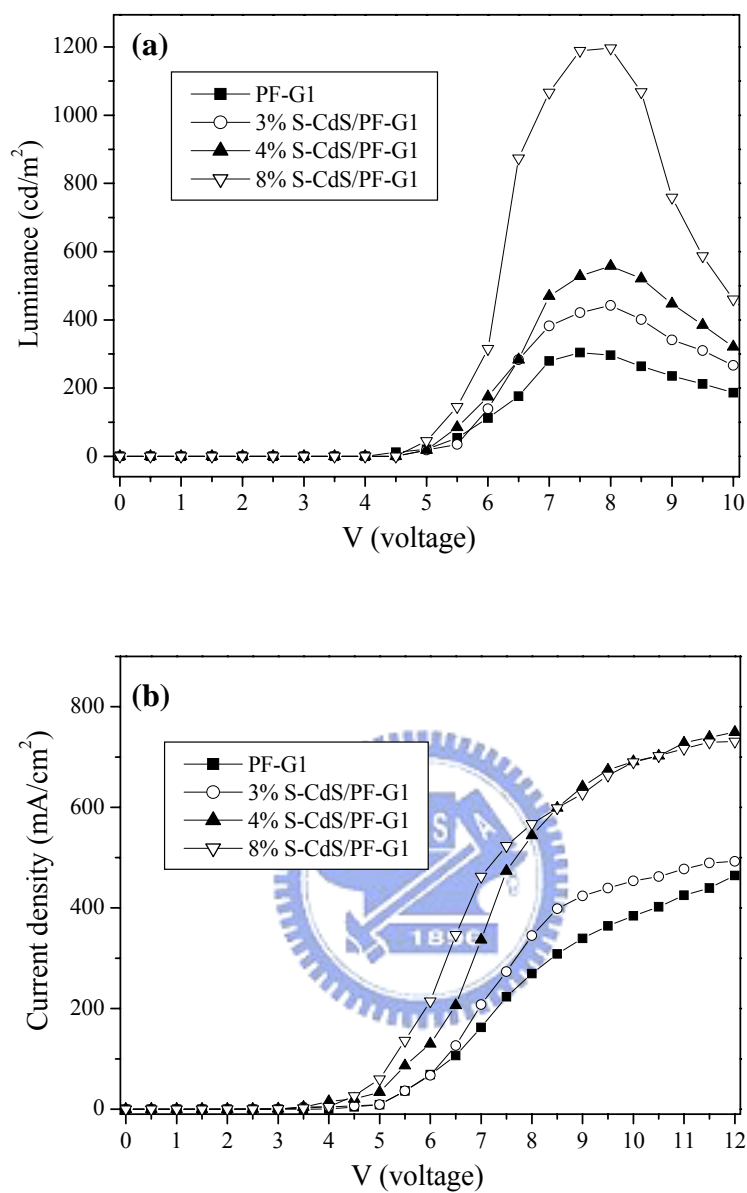


Figure 8. (a) I-V and (b) L-V curves of devices prepared from S-CdS/PF-G1 in the configuration ITO/PEDOT/polymer/Ca/Al.

Chapter 5: Blue Electroluminescence Enhancement of a Polyfluorene Copolymer Incorporating Side-Chain-Tethered Gold Nanoparticles

5-1 Introduction Materials

Hybrid polymer/inorganic nanoparticle materials have great potential for application in flexible optical and electronic devices^[118,119] because (a) modifying the molecular structure of the polymer and its solution processing are both relatively easy tasks and (b) colloidal nanoparticles can be fabricated with adjustable surface ligands for solution processing. Depending upon the type of material sought, three approaches are typically used to prepare these hybrids: in situ synthesis of nanoparticles in a polymer matrix,^[120] mixing polymers^[121,122] and nanoparticles in solvents, and polymerization of monomers in the presence of nanoparticles.^[123,124] In this study, we chose polyfluorene and gold nanoparticles (Au NPs) to be the components of a hybrid material, with chemical bonding of the Au NPs occurring through the side chains of the polyfluorene copolymer.

Polyfluorene and its derivatives are among the best performing of the blue light emitting polymers,^[49, 84] but their device applications are limited by poor emission spectral stability and the development of undesired emissions of green light^[125–127] arising from photo-oxidation of the carbon bridge or from aggregation of the polymer chains.^[128] The tethering of CdS semiconductor NPs of various sizes to the side chains of a dendritic polyfluorene—through π – π stacking between the ligands on the NPs and the dendritic groups—appears to produce a bluer and brighter light relative to that of the pure dendritic polyfluorene.^[129] Unfortunately, such π – π stacking in dendritic polyfluorene/NP hybrids can be sustained only at mild temperatures (ca. <60 °C) and at relatively semi-concentrated particle concentrations (ca. 8%). Moreover, the toxicity of CdS NPs prevents them from being used as major components of the hybrids for environmental reasons. On the other hand, Au NPs, which are used in, for example, DNA detection and other studies involving surface-enhanced Raman scattering, are considered to be friendlier to the environment and to living creatures. A recent study found that blending Au NPs with polyfluorene resulted in enhanced luminescent stability.^[32] The effect of

the Au NPs appears to be limited because the uniform distribution of gold NPs in polyfluorene—in the absence of any specific interaction or bonding to the polymer—is very difficult to achieve. In this paper, we describe how the tethering of Au NPs to the side chains of a poly(fluorene-*co*-DBMS), through chemical bonds, leads to enhanced electroluminescence with no detectable change in the emission wavelength of the polymer. To the best of our knowledge, Au NPs have never previously been attached to the side chains of luminescent polymers. Using this approach, the Au NPs appear to prevent aggregation of the polymer chains while serving as facilitators for electron transport. Scheme 1 provides a schematic illustration of this copolymer's molecular structure and how it incorporates the Au NPs. We synthesized poly{2,7-(9,9'-dioctylfluorene)-*co*-4-diphenylamino-4'-bipenylmethylsulfide}(PF-DBMS), dissolved it in toluene, and then added HAuCl₄—the precursor of the Au NPs—to the solution. Subsequently, NaBH₄ was added to reduce this precursor and form the Au NPs. The stability of Au NPs in various media is determined by the nature of their surface ligands, which are typically alkanethiols having various carbon chain lengths. Several groups have reported the chemisorption of alkane or polymer-terminated thiols onto the surfaces of gold NPs to form self-assembled monolayers. Other sulfur-containing ligands—such as disulfides (–S–S–),^[130–133] thioethers (–SCH₃),^[134] di-^[135] and trithiols,^[136] and resorcinarene tetrathiols^[137]—can also be used to stabilize AuNPs, but their binding abilities are not as high as those of the alkanethiols. To compensate for the weaker interactions between AuNPs and thioethers, polymers containing multiple thioether units are required to produce stable and well-ordered monolayers from such systems.^[138a] Because the use of end-grafting techniques to fix either thioether derivatives or polymer molecules onto the Au surfaces limits the number of NPs that can be bound to each chain, we prepared a series of polymers possessing multiple thioether bonding sites on their side chains (i.e., more bonding points per polymer molecule would be available for chemisorption). Thus, we brominated triphenylamine, reacted the tribromide with 4-(methylthio)benzeneboronic acid (Suzuki coupling), and then polymerized the dibromide/monothioether in the presence of fluorene monomers (Scheme 1).

5-2 Experimental

5-2-1. Materials

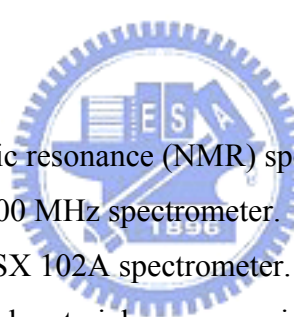
Synthesis of DBMS Tris(4-bromophenyl) amine (2.58 g, 5.36 mmol) and 4 (Methylthio)benzeneboronic acid (900mg, 5.36 mmol) was stirred with Aqueous potassium carbonate (2 M) and tetrakis(triphenylphosphine)palladium (2.0 mol%) in toluene (8mL) at 95°C overnight. The reaction mixture was then slowly poured into water (150 mL) and extracted with chloroform (3 × 30 mL). The combined extracts were dried (MgSO₄), the solvents were evaporated, and the residue was purified by column chromatography (hexane/ chloroform, 1:10) to afford DBMS (1.91g, 68%). ¹H NMR (CDCl₃): δ7.52-7.41 (m, 4H), 7.34 (d, *J* = 9Hz, 4H), 7.29 (d, *J* = 8.4 Hz, 2H), 7.08 (d, *J* = 8.4 Hz, 2H), 6.97 (d, *J* = 9 Hz, 4H), 2.50 (s, 3H) ppm. Anal. Calcd for C₂₆H₂₀Br₂S (%): C, 59.56; H, 3.84. Found: C, 59.11; H, 3.51.

General Procedure for the Synthesis of Alternating Copolymers PF-DBMS.

Aqueous potassium carbonate (2 M) and aliquate 336 were added to a solution of the DBMS, dibromide, and diboronate in toluene (1:4:5). The mixture was degassed and purged with nitrogen three times. The catalyst, tetrakis(triphenylphosphine)palladium (2.0 mol%), was added in one portion under a nitrogen atmosphere. The solution was then heated at 95 °C and vigorously stirred under nitrogen for 6 days. End-group capping was performed by heating the solution under reflux for 12 h sequentially with phenylboronic acid and bromobenzene. After cooling, the polymer was recovered by precipitating it into a mixture of methanol and acetone (3:1). The crude polymer was collected, purified twice by reprecipitation from THF into methanol, and subsequently dried under vacuum at 50 °C for 24 h. In this study, we have selected PF-DBMS10 (n: m= 9: 1) instead of PF-DBMS30 (n: m= 7: 3) as the polymer matrix to combine with Au NPs, because PF-DBMS10 has higher molecule weight, lower polydispersity (PDI), and better optical performance (in solid state).

Synthesis of Au/ PF-DBMS nanocomposites The synthesis of Au NPs was accomplished through a room-temperature, two-phase, one-pot reaction involving the reduction of HAuCl_4 in the presence of PF-DBMS. The HAuCl_4 was dissolved in H_2O and a phase-transfer reagent (tetraoctylammonium bromide) was employed to move the salt into toluene over a period of 3 h. PF-DBMS was then added to the organic solution, which was stirred for 1 h. Reduction of AuCl_4^- was accomplished upon the addition of NaBH_4 in H_2O , which produced an immediate dark-purple-colored organic layer. The mixture was stirred for 24 h after the addition of NaBH_4 . The dark-purple polymer/Au NP composites were precipitated into hexane, dried under vacuum at room temperature, and then redissolved for further studies. The diameters of the gold NPs were in the range 3.8 ± 0.3 nm, as determined using a JEOL JEM-2010 transmission electron microscope operating at 200 kV. PF-DBMS was synthesized according to Scheme 1.

5-2-2 Characterization.



^1H and ^{13}C nuclear magnetic resonance (NMR) spectra of the compounds were obtained using a Bruker DRX 300 MHz spectrometer. Mass spectra of the samples were obtained on a JEOL JMS-SX 102A spectrometer. Fourier transform infrared (FTIR) spectra of the synthesized materials were acquired using a Nicolet 360 FTIR spectrometer. Gel permeation chromatographic analyses were performed on a Waters 410 Differential Refractometer and a Waters 600 controller (Waters Styragel Column). All GPC analyses of polymers in THF solutions were performed at a flow rate of 1 mL/min at 40°C ; the samples were calibrated using polystyrene standards. UV–Vis absorption and photoluminescence (PL) spectra were recorded using an HP 8453 spectrophotometer and a Hitachi F-4500 luminescence spectrometer, respectively.

5-2-3 Device Fabrication and Testing

The electroluminescent (EL) devices were fabricated on an ITO-coated glass substrate that was precleaned and treated with oxygen plasma prior to use. A layer of

poly(ethylene dioxythiophene):poly(styrene sulfonate) (PEDOT:PSS, Baytron P from Bayer Co.; ca. 40-nm thick) was formed by spin-coating from an aqueous solution (1.3 wt%). The EL layer was spin-coated—at 1500 rpm from the corresponding toluene solution (15 mg mL⁻¹)—on top of the vacuum-dried PEDOT:PSS layer. The nominal thickness of the EL layer was 65 nm. Using a base pressure below 1×10^{-6} torr, a layer of Li (1 nm) and Ca (35 nm) was vacuum-deposited as the cathode and then a thick layer of Al was deposited as the protecting layer. The current–voltage characteristics were measured using a Hewlett–Packard 4155B semiconductor parameter analyzer. The power of the EL emission was measured using a Newport 2835-C multifunction optical meter. The brightness was calculated using the forward output power and the EL spectra of the devices; a Lambertian distribution of the EL emission was assumed.

5-3 Results and Discussions

A. Polyfluorene Side-Chain-Tethered Gold Nanoparticles

The chemical structures of the products were determined using ¹H NMR spectroscopy (Figure 1); in this paper, we use the acronym PF-DBMS to represent the copolymer containing a 10% molar ratio of DBMS repeat units in the polyfluorene. We used X-ray photoelectron spectroscopy (XPS) to confirm that chemical bonding occurred between the Au NPs and PF-DBMS (Figure 2). Because of spin-orbit splitting,^[138b] this spectrum exhibits two sets of doublets (S and S') that reveal the binding energies of the bound and unbound sulfur species, respectively. Peak fitting revealed that the binding energies of unbound S'(2P_{3/2}) and S'(2P_{1/2}) were 163.3 and 164.2 eV, respectively, while the peak of bound S(2P_{3/2}) and S(2P_{1/2}) were centered at 161.7 and 162.4 eV, respectively.^[138c-e] A reduction of 1.6 eV from S' to S corresponds to the effect of sulfur atoms bound to the gold—direct evidence for bonding of the ArSCH₃ functional groups to the Au NPs.

Figure 3 displays the UV–Vis absorption and photoluminescence spectra of PF-DBMS. In THF, PF-DBMS displayed signal maxima at 387 and 427 nm for its absorption and emission, respectively; the emission maximum shifted to 440 nm in the solid state. Moreover, the inset to Figure 3 clearly indicates an improved stability of the

PL emission characteristics of the PF-DBMS/Au NP hybrid, relative to those of PF-DBMS, after thermal treatment of 100 °C for 2 h. This situation results from the number of triplet excitons, which are the major cause of oxidation of PF-DBMS, being reduced as a result of energy transfer from the triplet emission band of PF-DBMS^[139–141] to the optical absorption bands of the Au NPs (ca. 520 nm). To obtain a quantitative assessment of the luminance of these hybrids, we used Beer's law to determine their quantum yields, which are listed in Table 1 along with the optical parameters of the composite films. Substantial improvements in the quantum yields of the composites occurred when a small weight percentage of Au NPs was present in the PF-DBMS. For instance, the quantum yield of PF-DBMS incorporating 1 wt% Au NPs improved to 0.86 (± 0.03) from 0.57 (± 0.02) for pure PF-DBMS—i.e., a 50% increase in quantum yield occurred upon adding the Au NPs. This increase in quantum yield in the presence of the Au NPs presumably results from reduced aggregation of the polymer chains upon their binding to the side-chain-tethered Au NPs. When we increased the concentration of Au NPs in PF-DBMS to 6 wt%, the quantum yield of this composite decreased to 0.54 (± 0.03). This phenomenon resulted both from the Au NPs also absorbing singlet exciton energy and from increased aggregation when the Au NP concentration reached a critical value. Thus, we found that the optimal quantum yield occurred for the composite containing 1 wt% Au NPs in PF-DBMS.

We determined the degree of dispersion of the Au NPs in PF-DBMS from transmission electron microscopy (TEM) images of the PF-DBMS/Au NP composites; Figure 4a indicates that the distribution of Au NPs (3.8 ± 0.3 nm in diameter) was uniform in terms of both their thickness and across a cross-sectional cut-away view. Figure 4b displays a histogram of the size distribution of the NPs. Figure 4c provides a cross-sectional view of the PF-DBMS/Au device used for the electroluminescence study; it appears that some of the Au NPs were located close to the interface of the electrode.

B. Electroluminescence (EL) Characteristics

Figure 5a displays the current–voltage characteristics of PF-DBMS and the

PF-DBMS/Au NP device. The most interesting phenomenon we observe is the dramatic increase in current that occurred when 0.5 wt% Au NPs were incorporated into the PF-DBMS, suggesting that the presence of the Au NPs in PF-DBMS enhances the transport of electrons. When we increased the concentration of the Au NPs further (to 1 wt%), the current density of PF-DBMS decreased, but remained larger than that of pure PF-DBMS. The turn-on threshold voltage for the EL device containing 0.5 wt% Au NPs was slightly lower than that of the pristine PF-DBMS device (6.5 vs. 7 V). A further increase in the Au content (to 6 wt %) led to a sudden increase in the turn-on threshold voltage to 9 V. The current density of the nanocomposite devices decreased upon increasing the number of Au NPs in excess of 1 wt%. This effect can be explained by considering the balance between a mild hole trapping effect^[142]—resulting from the difference in energy between the work function of the Au NPs and the highest occupied molecular orbital (HOMO) of the PEDOT:PSS layer—and enhanced electron injection (see the inset energy diagram in Figure 4a). At low concentrations of gold NPs, the enhanced electron injection is more dominant than the hole blocking effect caused by the Au NPs, and, thus, the current density in the device increased. When the concentration of the Au NPs in PF-DBMS increased further, the hole blocking effect of the NPs began to dominate, resulting in a decrease in the total current density. Figure 5b displays the luminescence–voltage characteristics of the device. A greater-than-threefold increase occurred in the maximum brightness of the 1 wt% Au/ PF-DBMS device, relative to that of the PF-DBMS device (1983 vs. 623 cd/m²), at a drive voltage of 12.5 V and a current density of 331 mA/cm². The trend in the luminescence behavior was similar to that of the current density, with the exception of the performance of the device containing 3 wt% Au NPs. Figure 6 displays the normalized electroluminescence of each device. The EL device prepared from pure PF-DBMS emitted blue light at 425 nm and an intense green light in the range 465–650 nm. For the 6 wt% Au/PF-DBMS device, the green emission was reduced sharply, while the peak at 425 nm sharpened to become the major emission signal. In addition, the full width at half maximum (FWHM) of the emission peak of the 6 wt% Au/ PF-DBMS device reduced to 110 nm (from 184 nm for pure PF-DBMS), indicating that this device emitted a purer form of blue light. Compared with its PL spectrum, the changes in the relative intensities of the vibronic structure

indicate that aggregate emission was dominant during the EL process.^[143, 144]

5-4 Conclusions

In summary, we have synthesized a series of side-chain-tethered Au NP/polyfluorene copolymer (PF-DBMS) hybrids by taking advantage of multiple ArSCH₃ anchor groups present on the polymer's side chains. The EL behavior of the PF-DBMS/Au NP devices indicates that they exhibit enhanced environmental stability and are suitable for use as nanocomposite emitting layers. The presence of the Au NPs appears to modify the device's interfacial morphology—they not only facilitate electron injection but also block hole migration. These Au/PF-DBMS nanocomposites display improved device performance relative to that of the pristine PF-DBMS device.



Table 1: Absorptions and Quantum Yields for Au NP/Polymer Nanocomposite Solid Films.

sample	$\epsilon^{[a]}$ ($M^{-1} \text{ cm}^{-1}$)	O.D. $^{[b]}$ $\lambda = 380 \text{ nm}$	L $^{[c]}$ (nm)	M $^{[d]}$ (mol cm^{-3})	$\eta^{[e]}$
PF-DBMS	4.71×10^4	0.321	102	0.768	0.57 ± 0.02
0. 5% $^{[f]}$ Au/PF-DBMS	4.62×10^4	0.312	90	0.750	0.73 ± 0.03
1% Au/PF-DBMS	4.68×10^4	0.324	86	0.805	0.86 ± 0.03
3% Au/PF-DBMS	4.72×10^4	0.294	79	0.788	0.80 ± 0.03
6% Au/PF-DBMS	4.70×10^4	0.292	76	0.817	0.54 ± 0.03

^[a] Values of the decadic molar extinction coefficient were determined from UV–Vis spectra recorded in THF ($\epsilon = \text{O.D.}/c l$), where c is the concentration of the compound in solution and l is the path length of the sample.

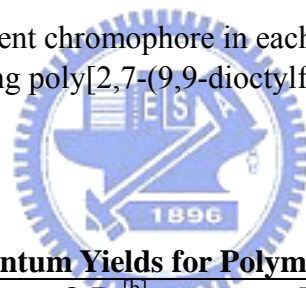
^[b] Optical density (absorbance) in the solid state.

^[c] Thickness of the thin film.

^[d] Concentration of the fluorescent chromophore in each composite film.

^[e] Quantum yield estimated using poly[2,7-(9,9-dioctylfluorene)] ($\eta = 0.55 \pm 0.03$) as the reference. See Ref. [146].

^[f] By weight.

**Table 2: Absorptions and Quantum Yields for Polymer Solid Films.**

sample	$\epsilon^{[a]}$ ($M^{-1} \text{ cm}^{-1}$)	O.D. $^{[b]}$ $\lambda = 380 \text{ nm}$	L $^{[c]}$ (nm)	M $^{[d]}$ (mol cm^{-3})	$\eta^{[e]}$
PF-DBMS10	4.71×10^4	0.321	102	0.768	0.57 ± 0.02
PF-DBMS30	4.91×10^4	0.383	83	0.939	0.40 ± 0.04

^[a] Values of the decadic molar extinction coefficient were determined from UV–Vis spectra recorded in THF ($\epsilon = \text{O.D.}/c l$), where c is the concentration of the compound in solution and l is the path length of the sample.

^[b] Optical density (absorbance) in the solid state.

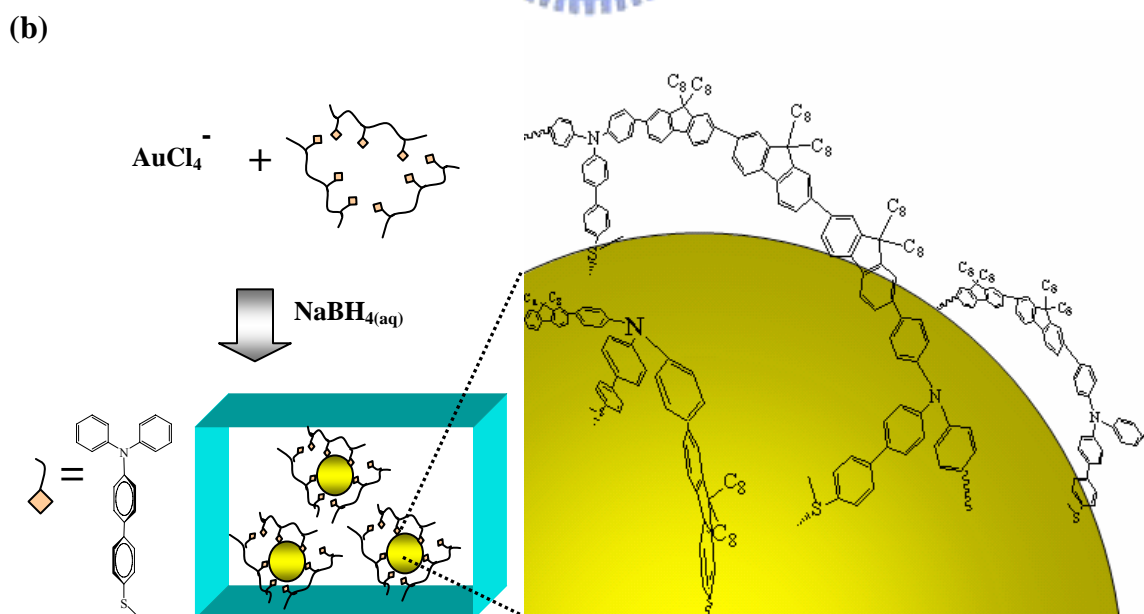
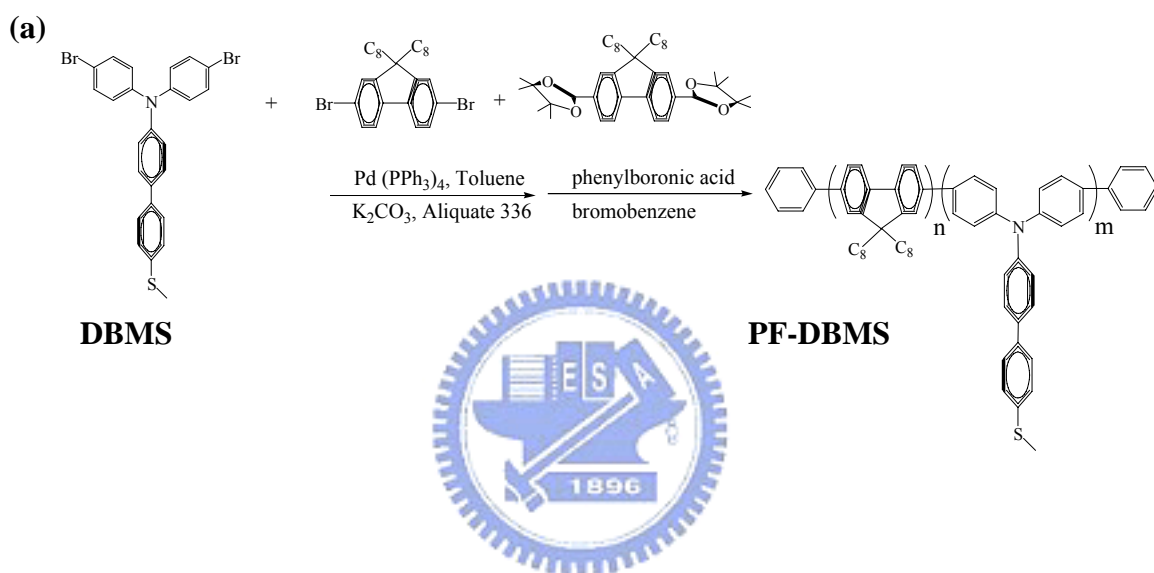
^[c] Thickness of the thin film.

^[d] Concentration of the fluorescent chromophore in each composite film.

^[e] Quantum yield estimated using poly[2,7-(9,9-dioctylfluorene)] ($\eta = 0.55 \pm 0.03$) as the reference.

Table 3: Molecular Weights of the Polymers.

polymer	M_w	M_n	M_w/M_n
PF-DBMS10	20,000	34,000	1.7
PF-DBMS30	14,000	27,000	1.9

**Scheme 1** Synthesis of (a) PF-DBMS copolymers (b) A schematic drawing of the architecture of Au/ PF-DBMS nanocomposites.

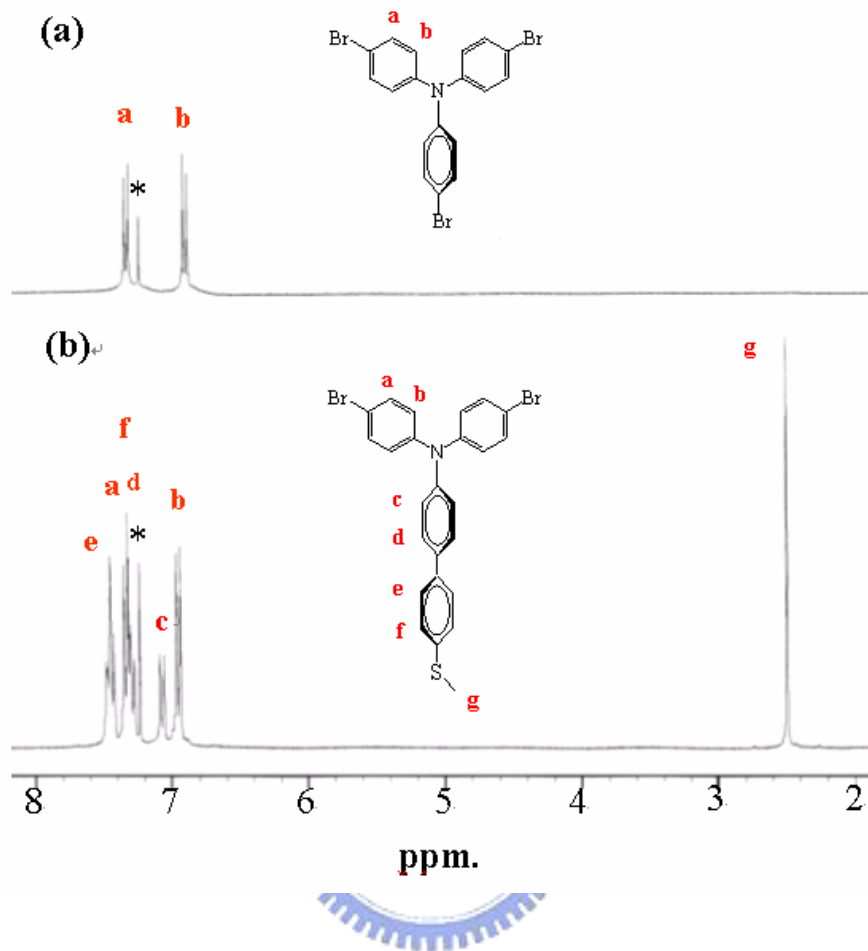


Figure 1. ¹H NMR spectra of (a) tris(4-bromophenyl)amine and (b) DBMS.

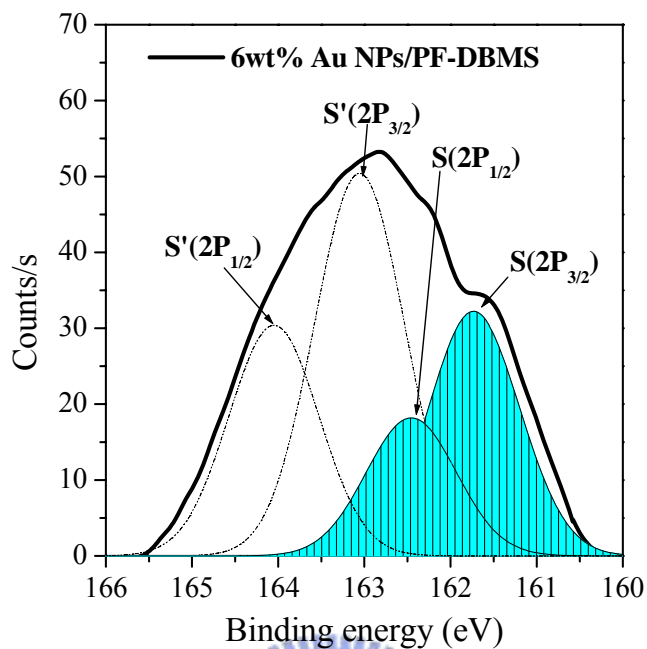


Figure 2. XPS spectra [S(2P) region] of PF-DBMS adsorbed onto Au NPs.

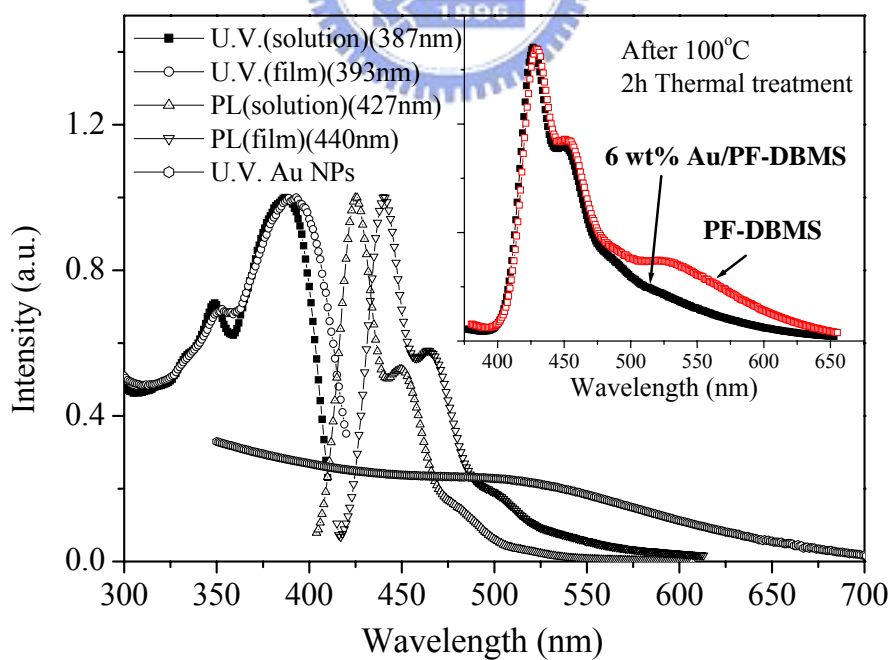


Figure 3. Normalized UV-Vis absorption spectra and PL emission spectra of PF-DBMS recorded in solution (THF) and from a thin film. The inset displays the thin film after thermal treatment at 100°C for 2 h.

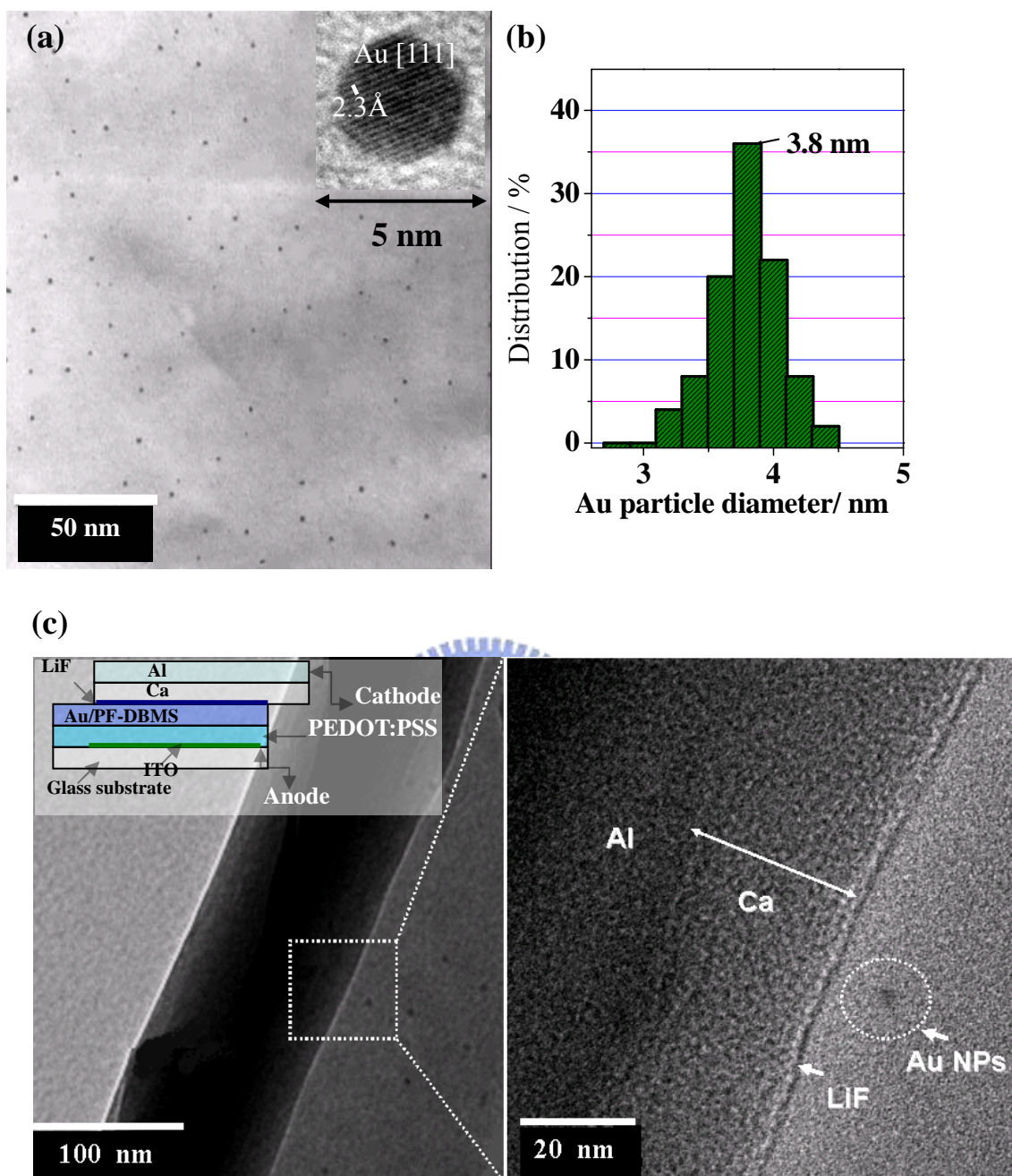


Figure 4. (a) Transmission electron microscopy images of Au/PF-DBMS films. The inset displays the lattice image (lattice spacing: ca. 2.3 Å) of the Au NPs. (b) Size distribution of Au NPs in the PF-DBMS polymer matrix. (c) TEM images of cross-sections of the device.

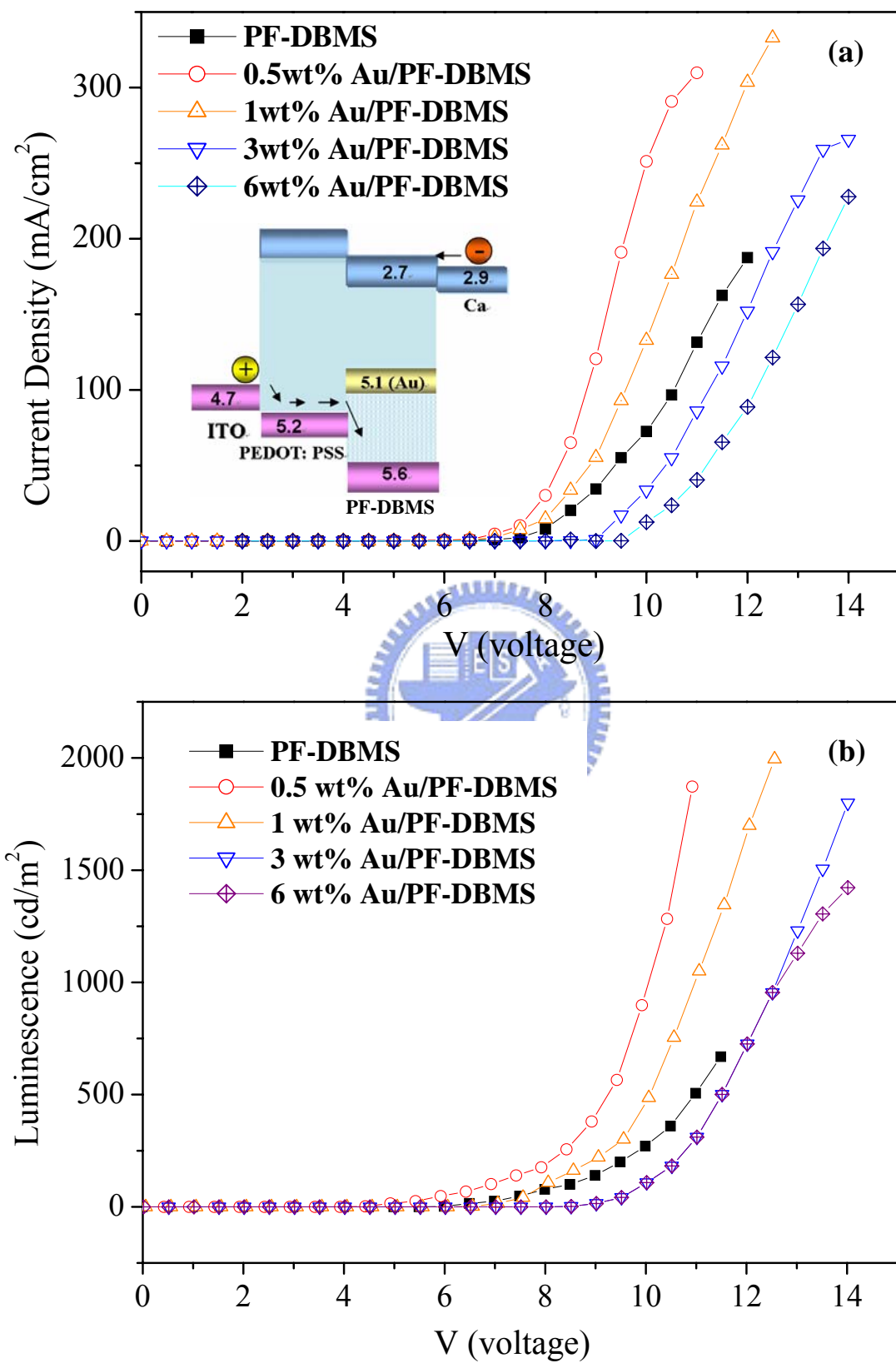


Figure 5. (a) I-V and (b) L-V curves of devices prepared from Au/PF-DBMS in the configuration ITO/PEDOT/polymer/Ca/LiF/Al.

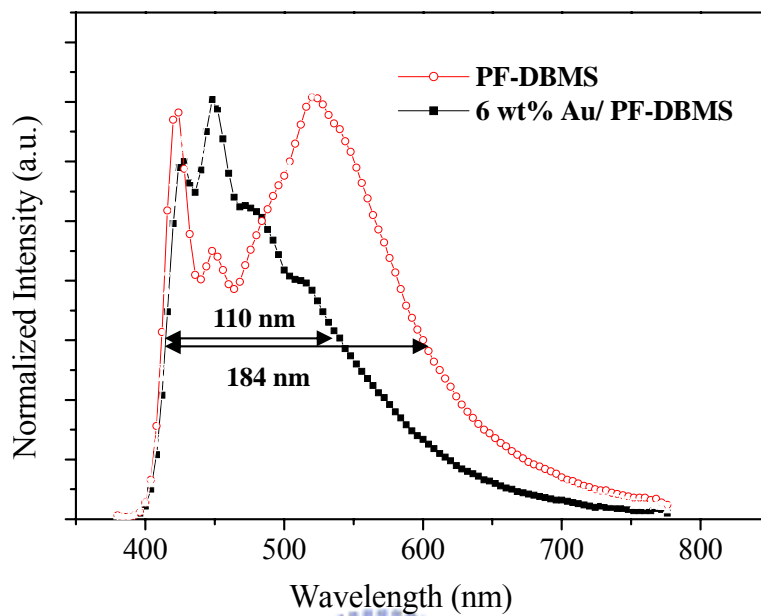
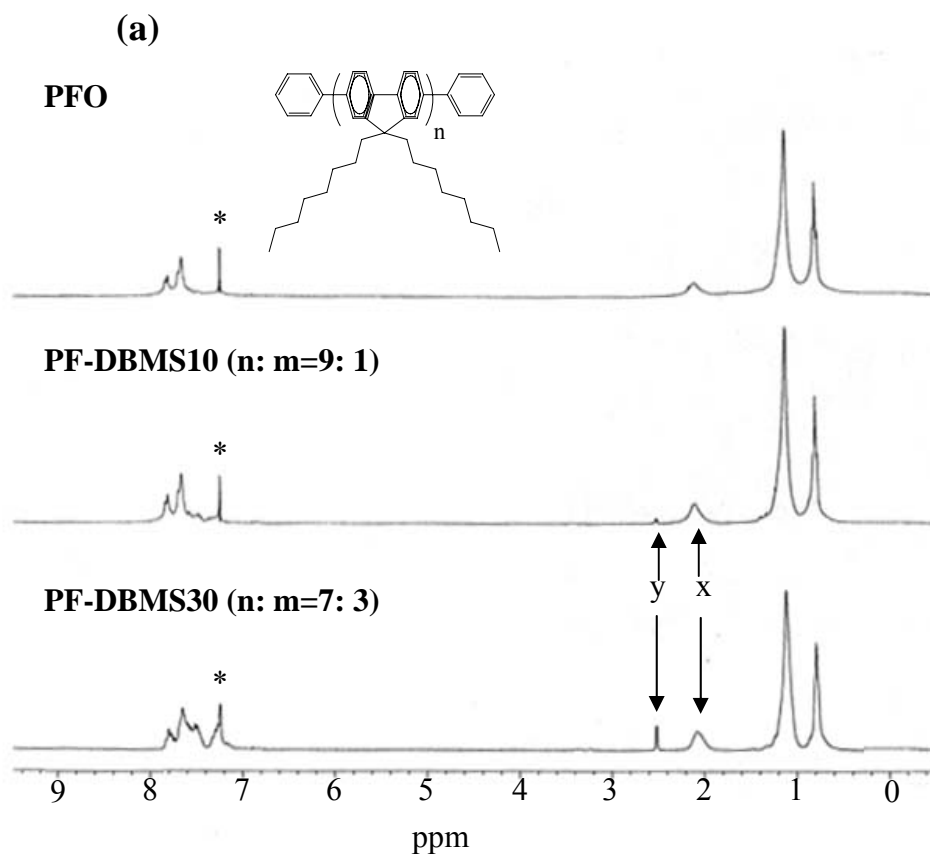


Figure 6. EL spectra of devices prepared from Au/PF-DBMS in the configuration ITO/PEDOT/polymer/LiF/Ca/Al.





(b)

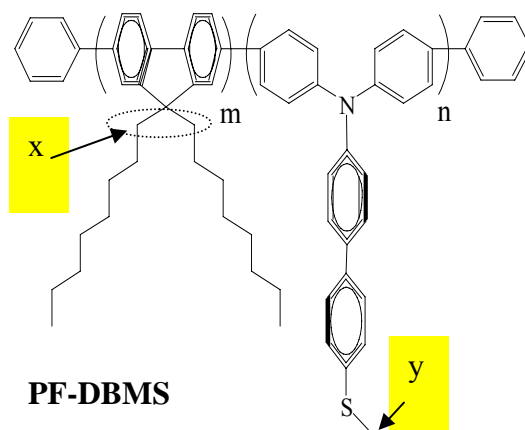
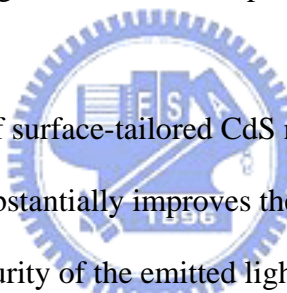


Figure 7. (a) ^1H NMR spectra of the chemical structure of all polymers. (b) The chemical structure of the PF-DBMS.

Chapter 6: Conclusions

We have synthesized a novel polyfluorene and poly(*p*-phenylenevinylene) side-chain-tethered polyhedral silsesquioxane that has a well-defined architecture. This particular molecular architecture of PFO-POSS increases the quantum yield of polyfluorene significantly by reducing the degree of interchain aggregation; it also results in a purer and stronger blue light being emitted from the EL device by preventing the formation of keto defects. Moreover, PPV-POSS also increases the quantum yield of MEHPPV significantly by reducing the degree of interchain aggregation; it also results in a much brighter red light from the EL device by decreasing the degree of aggregation between the polymer chains.



Placing a small amount of surface-tailored CdS nanoparticles into the dendritic structure of copolyfluorene substantially improves the efficiency of the polymer's light emission as well as the purity of the emitted light. The enhancements in photoluminescence and electroluminescence are due mainly to a reduction in the concentration of inter-polymer excimers through which energy transfer occurs from the excited polymer chains to their neighboring ground state polymer chains. In the other hand, side-chain-tethered Au NP/polyfluorene copolymer (PF-DBMS) hybrids by taking advantage of multiple ArSCH₃ anchor groups present on the polymer's side chains. The EL behavior of the PF-DBMS/Au NP devices indicates that they exhibit enhanced environmental stability and are suitable for use as nanocomposite emitting layers. The presence of the Au NPs appears to modify the device's interfacial morphology—they not only facilitate electron injection but also block hole migration. These Au/PF-DBMS nanocomposites display improved device performance relative to that of the pristine PF-DBMS device.

References and Notes

- [1] J. H. Burroughes, D. D. C. Bradley, A. R. Brown, R. N. Marks, K. Mackay, R. H. Friend, P. L. Burn, A. B. Holmes, *Nature* **1990**, *347*, 539.
- [2] R. J. Visser, *Application of Polymer Light-Emitting Materials in Light-Emitting Diodes, Backlights and Displays*, *Philips J. Res.* **1998**, *51*, 467.
- [3] Heeger, Alan. J., *Synthetic Metals* **2001**, *125*, 23.
- [4] U. Lemmer, S. Heun, R. F. Mahrt, U. Scherf, M. Hopmeier, U. Siegner, E.O. Goebel, K. Muellen, H. Baessler, *Chem. Phys. Lett.* **1995**, *240*, 373.
- [5] S. Pannozzo, J. -C. Vial, Y. Kervalla, O. Stephan, *J. Appl. Phys.* **2002**, *92*, 3495.
- [6] a) E. J. W. List, R. Güntner, P. Scandiucci de Freitas, U. Scherf, *Adv. Mater.* **2002**, *14*, 374. b) U. Scherf, E. J. W. List, *Adv. Mater.* **2002**, *14*, 477.
- [7] K. H. Weinfurtner, H. Fujikawa, S. Tokito, Y. Taga, *Appl. Phys. Lett.* **2000**, *76*, 2502.
- [8] S. Setayesh, A. C. Grimsdale, T. Weil, V. Enkelmann, K. Muellen, F. Meghdadi, E. J. W. List, G. Leising, *J. Am. Chem. Soc.* **2001**, *123*, 946.
- [9] N. Johansson, J. Salbeck, J. Bauer, F. Weissoertel, P. Broems, A. Anderson, W. R. Salaneck, *Adv. Mater.* **1998**, *10*, 1136.
- [10] J. I. Lee, G. Klämer, R. D. Miller, *Chem. Mater.* **1999**, *11*, 1083.
- [11] a) M. Bernius, M. Inbasekaran, E. Woo, W. Wu, L. Wujkowski, *J. Mater. Sci.: Mater. Electronics* **2000**, *11*, 111. b) M. T. Bernius, M. Inbasekaran, J. O'Brien, W. Wu, *Adv. Mater.* **2000**, *12*, 1737. c) M. Leclerc, *J. Polym. Sci. Part A: Polym. Chem.* **2001**, *39*, 2867.
- [12] R. H. Friend, D. D. C. Bradley, P. D. Townsend, *J. Phys. D: Appl. Phys.* **1987** *20*, 1367.
- [13] A. Kraft, A. C. Grimsdale, A. W. Holmes, *Angew. Chem. Int. Ed.* **1998**, *37*, 402.

- [14] a) H. A. Klok, S. Lecommandoux, *Adv. Mater.* **2001**, *13*, 1217. b) V. V. Tsukruk, *Prog. Polym. Sci.* **1997**, *22*, 247.
- [15] J. D. Lichtenhan, Y. A. Otonari, M. J. Carr, *Macromolecules* **1995**, *28*, 8435.
- [16] T. S. Haddad, J. D. Lichtenhan, *Macromolecules* **1996**, *29*, 7302.
- [17] A. Lee, J. D. Lichtenhan, *Macromolecules* **1998**, *31*, 4970.
- [18] F. J. Feher, D. Soulivong, A. G. Eklud, K. D. Wyndham, *Chem. Commun.* **1997**, 1185.
- [19] H. G. Jeon, P. T. Mather, T. S. Haddad, *Polym. Int.* **2000**, *49*, 453.
- [20] T. S. Haddad, P. T. Mather, H. G. Jeon, A. Romo-Uribe, R. Farris, J. D. Lichtenhan, In *Organic/Inorganic Hybrid Materials*; Laine, R., Sanchez, Brinker, Giannelis, Eds.; MRS Symp. Ser. 519; Materials Research Society: Warrendale, PA, **1998**; 381.
- [21] J. W. Gilman, D. S. Schlitzere, J. D. Lichtenhan, *J. Appl. Polm. Sci.* **1996**, *60*, 591.
- [22] R. I. Gonzalez, S. H. Phillips, G. B. Hoflund, *J. Spacecr. Rockets* **2000B**, *37*, 463.
- [23] C. Zhang, F. Babonneau, C. Bonhomme, R. M. Laine, C. L. Soles, H. A. Hristov, A. F. Yee, *J. Am. Chem. Soc.* **1998**, *120*, 8380.
- [24] R. M. Laine, J. Choi, I. Lee, *Adv. Mater.* **2001**, *13*, 800.
- [25] C. Zhang, R. M. Laine, *J. Am. Chem. Soc.* **2000**, *122*, 6979.
- [26] R. Tamaki, Y. Tanaka, M. Z. Asuncion, J. Choi, R. M. Laine, *J. Am. Chem. Soc.* **2001**, *123*, 12416.
- [27] L. Zheng, A. J. Waddon, R. J. Farris, E. B. Coughlin, *Macromolecules* **2002**, *35*, 2375.
- [28] J. H. Park, Y. T. Lim, O. O. Park, J. K. Kim, J. W. Yu, Y. C. Kim, *Chem. Mater.* **2004**, *16*, 688.

- [29] H. Skaff, K. Sill, T. Emrick, *J. Am. Chem. Soc.* **2004**, *126*, 11322.
- [30] M. R. Andersson, G. Yu, A. J. Heeger, *Synth. Metals* **1997**, *85*, 1275.
- [31] J. H. Kim, H. Lee, *Chem. Mater.* **2002**, *14*, 2270.
- [32] a) N. C. Greenham, S. C. Moratti, D. D. C. Bradley, R. H. Friend, A. B. Holmes, *Nature* **1993**, *365*, 628. b) G. Gustafsson, Y. Cao, G. M. Treacy, F. Klavetter, N. Colaneri, A. J. Heeger, *Nature* **1992**, *357*, 477. c) S. A. Jenekhe, J. A. Osaheni, *Science* **1994**, *620*, 765.
- [33] a) J. J. M. Halls, C. A. Walsh, N. C. Greenham, E. A. Marseglia, R. H. Friend, S. C. Moratti, A. B. Holmes, *Nature* **1995**, *376*, 498. b) G. Yu, J. Gao, J. C. Hummelen, F. Wudl, A. J. Heeger, *Science* **1995**, *270*, 1789. c) M. Granström, K. Petritsch, A. C. Arias, A. Lux, M. R. Andersson, R. H. Friend, *Nature* **1998**, *395*, 257.
- [34] a) Y. Yang, A. J. Heeger, *Nature* **1994**, *372*, 344. b) A. R. Brown, A. Pomp, C. M. Hart, D. M. de Leeuw, *Science* **1995**, *270*, 972. (c) H. Sirringhaus, N. Tessler, R. H. Friend, *Science* **1998**, *280*, 1741. (d) H. Sirringhaus, P. J. Brown, R. H. Friend, M. M. Nielsen, K. Bechgaard, B. M. W. Langeveld-Voss, A. J. H. Spiering, R. A. J. Janssen, E. W. Meijer, P. Herwig, D. M. de Leeuw, *Nature* **1999**, *401*, 685. (e) A. Babel, S. A. Jenekhe, *J. Am. Chem. Soc.* **2003**, *125*, 13656.
- [35] M. Ranger, D. Rondeau, M. Leclerc, *Macromolecules* **1997**, *30*, 7686.
- [36] W.-L. Yu, J. Pei, Y. Cao, W. Huang, A. J. Heeger, *Chem. Commun.* **1999**, 1837.
- [37] J. Pei, W.-L. Yu, W. Huang, A. J. Heeger, *Chem. Commun.* **2000**, 1631.
- [38] C. Ego, D. Marsitzky, S. Becker, J. Zhang, A. C. Grimsdale, K. Müllen, J. D. MacKenzie, C. Silva, R. H. Friend, *J. Am. Chem. Soc.* **2003**, *125*, 437.
- [39] G. Klärner, J. I. Lee, M. H. Davey, R. D. Miller, *Adv. Mater.* **1999**, *11*, 115.
- [40] a) W.-L. Yu, J. Pei, W. Huang, A. J. Heeger, *Adv. Mater.* **2000**, *12*, 828. b) G. Zeng, W.-L. Yu, S.-J. Chua, W. Huang, *Macromolecules* **2002**, *35*, 6907.
- [41] G. Klärner, J. I. Lee, V. Y. Lee, E. Chan, J. P. Chen, A. Nelson, D. Markiewicz,

- R. Siemens, J. C. Scott, R. D. Miller, *Chem. Mater.* **1999**, *11*, 1800.
- [42] a) D. Marsitzky, M. Klapper, K. Mullen, *Macromolecules* **1999**, *32*, 8685. b) D. Marsitzky, J. Murray, J. C. Scott, K. R. Carter, *Chem. Mater.* **2001**, *13*, 4285. c) C. Ego, A. C. Grimsdale, F. Uckert, G. Yu, G. Srdanov, K. Müllen, *Adv. Mater.* **2002**, *14*, 809. d) A. Pogantsch, F. P. Wenzl, E. J. W. List, G. Leising, A. C. Grimsdale, K. Müllen, *Adv. Mater.* **2002**, *14*, 1061. e) J. M. Lupton, P. Schouwink, P. E. Keivanidis, A. C. Grimsdale, K. Müllen, *Adv. Funct. Mater.* **2003**, *13*, 154.
- [43] C. F. Shu, R. Dodda, F. I. Wu, M. S. Liu, A. K. Y. Jen, *Macromolecules* **2003**, *36*, 6698.
- [44] G. Zeng, G. Yu, S. J. Chua, W. Huang, *Macromolecules* **2002**, *35*, 6907.
- [45] S. Xiao, M. Nguyen, X. Gong, Y. Cao, H. Wu, D. Moses, A. J. Heeger, *Adv. Funct. Mater.* **2003**, *13*, 25.
- [46] a) H. J. Cho, B. J. Jung, N. S. Cho, J. Lee, H. K. Shim, *Macromolecules* **2003**, *36*, 6704. b) E. Lim, B. J. Jung, H. K. Shim, *Macromolecules* **2003**, *36*, 4288.
- [47] A. P. Kulkarni, S. A. Jenekhe, *Macromolecules* **2003**, *36*, 5285.
- [48] a) L. Romaner, A. Pogantsch, P. S. Freitas, U. Scherf, M. Gaal, E. Zojer, J. W. List, *Adv. Funct. Mater.* **2003**, *13*, 597. b) A. P. Kulkarni, X. Kong, S. A. Jenekhe, *J. Phys. Chem. B.* **2004**, *108*, 8689.
- [49] a) C. M. Leu, Y. T. Chang, K. H. Wei, *Macromolecules* **2003**, *36*, 9122. b) A. Kraft, A. C. Grimsdale, A. B. Holmes, *Angew. Chem. Int. Ed.* **1998**, *37*, 402.
- [50] T. M. Miller, T. X. Neenan, R. Zayas, H. E. Bair, *J. Am. Chem. Soc.* **1992**, *114*, 1018.
- [51] M. Ranger, M. Leclerc, *Macromolecules* **1999**, *32*, 3306.
- [52] C. M. Leu, Y. T. Chang, K. H. Wei, *Chem. Mater.* **2003**, *15*, 3721.
- [53] M. Grell, D. D. C. Bradley, M. Inbasekaran, E. P. Woo, *Adv. Mater.* **1997**, *9*, 798.

- [54] F. I. Wu, D. S. Reddy, C. F. Shu, M. S. Liu, A. K. Y. Jen, *Chem. Mater.* **2003**, *15*, 269.
- [55] a) M. Grell, D. D. C. Bradley, X. Long, T. Chamberlain, M. Inbasekaran, E. P. Woo, M. Soliman, *Acta Polym.* **1998**, *49*, 439. b) A. W. Grice, D. D. C. Bradley, M. T. Bernius, M. Inbasekaran, W. W. Wu, E. P. Woo, *Appl. Phys. Lett.* **1998**, *73*, 629.
- c) R. H. Friend, R. W. Gymer, A. B. Holmes, J. H. Burroughes, R. N. Marks, C. Taliani, D. D. C. Bradley, D. A. Dos Santos, J. L. Bredas, M. Logdlund, W. R. Salaneck, *Nature* **1999**, *397*, 121.
- [56] A. C. Grimsdale, P. Leclère, R. Lazzaroni, J. D. MacKenzie, C. Murphy, S. Setayesh, C. Silva, R. H. Friend, K. Müllen, *Adv. Funct. Mater.* **2002**, *12*, 729.
- [57] W.-L. Yu, J. Pei, Y. Cao, W. Huang, A. J. Heeger, *Chem. Commun.* **1999**, 1837.
- [58] J. Pei, W.-L. Yu, W. Huang, A. J. Heeger, *Chem. Commun.* **2000**, 1631.
- [59] U. Mitschke, P. Bäuerle, *J. Mater. Chem.* **2000**, *10*, 1471.
- [60] A. Kraft, C. Grimsdale, A. B. Holmes, *Angew. Chem., Int. Ed.* **1998**, *37*, 402.
- [61] a) I. Sokolik, Z. Yang, F. E. Karasz, D. C. Morton, *J. Appl. Phys.* **1993**, *74*, 3584.
- b) B. R. Hsieh, Y. Yu, E. W. Forsythe, G. M. Schaaf, W. A. Feld, *J. Am. Chem. Soc.*, **1998**, 231.
- [62] a) Z. Yang, F. E. Karasz, H. J. Geise, *Macromolecules* **1993**, *26*, 6570. b) H. Spreitzer, H. Becker, E. Kluge, W. Kreuder, H. Schenk, R. Demandt, H. Schöo, *Advanced Materials*, **1998**, *10*, 1340. c) T. Ahn, M. S. Jang, H.-K. Shim, D.-H. Hwang, T. Zyung, *Macromolecules*, **1999**, *32*, 3279. d) H. Becker, H. Spreitzer, K. Ibrom, W. Kreuder, *Macromolecules* **1999**, *32*, 4925. e) H. Becker, H. Spreitzer, W. Kreuder, E. Kluge, H. Schenk, I. Parker, Y. Cao, *Advanced Materials*, **2000**, *12*, 42.
- [63] a) S. T. Pasco, P. M. Lahti, F. E. Karasz, *Macromolecules* **1999**, *32*, 6933. b) Z. K. Chen, N. H. S. Wei, H. Lee, Y. S. Xu, Y. Cao, *Macromolecules* **2003**, *36*, 1009.
- [64] S. H. Jin, J. E. Jung, D. K. Park, B. C. Jeon, S. K. Kwon, Y. H. Kim, D. K. Moon,

Y. S. Gal, *Eur. Polym. J.* **2001**, *37*, 921.

[65] S. H. Lee, S. H. Jin, S. B. Moon, I. S. Song, W. H. Kim, S. K. Kwon, N. K. Park, E. M. Han, *Mol. Cryst. Liq. Cryst.* **2000**, *349*, 507.

[66] a) S. H. Jin, W. H. Kim, I. S. Song, S. K. Kwon, K. S. Lee, E. M. Han, *Thin Solid Films* **2000**, *363*, 255. b) J. Huber, K. Mullen, J. Salbeck, H. Schenk, U. Scherf, T. Stehlin, R. Stern, *Acta Polym.* **1994**, *45*, 244. c) M. Grell, D. D. C. Bradley, G. Ungar, J. Hill, Whitehead, K. S. *Macromolecules*, **1999**, *32*, 5810.

[67] a) W. J. Lin, W. C. Chen, W. C. Wu, Y. H. Niu, A. K. Y. Jen, *Macromolecules* **2004**, *37*, 2335. b) J. Lee, H.-J. Cho, B.-J. Jung, N. S. Cho, H.-K. Shim, *Macromolecules* **2004**, *37*, 8523.

[68] J. D. Lichtenhan, N. Q. Vu, J. A. Carter, J. W. Gilman, F. J. Feher, *Macromolecules* **1993**, *26*, 2141.

[69] F. J. Feher, D. Soulivong, A. G. Eklud, K. D. Wyndham, *Chem. Commun.* **1997**, 1185.

[70] a) S. Aratani, C. Zhang, K. Pakbaz, S. Hoger, F. Wudl, A. J. Heeger, *J. Elec. Mater.* **1993**, *22*, 745. b) Y. Yang, A. J. Heeger, *Appl. Phys. Lett.* **1994**, *64*, 1245. c) D. Braun, A. J. Heeger, *Appl. Phys. Lett.* **1991**, *58*, 1982.

[71] a) C. M. Leu, G. M. Reddy, K. H. Wei, C. F. Shu, *Chem. Mater.* **2003**, *15*, 2261. b) C. M. Leu, Y. T. Chang, K. H. Wei, *Macromolecules*, **2003**, *36*, 9122.

[72] S. H. Chen, A. C. Su, H. L. Chou, K. Y. Peng, S. A. Chen, *Macromolecules* **2004**, *37*, 167.

[73] A. Kurian, N. A. George, B. Paul, V. P. N. Nampoore, C. P. G. Vallabhan, *Laser Chemistry* **2002**, *20*, 99.

[74] J. R. Heldt, J. Heldt, M. Obarowska, B. Mielewska, J. Kamiński, *Journal of Fluorescence* **2002**, *11*, 335.

[75] D. Magde, R. Wong, P. G. Seybold, *Photochem. Photobiol.* **2002**, *75*, 327.

[76] a) Y. Shi, J. Liu, Y. Yang, *J. Appl. Phys.* **2000**, *87*, 4254. b) T.-Q. Nguyen, I. Martini, J. Liu, B. J. Schwartz, *J. Phys. Chem. B.* **2000**, *104*, 237. c) T.-Q. Nguyen, V. Doan, B. J. Schwartz, *J. Chem. Phys.* **1999**, *110*, 4068.

[77] a) T.-Q. Nguyen, B. J. Schwartz, R. D. Schaller, J. C. Johnson, L. F. Lee, L. H. Haber, R. J. Saykally, *J. Phys. Chem. B.* **2001**, *105*(22), 5153. b) T.-Q. Nguyen, B. J. Schwartz, *Journal of Chemical Physics*, **2002**, *116*(18), 8198.

[78] a) J. Liu, Y. Shi, Y. Yang, *Advanced Functional Materials*, **2001**, *11*(6), 420. b) Y. Shi, J. Liu, Y. Yang, *Journal of Applied Physics*, **2000**, *87*(9), 4254.

[79] S. Tretiak, A. Saxena, R. L. Martin, A. R. Bishop, *J. Phys. Chem. B.* **2000**, *104*(30); 7029.

[80] a) PL quantum yield was determined by using a standard of Rhodamine 6G ($\Phi_r = 0.95$) dispersed in Poly(methyl methacrylate) (PMMA) at low concentration (10^{-3} M) with the film thickness being 100 ± 10 nm. The quantum yield of a sample, Φ_s , can be calculated by the following equation: $\Phi_s = (A_r/A_s)(F_s/F_r) \Phi_r$; A_s and A_r are the respective optical density of the sample and the reference at their excitation wavelengths, F_r and F_s are the corresponding areas under their emission peaks. b) B. S. Kang, D. H. Kim, S. M. Lim, J. Kim, M.-L. Seo, K.-M. Bark, S. C. Shin, K. Nahm, *Macromolecules*, **1997**, *30*, 7196.

[81] Transmission electron microscopy was performed on a Hitachi H-600 instrument operated at 100 kV and on a JEOL-2010 TEM operated at 200 kV at the Center for Nano Science & Technology (CNST). The ultrathin sections of POSS-PPV-co-MEHPPV copolymer prepared for TEM studies were microtomed using a Leica Ultracut Uct apparatus equipped with a diamond knife and subsequently deposited on copper grids. The microtomed thin films, corresponding to the section of the POSS-PPV-co-MEHPPV copolymer, were also observed using a Digital Nanoscope IIIa atomic force microscope (AFM).

- [82] I. Prieto, J. Teetsov, M. A. Fox, D. A. V. Bout and A. J. Bard, *J. Phys. Chem. A*, **2001**, *105*, 520.
- [83] D. Marsitzky, R. Vestberg, P. Blainey, B. T. Tang, C. J. Hawker and K. R. Carter, *J. Am. Chem. Soc.*, **2001**, *123*, 6965.
- [84] Q. Pei and Y. Yang, *J. Am. Chem. Soc.*, **1996**, *118*, 7416.
- [85] D. Y. Kim, H. N. Cho and C. Y. Kim, *Prog. Polym. Sci.*, **2000**, *25*, 1089.
- [86] D. M. Johansson, G. Srdanov, G. Yu, M. Theander, O. Inganäs and M. R. Andersson, *Macromolecules*, **2000**, *33*, 2525.
- [87] R. M., Gurge, A. M. Sarker, P. M. Lahti, B. Hu and F. E. Karasz, *Macromolecules*, **1997**, *30*, 8286.
- [88] G. Padmanaban and S. Ramakrishnan, *J. Am. Chem. Soc.*, **2000**, *122*, 2244.
- [89] J. Grimme, K. Martin, F. Uckert, K. Mullen and U. Scherf, *Adv. Mater.*, **1995**, *7*, 292.
- [90] S. H. Jin, M. S. Jang, H. S. Suh, H. N. Cho, J. H. Lee and Y. S. Gal, *Chem. Mater.*, **2002**, *14*, 643.
- [91] H. Yang and P. H. Holloway, *J. Phys. Chem. B*, **2003**, *107*, 9705.
- [92] J. Cheng, S. Wang, X. Y. Li, Y. J. Yan, S. Yang, C. L. Yang, J. N. Wang and W. K. Ge, *Chem. Phys. Lett.*, **2001**, *333*, 375.
- [93] F. Hide, B. J. Schwartz, M. A. Diaz-Garcia and A. J. Heeger, *Chem. Phys. Lett.*, **1996**, *256*, 424.
- [94] B. O. Dabbousi, M. G. Bawendi, O. Onitsuka and M. F. Rubner, *Appl. Phys. Lett.*, **1995**, *66*, 1316.
- [95] W. U. Huynh, J. J. Dittmer and A. P. Alivisatos, *Science*, **2002**, *295*, 2425.
- [96] D. J. Milliron, A. P. Alivisatos, C. Pitois, C. Edder and J. M. J. Fréchet, *Adv. Mater.*, **2003**, *15*, 58.
- [97] P. A. Van Hal, M. P. T. Christiaans, M. M. Wienk, J. M. Kroon and R. A. J.

Janssen, *J. Phys. Chem. B*, **1999**, *103*, 4352.

[98] H. Mattoussi, L. H. Radzilowski, B. O. Dabbousi, E. L. Thomas, M. G. Bawendi and M. F. Rubner, *J. Appl. Phys*, **1998**, *83*, 7698.

[99] M. C. Schlamp, X. Peng and A. P. Alivisatos, *J. Appl. Phys*, **1997**, *82*, 5837.

[100] a) L. Sheeney-Haj-Ichia, Z. Cheglakov and I. Willner, *J. Phys. Chem. B*, **2004**, *108*, 11. b) T. Trindade, P. O'Brien and N. L. Pickett, *Chem. Mater.*, **2001**, *13*, 3843.

[101] N. C. Greenham, X. Peng and A. P. Alivisatos, *Phys. Rev. B*, **1996**, *54*, 17628.

[102] C. H. Chou and C. F. Shu, *Macromolecules*, **2002**, *35*, 9673.

[103] R. G. Dondon, V. P. Khilya, A. D. Roshal and S. Fery-Forgues, *New J. Chem.*, **1999**, *23*, 923.

[104] T. Q. Nguyen, I. B. Martini, J. Liu and B. J. Schwartz, *J. Phys. Chem. B*, **2000**, *104*, 237.

[105] C. H. Chou, S. L. Hsu, K. Dinakaran, M. Y. Chiu and K. H. Wei, *Macromolecules*, **2005**, *38*, 745.

[106] J. G. C. Veinot, M. Ginzburg and W. J. Pietro, *Chem. Mater.*, **1997**, *9*, 2117.

[107] N. Herron, Y. Wang and H. Eckert, *J. Am. Chem. Soc.*, **1990**, *112*, 1322.

[108] L. Brus, *J. Phys. Chem.*, **1986**, *90*, 2555.

[109] M. Moffitt, H. Vali and A. Eisenberg, *Chem. Mater.*, **1998**, *10*, 1021.

[110] J. Hofkens, M. Cotlet, T. Vosch, P. Tinnefeld, K. D. Weston, C. Ego, A. Grimsdale, K. Mullen, D. Beljonne, J. L. Brédas, S. Jordens, G. Schweitzer, M. Sauer and F. D. Schryver, *Proc. Natl. Acad. Sci. U.S.A.*, **2003**, *100*, 13146.

[111] Wide-angle X-ray scattering (WAXS) is used for characterizing the d spacing of polymeric materials. The scattering experiments were carried out on a Siemens Hi-Star area detector with Cu K(α) radiation $\lambda = 1.5406 \text{ \AA}$ operated at 40 kV and 45 mA. The 2θ range was from 1° to 40° , and the sample was a film about $1 \mu\text{m}$ thickness on a glass substrate.

- [112] a) S. H. Chen, A. C. Su, C. H. Su, S. A. Chen, *Macromolecules*, **2005**, *38*, 379.
b) S. Choi, J. H. Kim, Y. S. Kang, *Macromolecules*, **2001**, *34*, 9087. c) D. A. Shultz, R. M., Jr. Fico, P. D. Boyle, J. W. Kampf, *J. Am. Chem. Soc.*, **2001**, *123*, 10403.
- [113] a) G. Maruta, S. Takeda, K. Yamaguchi, K. Ueda, T. Sugimoto, *Synth. Met.* **1999**, *103*, 2333. b) H. Adams, C. A. Hunter, K. R. Lawson, J. Perkins, S. E. Spey, C. J. Urch, J. M. Sanderson, *Chem.-Eur. J.* **2001**, *7*, 4863.
- [114] R. Rathore, S. H. Abdelwahed, I. A. Guzei, *J. Am. Chem. Soc.*, **2003**, *125*, 8712.
- [115] a) G. B. Schuster, *Acc. Chem. Res.* **2000**, *33*, 253. b) B. G. Maiya, T. Ramasarma, *Curr. Sci.* **2001**, *80*, 1523. c) F. D. Lewis, R. L. Letsinger, M. R. Wasielewski, *Acc. Chem. Res.* **2001**, *34*, 159.
- [116] In Figure 5D, polymer in solid state (in the presence of tetra *n*-butylammonium hexafluorophosphate as a supporting electrolyte) at a scan rate of 50 mV s⁻¹ showed reversible cyclic voltammograms with oxidation potentials (E_{ox}) that progressively decreased with an increasing S-CdS nanoparticles concentration.
- [117] W. Wang, J. Xu, Y.-H. Lai, F. Wang, *Macromolecules*, **2004**, *37*, 3546.
- [118] A. P. Alivisatos, *Science* **1996**, *271*, 933.
- [119] J. Shi, S. Gider, K. Babcock, D. D. Awschalom, *Science* **1996**, *271*, 937.
- [120] M. Krishnan, J. R. White, M. A. Fox, A. J. Bard, *J. Am. Chem. Soc.* **1983**, *105*, 7002.
- [121] Y. Lin, J. Zhang, E. H. Sargent, E. Kumacheva, *J. Mater. Sci.* **2004**, *39*, 993.
- [122] H. Mattoussi, L. H. Radzilowski, B. O. Dabbousi, D. E. Fogg, R. R. Schrock, E. L. Thomas, M. F. Rubner, M. G. Bawendi, *J. Appl. Phys.* **1999**, *86*, 4390.
- [123] H. Zhang, C. Zhanchen, Y. Wang, K. Zhang, J. Xiulei, L. Changli, B. Yang, *Adv. Mater.* **2003**, *15*, 777.
- [124] M. J. Percy, C. Barthet, J. C. Lobb, M. A. Khan, S. F. Lascelles, M. Vamvakaki, S. P. Armes, *Langmuir* **2000**, *16*, 6913.

- [125] M. Kreyenschmidt, G. Klärner, T. Fuhrer, J. Ashenurst, S. Karg, W. D. Chen, V. Y. Lee, J. C. Scott, R. D. Miller, *Macromolecules* **1998**, *31*, 1099.
- [126] D. Marsitzky, M. Klapper, K. Mullen, *Macromolecules* **1999**, *32*, 8685.
- [127] a) C. F. Shu, R. Dodda, F. I. Wu, M. S. Liu, A. K. Y. Jen, *Macromolecules* **2003**, *36*, 6698. b) E. Lim, B. J. Jung, H. K. Shim, *Macromolecules* **2003**, *36*, 4288. c) A. P. Kulkarni, S. A. Jenekhe, *Macromolecules* **2003**, *36*, 5285.
- [128] A. P. Kulkarni, X. Kong, S. A. Jenekhe, *J. Phys. Chem. B.* **2004**, *108*, 8689.
- [129] C. H. Chou, H. S. Wang, K. H. Wei, J. Y. Huang, *Adv. Funct. Mater.* **2006**, *16*, 909.
- [130] L. A. Porter, Jr., D. Ji, S. L. Westcott, M. Graupe, R. S. Czernuszewicz, N. J. Halas, T. R. Lee, *Langmuir* **1998**, *14*, 7378.
- [131] T. Yonezawa, K. Yasui, N. Kimizuka, *Langmuir* **2001**, *17*, 271.
- [132] A. Manna, P.-L. Chen, H. Akiyama, T.-X. Wei, K. Tamada, W. Knoll, *Chem. Mater.* **2003**, *15*, 20.
- [133] K. Torigoe, K. Esumi, *J. Phys. Chem. B* **1999**, *103*, 2862.
- [134] K. Furukawa, K. Ebata, H. Nakashima, Y. Kashimura, K. Torimitsu, *Macromolecules* **2003**, *36*, 9.
- [135] R. Resch, C. Baur, A. Bugacov, B. E. Koel, P. M. Echternach, A. Madhukar, N. Montoya, A. A. G. Requicha, P. Will, *J. Phys. Chem. B* **1999**, *103*, 3647.
- [136] N. Felidj, J. Aubard, G. Levi, J. R. Krenn, A. Hohenau, G. Schider, A. Leitner, F. R. Aussenegg, *Appl. Phys. Lett.* **2003**, *82*, 3095.
- [137] R. Balasubramanian, B. Kim, S. L. Tripp, X. Wang, M. Lieberman, A. Wei, *Langmuir* **2002**, *18*, 3676.
- [138] a) X.-M. Li, M. R. de Jong, K. Inoue, S. Shinkai, J. Huskens, D. N. Reingoudt, *J. Mater. Chem.* **2001**, *11*, 1919. b) C. Zubrägel, C. Deuper, F. Schneider, M. Neumann, M. Grunze, A. Schertel, C. Wöll, *Chem. Phys. Lett.* **1995**, *238*, 308. c) R.

- Balasubramanian, B. Kim, S. L. Tripp, X. Wang, M. Lieberman, A. Wei, *Langmuir* **2002**, *18*, 3676. d) Z. Li, M. Lieberman, W. Hill, *Langmuir* **2001**, *17*, 4887. e) C. R. Mayer, S. Neveu, C. Simonnet-Jégat, C. Debiemme-Chouvy, V. Cabuil, F. Secheresse, *J. Mater. Chem.* **2003**, *13*, 338.
- [139] G. D. Hale, J. B. Jackson, O. E. Shmakova, T. R. Lee, N. J. Halas, *Appl. Phys. Lett.* **2001**, *78*, 1502.
- [140] J. H. Park, Y. T. Lim, O. O. Park, Y. C. Kim, *Macromol. Rapid Commun.* **2003**, *24*, 331.
- [141] A. P. Monkuan, H. D. Burrows, L. J. Hartwell, L. E. Horsburgh, I. Hamblett, S. Navaratnam, *Phys. Rev. Lett.* **2001**, *86*, 1358.
- [142] F. Wang, Z. J. Chen, Q. H. Gong, K. W. Wu, X. S. Wang, B. W. Zhang, F. Q. Tang, *Appl. Phys. Lett.* **1999**, *75*, 3243.
- [143] T. Q. Nguyen, I. B. Martini, J. Liu, B. J. Schwartz, *J. Phys. Chem. B* **2000**, *104*, 237.
- [144] S. H. Chen, A. C. Su, Y. F. Huang, C. H. Su, G. Y. Peng, S. A. Chen, *Macromolecules* **2002**, *35*, 4229.
- [145] L. O. Brown, J. E. Hutchison, *J. Phys. Chem. B* **2002**, *105*, 8911.
- [146] R. G. Dondon, V. P. Khilya, A. D. Roshal, S. Fery-Forgues, *New J. Chem.* **1999**, *23*, 923.

著作目錄

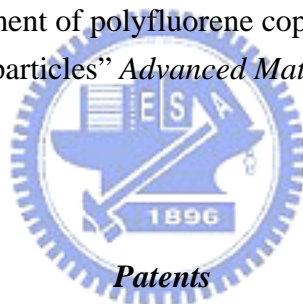
- 1. Chia-Hung Chou** and Ching-Fong Shu*. Synthesis and Characterization of Dendronized Polyfluorenes. *Macromolecules* **2002**, *35*, 9673. (Impact Factor =3.898)
- 2. Chia-Hung Chou**, D. Sahadeva Reddy, Ching-Fong Shu*. Synthesis and characterization of spirobifluorene-based polyimides. *Journal of Polymer Science Part A: Polymer Chemistry* **2002**, *40*, 3615. (Impact Factor =2.773)
- 3. D. Sahadeva Reddy**, **Chia-Hung Chou**, Ching-Fong Shu*, Synthesis and characterization of soluble poly(ether imide)s based on 2,2'-bis(4-aminophenoxy)-9,9'-spirobifluorene. *Polymer* **2003**, *44*, 557. (Impact Factor =2.433)
- 4. Jingdong Luo**, Marnie Haller, Hongxiang Li, Hong-Zhi Tang, Alex K.-Y. Jen*, Kavitha Jakka, **Chia-Hung Chou**, and Ching-Fong Shu. A Side-Chain Dendronized Nonlinear Optical Polyimide with Large and Thermally Stable Electrooptic Activity. *Macromolecules* **2004**, *37*, 248. (Impact Factor =3.898)
- 5. K.Dinakaran**, **Chia-Hung Chou**, So-Lin Hsu, Kung-Hwa Wei*. Synthesis and characterization of fluorescent poly(fluorene-co-phenylene-1-(di-2-pyridylamine)) copolymer and its Ru(II) complex. *Journal of Polymer Science Part A: Polymer Chemistry* **2004**, *42*, 4838. (Impact Factor =3.898)
- 6. Siao-Wei Yeh**, Yao-Te Chang, **Chia-Hung Chou**, Kung-Hwa Wei* "Effect of Surface-Hydroxylated CdS Nanoparticles on the Morphological Transformation of Polystyrene-block-Poly(ethylene oxide) Thin Films" *Macromolecular Rapid Communications* **2005**, *25*, 1679. (Impact Factor =3.366)
- 7. Kannaiyan Dinakaran**, Shu-Min Hsiao, **Chia-Hung Chou**, So-Lin Shu and Kung-Hwa Wei* "Synthesis and characterization of an efficiently fluorescent polyphenylenevinylene possessing pendant dendritic phenyl groups" *Macromolecules* **2005**, *38*, 10429. (Impact Factor =3.898)
- 8. Chin-Cheng Weng**, **Chia-Hung Chou**, Kung-Hwa Wei*, Jung Y. Huang. "Luminescence enhancement of MEHPPV Solid Film by Needle-like TiO₂ nanostructures" *Journal of Polymer Research*, **2006**, *13*, 229. (Impact Factor =0.375)

9. Chia-Hung Chou, So-Lin Hsu, Siao-Wei Yeh, Hsu-Shen Wang, Kung-Hwa Wei* “Enhanced Luminance and Thermal Properties of Polyphenylenevinylene Copolymer Presenting Side-Chain-Tethered Silsesquioxane Units” *Macromolecules* **2005**, *38*, 9117. (Impact Factor =3.898)

10. Chia-Hung Chou, So-Lin Hsu, K. Dinakaran, Mao-Yuan Chiu, and Kung-Hwa Wei* ”Synthesis and Characterization of Luminescent Polyfluorenes Incorporating Side-Chain-Tethered Polyhedral Oligomeric Silsesquioxane Units” *Macromolecule* **2005**, *38*, 745. (Impact Factor = 3.898)

11. Chia-Hung Chou, Kung-Hwa Wei*, Jung Y. Huang. Enhancement of luminescence efficiency of dendritic polyfluorene copolymers by CdS nanoparticles. *Advance Functional Materials* **2006**, *16*, 909. (Impact Factor =5.679)

12. Chia-Hung Chou, Chen-Ping Chen, So-Lin Hsu, and Kung-Hwa Wei* “Blue electroluminescence enhancement of polyfluorene copolymer incorporating side-chain-tethered gold nanoparticles” *Advanced Materials* **2006**, submitted. (Impact Factor = 8.079)



1. Inventor: Kung-Hwa Wei, **Chia-Hung Chou**

Title: Surface-modified quantum dots enhanced luminescence in polymer nanocomposites light emitting diode.

Status: US/Taiwan Patent pending.

2. Inventor: Kung-Hwa Wei, **Chia-Hung Chou**

Title: Luminescent polymers Incorporating Side-Chain-Tethered Polyhedral Oligomeric Silsesquioxane.

Status: US/Taiwan Patent pending.

學經歷資料

- 姓名：周嘉宏
- 性別：男
- 生日：67年4月10日，台北人
- 電子郵件信箱：vic.mse91g@nctu.edu.tw
- 聯絡電話：(學校) 03-5731771 (手機) 0953948108
- 通訊地址：新竹市 300 大學路 1001 號



國立交通大學材料與工程研究所
永久地址：台北縣永和市保順路 51 巷 15 號 8F

學歷

博士候選人：國立交通大學材料科學與工程研究所	2002. 9 ~ 2006. 6
研究所：國立交通大學應用化學研究所	2000. 9 ~ 2002. 6
大學：文化大學化學系	1996. 9 ~ 2000. 6

專長

- 有機光電材料(OLED/PLED)：
 1. 新穎材料分子設計及合成。
 2. 量子點及奈米複合材料。
- 有機/無機奈米複合材料：
 1. 奈米結構之無機物/高分子混成材及界面改質分散技術。
 2. 低介電聚亞醯(PI)與/無機物奈米複合材料。
- 分析儀器操作：

平面顯示器元件製程機台 (Hewlett-Packard 4155B semiconductor parameter analyzer、Newport 2835-C multi-function optical meter(EL)、Spin coater、蒸鍍機、真空手套箱(Dry Box)、UV0-Cleaner、元件封膠機、偏光顯微鏡。) 穿透式電子顯微鏡(TEM)、超薄切片機、原子力顯微鏡(AFM)、輝度計(PR-450)、拉曼光譜儀、紅外線光譜儀(FT-IR)、XRD、核磁共振光譜儀(Varian NMR and Bruker NMR)、微差掃描卡計(DSC)、熱重量分析儀(TGA)、質譜儀(Mass)、流變儀、凝膠滲透層析儀(GPC)、微光光譜儀(Uv-vis)、螢光光譜儀(PL)、旋轉塗佈機(Spin coater)、循環伏安計(CV)、熱蒸鍍機、片電阻四點破針、 α -step 薄膜測厚儀。